MUTATIONS IN PI(3,5)P2 SIGNALING AND NEURODEGENERATION IN MOUSE AND HUMAN

by

Clement Y. Chow

A dissertation submitted in partial fulfillment
of the requirements for the degree of
Doctor of Philosophy
(Human Genetics)
in The University of Michigan
2008

Doctoral Committee:

Professor Miriam H. Meisler, Chair
Professor Sally A. Camper
Professor David Ginsburg
Associate Professor David C. Kohrman
Assistant Professor Geoffrey G. Murphy

To my wife, Candace

For all her love and support

ACKNOWLEDGEMENTS

I would first like to thank my mentor, Miriam Meisler. She is the consummate scientist. Miriam is inquisitive and interested in a wide range of topics. This trait has taught me to always ask the right questions and be skeptical of conclusions that are not supported by data. Miriam's unending desire to make each oral presentation perfect drove me to improve my own skills. I came to this lab without any public presentation skills, but I am now greatly improved in my presentation abilities, a skill crucial for a successful scientific career. Miriam is a perfectionist when it comes to writing and always encouraged me to do the same. I will continue to strive to perfect my writing abilities. I came to the lab wanting to positionally clone a mouse mutant. I told Miriam that I would stay in the lab if she allowed me to do so. She was supportive and excited from the beginning, allowing me to pursue a project with an unknown future. This allowed me to learn, first hand, many aspects of genetics that such a project provides. Her scientific guidance was invaluable, as it led to many new discoveries that have allowed me to publish great papers, and attend and present at the best scientific meetings. I thank Miriam for her guidance during my graduate career and I will always look to her as a role model.

I would also like to thank all the members of the Meisler lab, both past and present. Everyone has been helpful with their technical advice and their scientific

conversations. I am indebted to Susannah Cheek, Sarah Bergren and Adrienne Grant for their assistance in mouse genotyping, an often thankless job. Julie Jones was amazing in her technical knowledge and helped me improve my experiments every step of the way. I would like to thank Maja Adamska for initially detecting *pale tremor* in our mouse room. This initial observation led to all the experiments described in this thesis. Jennifer Kearney and Viive Howell were extremely helpful with their scientific discussions and career advice. Though they have only been with the lab for a short time, I would like to thank Guy Lenk and Cole Ferguson for showing interest in my project. I leave the Fig4 project in your hands. Lois Weisman and her lab have been instrumental in the success of my thesis. They provided the expertise and technical skills that greatly improved many aspects of each project. I specifically would like to thank Yanling Zhang, Emily Kaufman, Sergey Zolov, and Natsuko Jin for their contributions of crucial data to my thesis. I would also like to thank all the students in Human Genetics and other departments that have supported me. My thesis committee, Sally Camper, David Ginsburg, David Kohrman, and Geoff Murphy, have all been very helpful with their advice and support. I especially thank them for taking the time to speak with me about specific aspects of my project and taking the time to give me career advice. I thank my wife Candace for all the sacrifices she has made to be with me. Her support, love and patience have been invaluable to my success. Finally, the success of my thesis project would not have been possible without the strength I receive from my faith in God.

TABLE OF CONTENTS

LIST OF FIGURES

Figure

LIST OF TABLES

Table

CHAPTER I

INTRODUCTION

Mouse genetics is an important tool for identifying genes involved in human disease and for understanding their biological roles. The mouse is well suited for this purpose because of genetic tools that have been developed, its short life span, and its similar physiology to humans. Forward genetics is an unbiased, phenotype driven method to identify novel disease genes. Forward genetics ensures that the disease gene identified is involved in the phenotype being studied. Reverse genetics is a gene driven approach, whereby mutations are engineered into the mouse to study or confirm the function of the gene of interest. Both forward and reverse genetics are tools that can advance understanding of disease processes.

In this thesis, I have used both forward and reverse genetics to identify genes involved in phosphoinositide metabolism that cause neurodegeneration in mouse and human. Cloning of a spontaneous mouse mutant led to identification of a novel human disease, Charcot-Marie-Tooth disease type 4J (CMT4J). To study CMT4J pathogenesis, a forward genetics approach was undertaken to

produce a mouse model of CMT4J. Further search for mouse mutants with similar phenotypes identified another mutant that affects the same pathway. The work described in this thesis demonstrates the importance of mouse genetics to the study of human neurological disease.

Charcot-Marie-Tooth disease

Charcot-Marie-Tooth disease (CMT) is the most common type of inherited peripheral neuropathy, affecting 1 in 2500 people (Martyn and Hughes, 1997). CMT is a genetically heterogeneous group of disorders that affect the peripheral nerves. CMT is characterized by muscular atrophy and weakness of the distal limbs. This can also be accompanied by distal sensory loss, skeletal deformities and loss of tendon reflexes (Pareyson et al., 2006).

The clinical presentation can be very similar between individuals with mutations in different genes. More than 25 genes are implicated in CMT with diverse functions including, cytoskeletal elements, enzymes, transcription factors, and myelin structural proteins (Niemann et al., 2006). Long distal nerves are first affected because dysfunction of any of these genes results in primary or secondary axonal degeneration that is highly length dependent. The disease can affect either peripheral sensory nerves, motor nerves, or both (Niemann et al., 2006).

CMT is subdivided based on inheritance and disease pattern (Table 1-1). CMT1 is autosomal dominant, primarily causing demyelination (Houlden and Reilly, 2006). CMT2 is autosomal dominant, primarily causing degeneration of axons (Zuchner and Vance, 2006). CMTX is X-linked, comprising up to 10% of CMT. CMTX is associated with mutations in the *GJB1/Cx32* gene (Kleopa and Scherer, 2006). The majority of autosomal recessive forms fall into the CMT4 group. These are primarily demyelinating, though exceptions do exist. CMT4 is rare and generally has an earlier onset and more severe disease than autosomal dominant forms (Dubourg et al., 2006). Each form of CMT is further subdivided by the gene or locus responsible (i.e., CMT1A, CMT1B etc).

Diagnosis is based on inheritance of the disease, as well as electrophysiological measurements of peripheral nerves from the affected patient. Reduction in nerve conduction velocity (NCV) is a hallmark of a primary myelinopathy (CMT1). A reduction of the nerve action potential with no change in the NCV is a sign of a primary axonopathy (CMT2). A study resulting in a mix of both findings is classified as intermediate CMT (Pareyson et al., 2006).

In some forms of CMT, the disease mechanism is straightforward. For example, CMT1A is caused by duplications of (Lupski et al., 1991; Raeymaekers et al., 1991) or point mutations (Valentijn et al., 1992) in the *PMP22* gene. PMP22 is a glycoprotein that is primarily expressed in myelinating Schwann cells. It is a highly abundant protein, comprising a total of 2-5% of all PNS myelin

protein. PMP22 is critically important for the formation and maintenance of compact myelin (Naef and Suter, 1998; Snipes et al., 1992). Thus, it is not surprising that mutations in PMP22 cause demyelinating CMT. However, for the majority of CMT subtypes, the pathophysiology is not as obvious.

Genes involved in CMT can span the range of cellular functions. Indeed, many CMT genes are ubiquitous “housekeeping” genes (Niemann et al., 2006). This poses a unique challenge to identifying the mechanism of disease, as CMT mainly affects peripheral nerves. How dysfunction in ubiquitously expressed genes result in only a peripheral neuropathy and not a multi-organ disorder is a persistent question. Both peripheral sensory neurons and spinal motor neurons have very long axons, up to one meter in some instances. It has been proposed that the increased amount of trafficking required to maintain long axons may make these neurons highly sensitive to perturbations in ubiquitous, basic cellular pathways (Niemann et al., 2006). Understanding this sensitivity will shed light on disease mechanism as well as basic peripheral nerve biology.

Phosphoinositides

The phosphoinositide pathway provides one such challenge. Phosphoinositides are a family of low abundance, signaling phospholipids that are generated from the phosphatidylinositol precursor. Phosphatidylinositol is made up of two fatty acids and an inositol ring esterified to phosphatidic acid (Figure 1-1). Phosphatidylinositol can be phosphorylated at the D3, D4, and D5

position of the inositol ring, resulting in seven naturally occurring phosphoinositides (Figure 1-2). Phosphoinositides regulate a host of basic cellular functions including membrane and vesicle trafficking, cytoskeleton rearrangements, apoptosis, cell motility, and synaptic function (Di Paolo and De Camilli, 2006).

Phosphoinositides are localized in specific functional pools throughout the membrane system of the cell and are synthesized on the cytosolic face of membranes. Phosphoinositide signaling occurs via recruitment of specific effector proteins. These proteins often contain one or more binding domains that recognize a phosphoinositide. Phosphoinositide binding domains include PH, ENTH/ANTH, FYVE, PX, Tubby and lysine/arginine-rich patches (Lemmon, 2003). Some domains have very strong affinity to one phosphoinositide, whereas other domains bind several different phosphoinositides dependent on the context of the interaction. Binding of phosphoinositides not only localizes the proteins, but can also induce conformational and enzymatic changes (Di Paolo and De Camilli, 2006).

Tight regulation of phosphoinositides is essential to proper signaling throughout the cell. Phosphatases and kinases work in concert to interconvert and turnover the phosphate tags (Figure 1-2). For example, PI(3)P is the predominant tag on early endosomes. As the endosome progresses to late

endosome and lysosome, PI(3)P is converted to PI(3,5)P2 and becomes the predominant lipid signal (Figure 1-3) (Michell et al., 2006).

CMT and phosphoinositides

The cells involved in CMT, neurons and Schwann cells, are specialized in function. Neurons with long axons, mainly innervating the distal portions of the body, are unique in several ways. Neurons are post-mitotic and are sensitive to many insults because they are not replaced. Neurons with long axons also have special challenges to maintain these complex structures. Both retrograde and anterograde vesicle trafficking must be functional. Anterograde trafficking allows transport of new membrane elements, proteins and neurotransmitters from the soma through the axon to the synapse. Retrograde trafficking allows signaling proteins as well as cellular elements marked for recycling to be delivered to the soma for processing.

Schwann cells also face unique challenges to proper function. Schwann cells are the myelinating cells of the peripheral nervous system. One Schwann cell myelinates multiple axons. These cells produce large amounts of lipids and proteins to form and maintain the multi-laminar myelin sheaths on each axon. Cellular vesicle trafficking is critically important for transport of myelin proteins and lipids.

CMT subtypes differentially affect neurons and Schwann cells. CMT1 primarily affects Schwann cells and CMT2 primarily affects neuronal axons. However, neurons and Schwann cells do not function independently (Figure 1-4). Each must maintain its own integrity, but signaling is required between both cell types for either to function properly (Berti et al., 2006). It is still unclear how exactly each cell type contributes to disease.

Phosphoinositides are intimately involved in vesicle trafficking and cytoskeletal rearrangements, processes that are essential to the proper function of neurons and Schwann cells. Dysfunction in ubiquitous phosphoinositide signaling genes have been implicated in several forms of CMT, including CMT4B1, CMT4B2, CMT4H, CMTDIB (Suter, 2007), and in work described in this thesis, CMT4J (Table 1-2).

CMT4B1 and CMT4B2 are clinically indistinguishable severe, early onset demyelinating peripheral neuropathies. Both diseases are characterized by myelin outfoldings, abnormal myelin formations, and loss of myelinated axons. CMT4B1 and CMT4B2 are caused by mutations in *MTMR2* (myotubularin-related protein 2) and *MTMR13*, respectively (Previtali et al., 2007). MTMR2 and MTMR13 belong to a large family of proteins related to myotubularin. MTMR2 is a phosphoinositide phosphatase that dephosphorylates PI(3)P and PI(3,5)P2 at the D3 position (Bolis et al., 2007). The majority of CMT4B1 mutations result in loss of phosphatase activity (Previtali et al., 2007). MTMR13 is a

pseudophosphatase with an inactive phosphatase domain. MTMR13 forms a tetrameric complex with MTMR2 to increase the phosphatase activity of MTMR2 (Berger et al., 2006).

CMT4H is a recessive demyelinating neuropathy characterized by myelin outfoldings. Mutations in *Frabin/FGD4* are implicated in CMT4H (Delague et al., 2007; Stendel et al., 2007b). Frabin is a guanine-exchange factor (GEF) for the RhoGTPase Cdc42 (Umikawa et al., 1999). Frabin contains a FYVE domain and two PH domains. Both motifs are known phosphoinositide binding domains (Lemmon, 2003). While MTMR2 and MTMR13 function to metabolize phosphoinositides, Frabin function requires the presence of phosphoinositide tags, suggesting the potential interplay between enzymes and effectors.

CMTDIB is an autosomal dominant peripheral neuropathy, affecting both axons and Schwann cells. Mutations in Dynamin 2 (*DNM2*) cause CMTDIB (Zuchner et al., 2005). DNM2 also contains a PH domain. Interestingly, all the CMTDIB mutations are clustered in the PH domain (McNiven, 2005; Zuchner et al., 2005), suggesting that disease is a direct effect of loss of interaction with phosphoinositides.

Phosphoinositide-related CMT mouse models

It is counterintuitive that changes in phosphoinositide signaling cause only a peripheral neuropathy and not a systemic disease. On the one hand,

phosphoinositides are essential for all the processes described above. Thus, it would be expected that neurons or Schwann cells would be compromised if the phosphoinositide pathways were abnormal. On the other hand, phosphoinositides are essential to many basic cellular processes. Perturbations of the phosphoinositide pathway would be expected to be incompatible with life due to their potential global effects.

To better understand the exact pathophysiology of phosphoinositide dysfunction and CMT, it is important to study mouse models of these diseases. Mouse models are invaluable tools for disease research. In order to fully understand the disease mechanism and develop viable therapies, the mouse model should closely mimic the human disease. Technological advancements have allowed the mouse to become even more powerful. Temporal conditional alleles allow the investigator to overcome biological difficulties such as embryonic lethality. Spatial conditional alleles allow the investigator to answer questions involving cell autonomy as well as isolating an organ specific disease process.

To date, only mouse models of CMT4B1 and CMT4B2 have been reported. To model CMT4B1, two separate groups produced loss-of-function *Mtmr2* mouse models. The first mouse reported was a floxed allele of *Mtmr2* (Bolino et al., 2004). Exon 4 was flanked by LoxP sites. Floxed alleles allow for conditional deletion of the gene when crossed with a mouse carrying a CRE-recombinase under the control of a temporal or spatial specific promoter. The

floxed allele of *Mtmr2* was crossed with a ubiquitous expressing Cre line. This resulted in loss of Mtmr2 protein (Bolino et al., 2004).

Mtmr2 null mice were viable and healthy, with no major neurological disease. A minor gait abnormality was noted at 6 months of age. Accompanying this was mildly reduced nerve conduction velocity and prolonged f-wave latencies, indications of sciatic nerve dysfunction. These findings are consistent with peripheral neuropathy. Little visible phenotype was observed before six months of age. *Mtmr2* null mice showed progressive changes in the myelin of peripheral nerves. Myelin outfoldings were observed and the complexity of myelin structures increased with age. Myelin outfoldings occurred prominently at the paranodal regions. Both motor and sensory nerves were affected (Bolino et al., 2004). Overall, the dysmyelinating phenotype of the *Mtmr2* null mice resembled CMT4B1.

A second *Mtmr2* mouse model was also developed. The nonsense mutation, E276X was knocked into the *Mtmr2* locus (Bonneick et al., 2005). E276X was previously identified in a CMT4B1 family (Bolino et al., 2000). While it was unclear whether the E276X protein was expressed in the mice (Bonneick et al., 2005), the putative truncated protein was shown to be nonfunctional and could not dephosphorylate PI(3)P and PI(3,5)P2, *in vitro* (Berger et al., 2002). Overall the pathology in the E276X mouse was similar to the *Mtmr2* null mouse.

However, the E276X mouse showed no electrophysiological abnormalities up to 16 months of age (Bonneick et al., 2005).

It is important to note that *Mtmr2* mouse models are not as severely affected as CMT4B1 patients. CMT4B1 is a clinically homogenous, severe, childhood onset disease. *Mtmr2* mutant mice are marginally affected late in life and disease is best detected with careful histopathology. It remains to be seen whether aged mice will show a more profound phenotype.

While myelin outfoldings are a primary pathology in *Mtmr2* mutant mice and CMT4B1 patients, it is unclear whether dysfunction resides in the axon, the Schwann cell, or both. *Mtmr2* is expressed in both neurons and Schwann cells. Myelin is produced by Schwann cells, but myelination requires communication between the axon and the Schwann cell. To address this question, Bolis and colleagues (2005) made conditional *Mtmr2* mutant mice. The previously described floxed allele of *Mtmr2* (Bolino et al., 2004) was deleted by a motor neuron specific Cre and a Schwann cell specific Cre. This created mice with motor neurons that lacked *Mtmr2* and mice with Schwann cells that lacked *Mtmr2*. Mice lacking *Mtmr2* in the motor neurons showed no signs of disease (Bolis et al., 2005). There was no myelin pathology or functional evidence of any peripheral neuropathy. However, conditional deletion of *Mtmr2* in Schwann cells completely recapitulated the peripheral neuropathy observed in complete *Mtmr2*

null mice. This data indicates that CMT4B1 pathology is a Schwann cell autonomous disease (Bolis et al., 2005).

The role of Schwann cells is also demonstrated by the interaction between Mtmr2 and Dlg1, a scaffolding protein which links transmembrane proteins with the cytoskeleton. In Schwann cells, Dlg1 is located at the paranodal junctions, where myelin outfoldings are often found (Bolino et al., 2004; Bolis et al., 2005). It remains to be seen what function Mtmr2 plays in neurons and if there are compensatory myotubularin-related proteins in neurons, but not Schwann cells.

Two *Mtmr13* deficient mice have also been reported (Robinson et al., 2008; Tersar et al., 2007). Not surprisingly, *Mtmr13* mutant mice are similar to *Mtmr2* mutant mice. Both *Mtmr13* mouse models were generated from gene-trap ES cell lines and were completely null. Both models showed myelin outfoldings at the paranodes as well as other abnormal myelin structures. Beginning at 6 months, the myelin abnormalities progressively increased with age. Accompanying this pathology was also slowed nerve conduction velocity in both models, though one was more severe than the other (Robinson et al., 2008; Tersar et al., 2007). One model demonstrated no functional deficits until 12 months of age (Tersar et al., 2007).

Mtmr13 mice are also much less severely affected than CMT4B2 patients. *Mtmr2* and *Mtmr13* double mutant mice were generated (Tersar et al., 2007).

The double mutant mice appeared to be no different from either single mutant mouse, consistent with a required Mtmr2 and Mtmr13 interaction.

Mtmr2 and *Mtmr13* mutant mice do not completely mimic CMT4B1 and CMT4B2. While they do recapitulate key features such as myelin outfoldings, both mouse mutants are much less severe than the human diseases. There are several reasons that can account for this. First, the myotubularin gene family includes myotubularin and 13 related genes (Bolis et al., 2007). Another myotubularin-related protein could be compensating for the loss of *Mtmr2* and *Mtmr13* in mouse, but not in human. Second, the smaller size of the mouse may make the mouse peripheral nervous system less sensitive to perturbations. Because mice are smaller, axons extend a shorter distance and vesicle trafficking may be an easier task. With shorter axons, Schwann cells produce much less myelin.

Despite differences, these mouse models are valuable tools. They have established the Schwann cell autonomous nature of CMT4B1. This finding will help direct therapeutic interventions by focusing research on dysfunction of Schwann cells, rather than neurons. These mouse models shed light on the molecular mechanism of disease when *Mtmr2* and *Mtmr13* are lost. Levels of phosphoinositides have not been measured in these mice. Further research is needed to identify which phosphoinositides are dysregulated due to mutations in

Mtmr2 and *Mtmr13*. It is unknown if different phosphoinositides are dysregulated in neurons versus Schwann cells that cause a Schwann cell specific disease.

To date, no mouse models of CMT4H (*Frabin/FGD4*) or CMTDIB (*DNM2*) have been reported. It will be only a matter of time before these mice will be developed. Mouse models of phosphoinositide-related CMT disease will continue to be a rich resource for the peripheral nerve community and will contribute to understanding of phosphoinositide function in the peripheral nerve.

The data presented in this thesis demonstrates the importance of PI(3,5)P2 to health and disease. Both reverse and forward mouse genetics were crucial in demonstrating this. As known genes involved in phosphoinositide pathways are identified in disease, reverse genetics will provide a pathway to molecular understanding. Forward genetics will identify new disease genes and new human diseases. Mouse genetics remains a very powerful tool for human disease research.

Table 1-1. CMT subtypes and genetic loci that account for ~85% of CMT

type	inheritance	major feature(s)	genes/loci identified
CMT1	AD	Demyelinating Most common subtype	6
CMT2	AD	Axonopathy	11
	AR	Axonopathy Very rare	3
DI CMT*	AD	Demyelinating and axonopathy	3
CMT4	AR	Demyelinating Early onset, severe	11
CMTX	X-linked	Demyelinating and axonopathy	5**
dHMN#	AR, AD, and X-linked	Neuronopathy/axonopathy Motor neurons only	13

*dominant intermediate CMT

**Mutations in Cx32/GJB1 are the overwhelming majority with >220 mutations to date. The four other loci are from one or two extended pedigrees.

#distal hereditary motor neuropathy

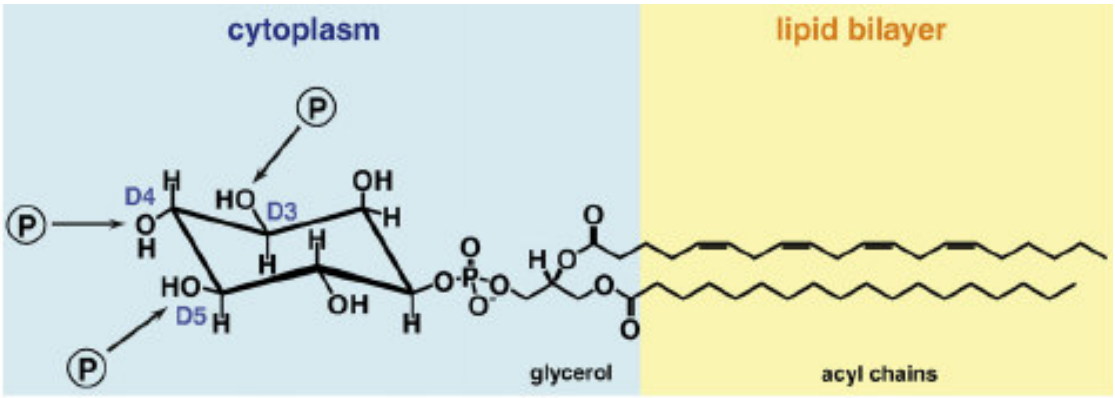

Figure 1-1. The structure of a phosphoinositide molecule. The acyl fatty acid chain is inserted into the lipid bilayer and the inositol head group is exposed to the cytoplasm. Positions D3, D4, and D5 can be phosphorylated in different combinations. Modified from (Strahl and Thorner, 2007)

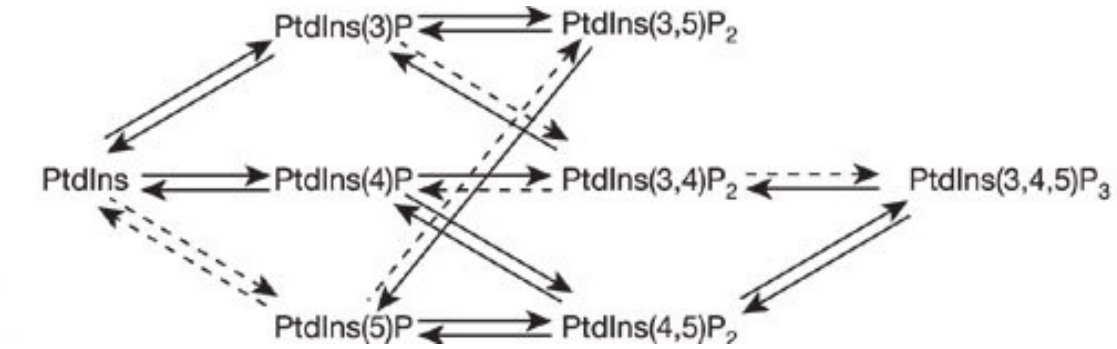

Figure 1-2. Interconversion of phosphoinositides. Seven different phosphoinositides can be produced. Solid arrows indicate proven *in vivo* reactions. Dotted arrows indicate established *in vitro* reactions. PtdIns, phosphoinositide. Modified from (Di Paolo and De Camilli, 2006).

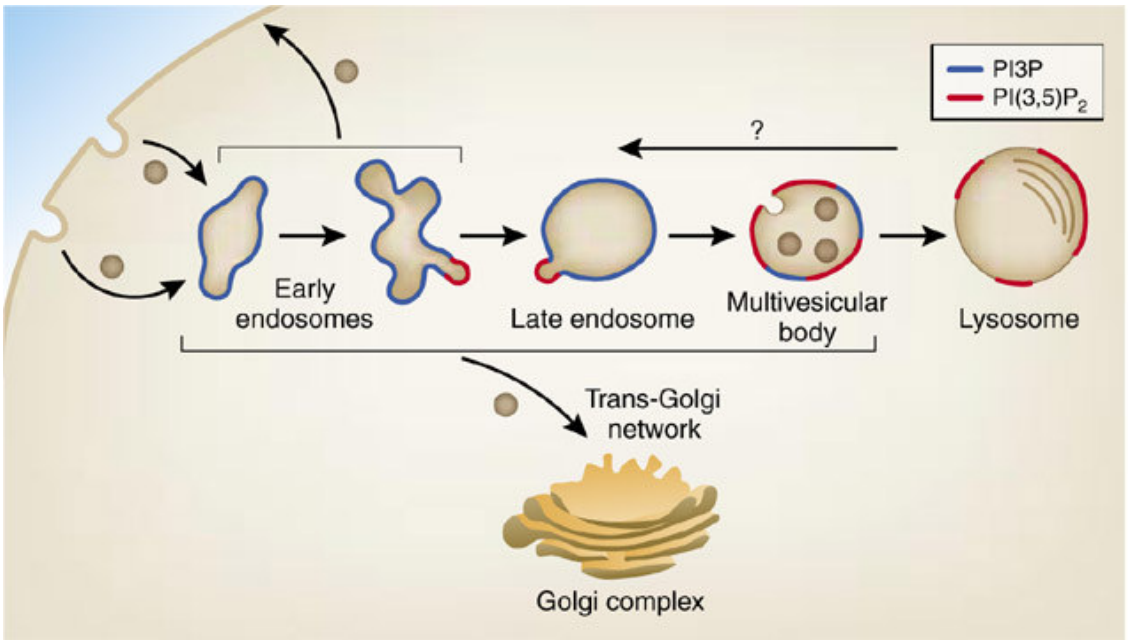

Figure 1-3. PI3P and PI(3,5)P2 label endosomes and lysosomes. PI3P labels endosomes. As endosomes progress to late endosomes, mutivesicular bodies, and lysosomes, PI3P is increasingly converted to PI(3,5)P2. PI(3,5)P2 is the predominant tag on late endosomes and lysosomes. Adapted from (Volpicelli-Daley and De Camilli, 2007)

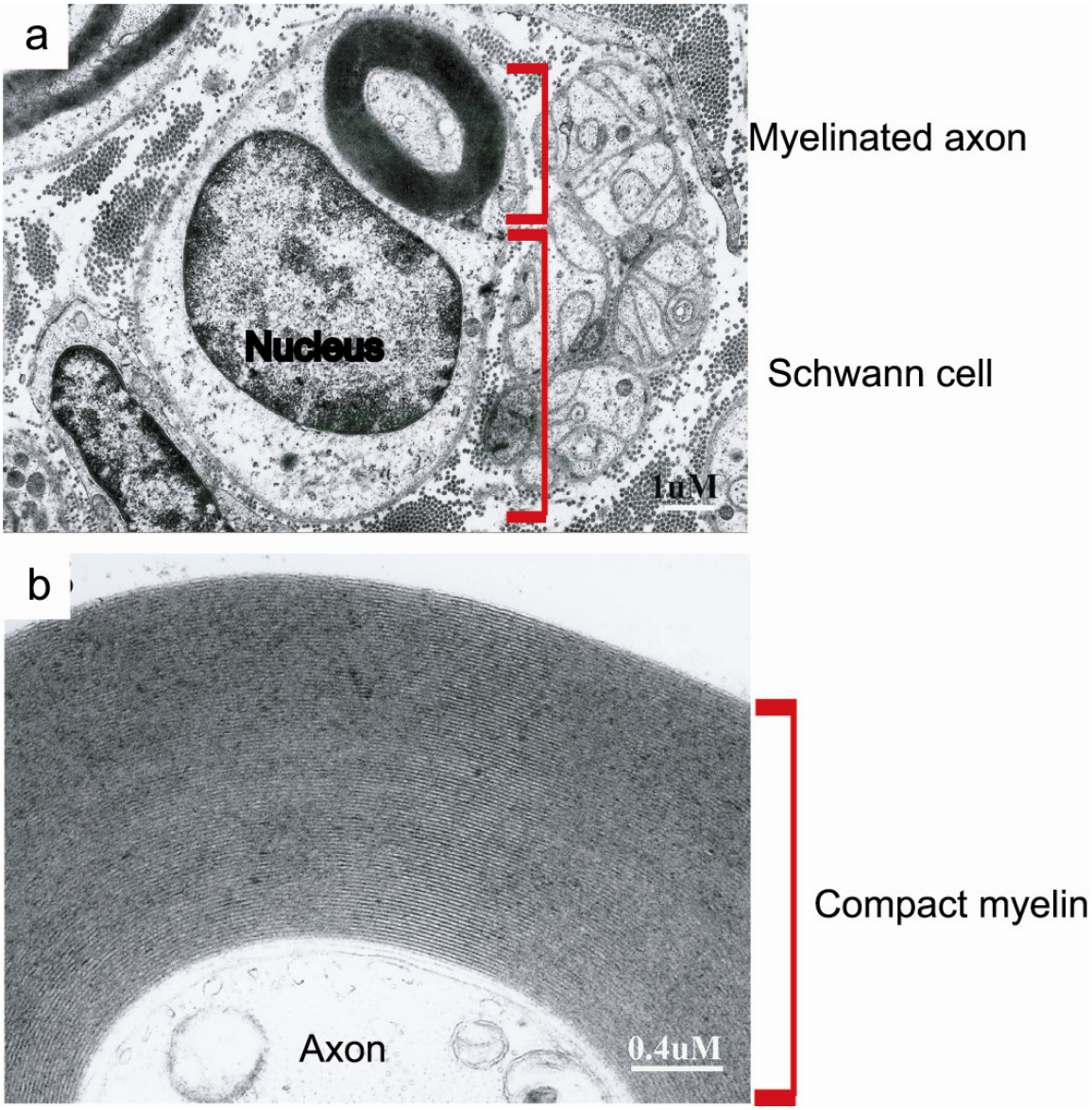

Figure 1-4. Schwann cells and axons. **a.** A single Schwann cell axon unit. The Schwann cell ensheathes the axon in a thick layer of compact myelin. **b.** High resolution image of the compact myelin surrounding an axon. Modified from (Li et al., 2005a).

Table 1-2. CMT subtypes with mutations in phosphoinositide-related genes

disease	gene mutated	phosphoinositide function
CMT4B1	*MTMR2*	PI3P and PI(3,5)P2 3-phosphatase
CMT4B2	*MTMR13*	Enhances function of MTMR2
CMT4H	*Frabin/FGD4*	Binds phosphoinositides via FYVE and PH domains
CMT4J	*FIG4*	PI(3,5)P2 5-phosphatase
CMTDIB	*DNM2*	Binds phosphoinositides via PH domain

CHAPTER II

MUTATION OF *FIG4* CAUSES NEURODEGENERATION IN THE *PALE TREMOR* MOUSE AND PATIENTS WITH CMT4J*

Abstract

Membrane-bound phosphoinositides are signaling molecules that play a key role in vesicle trafficking in eukaryotic cells (Di Paolo and De Camilli, 2006). Proteins that bind specific phosphoinositides mediate interactions between membrane-bounded compartments whose identity is partially encoded by cytoplasmic phospholipid tags. Little is known about the localization and regulation of mammalian PI(3,5)P2, a quantitatively minor phosphoinositide that regulates membrane trafficking in the endosome-lysosome axis in yeast (Michell et al., 2006). We describe a multi-organ disorder with neuronal degeneration in the CNS, peripheral neuronopathy, and diluted pigmentation, in the *pale tremor* mouse. Positional cloning identified an Etn2β retrotransposon insertion in intron 18 of *Fig4*, the homolog of a yeast SAC-domain PI(3,5)P2 5-phosphatase located in the vacuolar membrane. The abnormal concentration of PI(3,5)P2 in cultured fibroblasts from *pale tremor* mice demonstrates conserved biochemical function of mammalian FIG4. The cytoplasm of affected cells is filled with large LAMP2-immunoreactive vacuoles, consistent with dysfunction of the late endosome-

lysosome. Neonatal neurodegeneration in sensory and autonomic ganglia is followed by loss of neurons from layers 4 and 5 of the cortex, deep cerebellar nuclei, and other localized brain regions. Sciatic nerve exhibits reduced numbers of large diameter myelinated axons, slowed nerve conduction velocity, and reduced amplitude of compound muscle action potentials. We identified pathogenic mutations of human *FIG4* (KIAA0274) on chromosome 6q21 in four unrelated patients with hereditary motor and sensory neuropathy. This novel form of autosomal recessive Charcot-Marie-Tooth disorder is designated CMT4J.

Results and Discussion

Mutant mice with severe tremor, abnormal gait, and diluted pigmentation were identified in our mouse colony on a mixed inbred strain background. One breeding pair generated 8/30 affected progeny, consistent with inheritance of an autosomal recessive mutation designated *pale tremor* (*plt*). At postnatal day 3 (P3), affected homozygotes have diluted pigmentation and reduced size (Figure 2-1a). Intentional tremor develops during week 2, and abnormal limb postures are evident by week 3 (Figure 2-1b). The impaired motor coordination, muscle weakness, and "swimming" gait of *plt* mice are demonstrated in the Supplementary video (http://www.nature.com/nature/journal/v448/n7149/suppinfo/nature05876.html). There is progressive loss of mobility, reduction in body weight and juvenile lethality (Figure 2-1c).

To genetically map *plt*, a cross was carried out with strain CAST/Ei. The recovery of affected F2 offspring was 9% (50/532), indicative of prenatal loss on this genetic background. We genotyped 532 F2 animals with microsatellite and SNP markers to map *plt* to a 2 Mb interval of mouse chromosome 10 between D10Umi13 and D10Mit184 (Figure 2-1d). There are 21 annotated genes in the nonrecombinant interval (www.ensembl.org; mouse build 35) and these were tested as candidates by sequencing RT-PCR products from brain RNA. The *plt* transcript of A530089I17Rik lacks exons 19 through 23 from the 3' end of the gene (Figure 2-2a). Hybridization of a polyA$^+$ Northern blot with a cDNA probe containing exons 8 to 15 identified a wildtype transcript of 3.3 kb that is not present in *plt* RNA (Figure 2-2c). No abnormal transcripts were detected in the mutant, even when the exposure time was increased from 3 hrs to 63 hrs (not shown). We were able to amplify exons 19-23 from genomic DNA, eliminating the possibility of a genomic deletion (Figure 2-2b).

To identify the genomic mutation, we examined the structure of intron 18 by PCR. A wildtype product of 0.65 kb and a mutant product of 6.2 kb were amplified from the 3' end of intron 18 (Figure 2-2d). The sequence of the mutant product (GenBank DQ813648) contains a 5,547 bp insert with 99% sequence identity to mouse retrotransposon Etn2β (GenBank Y17106). The transposon is inserted 384 bp upstream of exon 19, in the same orientation as the gene, and flanked by a duplication of the hexanucleotide CCCCTG (Figure 2-2g), characteristic of Etn2β insertions (Maksakova et al., 2006). The mutant allele

can be detected by PCR with a primer in the LTR (Figure 2-2e). Since the background strains do not contain the Etn2β element (data not shown), the *plt* mutation appears to be a result of transposon insertion. The data are consistent with abnormal splicing from exon 18 of *FIG4* to one of the cryptic splice acceptor sites in the Etn2β element (Maksakova et al., 2006), generating a transcript of very low abundance that is detected by RT-PCR but is below the sensitivity of the polyA+ Northern blot.

RT-PCR of tissues from wildtype mice demonstrated widespread expression (Figure 2-2f), consistent with public EST and microarray databases. *In situ* hybridization data demonstrates distribution of the transcript throughout the brain (www.brainatlas.org/aba/ and unpublished). The human ortholog, KIAA0274, is located on human chromosome 6q21. The mutated protein is most closely related to the yeast SAC-domain phosphatase Fig4, with overall amino acid sequence identity of 35% and similarity of 66%. The SAC domain with the active site motif $CX_5R(S/T)$ is characteristic of phosphatases with specificity for phosphoprotein or phospholipid substrates (Hughes et al., 2000) and exhibits 44% sequence identity (191/435 aa) (Figure 2-3a). The four other mammalian genes with SAC domains (synaptojanin 1, synaptojanin 2, INPP5F and SAC1) differ from Fig4 at other domains (Hughes et al., 2000), indicating that mouse A530089I17Rik and human KIAA0274 are homologs of yeast Fig4.

Yeast Fig4p is localized to the vacuolar membrane and is required for both

generation and turnover of PI(3,5)P2 (Duex et al., 2006b). Fig4p exhibits lipid phosphatase activity towards the 5-phosphate residue of PI(3,5)P2 (Rudge et al., 2004), and also appears to activate the Fab1/PIKfyve kinase that synthesizes PI(3,5)P2 from PI3P, possibly by dephosphorylating the kinase or one of its regulators (Duex et al., 2006b). As a result, deletion of yeast Fig4 reduces rather than increases the intracellular concentration of PI(3,5)P2 (Duex et al., 2006a), leading to defects in vacuole fission, formation of enlarged vacuoles, and impaired retrograde traffic to the late endosome (Bonangelino et al., 2002; Gary et al., 2002; Michell et al., 2006). Knock-down of mammalian Fab1/PIKfyve kinase causes a similar defect in retrograde endosome traffic and enlarged vacuoles (Rutherford et al., 2006).

Analysis of phosphoinositides from cultured fibroblasts of *plt* mice demonstrated a three-fold reduction in PI(3,5)P2 ($p=0.04$), with no change in 3 other phosphoinositides (Figure 2-3b). Enlarged cytoplasmic vacuoles accumulate in 40% of cultured fibroblasts from plt mice (174/435) compared with 5% of wildtype cells (22/403) (Figure 2-3c). These vacuoles stain positively for the lysosomal membrane protein LAMP2 (Figure 2-3d), indicating that they represent late-stage endosomes. The altered levels of PI(3,5)P2 demonstrate a conserved enzymatic function of FIG4 from yeast to mammals, while the enlarged vacuoles demonstrate a conserved cellular role in regulation of the size of late endosomes.

In vivo loss of FIG4 results in a striking pattern of selective neurodegeneration. Extensive loss of neurons from sensory and autonomic ganglia is evident during the neonatal period (Figure 2-4a-d). The presence of neurons with enlarged cytoplasmic vacuoles suggests that vacuole accumulation may precede cell loss (Figure 2-4 inserts). Spinal motor neurons exhibit normal morphology at 3 weeks (Figure 2-4e-f) but contain vacuoles at 6 weeks of age (Figure 2-4g-h).

Peripheral nerves are also affected. Cross-sections of sciatic nerve reveal substantial reduction in the number of large diameter myelinated axons in the mutant (Figure 2-5a-b). Nerve conduction velocity and amplitude of compound muscle action potentials are reduced (Figure 2-5c-d), consistent with the axonal loss visible in the semithin sections of the sciatic nerve and the pathological abnormalities in the motor neurons. There was no response when recording from tail sensory fibers, consistent with the severe loss of sensory neurons from the DRG.

In the brain, neuronal loss in the thalamus, pons, medulla and deep cerebellar nuclei is visible at 1 week of age (not shown). By 3 weeks of age there is additional loss of neurons from cortical layers 4 and 5, the deep layers of the superior and inferior colliculus and the olfactory bulb (Figure 2-6a). Some neuronal cell bodies contain enlarged vacuoles (Figure 2-6b); these vacuoles are not stained by Oil Red O (for lipid) or PAS (for carbohydrate) (not shown).

Hippocampus, cerebellar cortex, and cerebral cortex layers 1, 2, 3 and 6 remain relatively unaffected throughout the course of the disease, although under culture conditions hippocampal neurons become vacuolated (not shown). The abnormal gait and motor coordination in the *plt* mutant may be accounted for by abnormal proprioception due to degeneration of DRG neurons, in combination with degeneration of neurons from brain regions directly involved in motor control (layer 5 of the cortex, thalamus and deep cerebellar nuclei).

Abnormalities are visible in skin and spleen. Pigment-containing hair follicles are greatly reduced in number and the few pigmented hairs contain clumped melanosomes (Figure 2-7a-d), similar to mouse mutants with defects in lysosome-melanosome biogenesis (Marks and Seabra, 2001). There is extensive cell loss in the spleen (Figure 2-7e-f). White blood cell profiles are normal, and liver, kidney, and testis appear normal by light microscopy.

The clinical and pathological features of peripheral neuropathy in *pale tremor* mice resemble some types of Charcot-Marie-Tooth disease (Schroder, 2006; Szigeti et al., 2006). We tested FIG4 as a candidate gene by screening 95 individuals diagnosed with CMT but lacking mutations in known genes (Szigeti et al., 2006). The 23 coding exons of FIG4 were amplified from genomic DNA, screened by heteroduplex analysis and sequenced. Patient BAB 1079 has a severe, early onset disorder. We identified the protein truncation mutation F98fsX102 in exon 4 and the missense mutation I41T in exon 2 of *FIG4* (Figure

2-8a). F98fsX102 truncates the protein within the SAC domain and is likely to be a loss of function allele. Pedigree analysis demonstrated autosomal recessive inheritance. Each mutation was inherited from a heterozygous parent (Figure 2-8b). Two heterozygous carriers of F98fsX102 are unaffected, indicating that *FIG4* is not haploinsufficient. Heterozygous *plt/+* mice aged to 18 months are also unaffected.

Patient BAB1372 was also found to be a compound heterozygote with a nonsense mutation R183X in exon 6 together with I41T (Figure 2-8a). R183X was inherited from the patients' father (Figure 2-8b). The mother is an obligate carrier of I41T, and the affected sibling inherited both mutations (Figure 2-8b). The siblings have severe disease: BAB1372 is functionally quadriplegic and BAB1373 is wheelchair-bound while retaining normal use of his arms. Both have slow nerve conduction velocities. A sural nerve biopsy for BAB1373 demonstrated profound axonal loss, thinly myelinated nerve fibers, and evidence of de- and remyelination.

Two additional patients, BAB1161 and BAB1369, carry unique truncation mutations together with I41T (Figure 2-8a). Both patients developed disease by 5 years of age and demonstrate reduced nerve conduction velocity (2 to 7 m/s, compared with normal values of 40-50 m/s). One patient had motor developmental delay consistent with Dejerine-Sottas neuropathy.

It is remarkable that four unrelated Caucasian patients carry the same missense mutation. No additional coding or splice site variants were detected in these patients when all 23 exons of FIG4 were sequenced. Isoleucine 41 is located upstream of the SAC phosphatase domain and is evolutionarily invariant in FIG4 from yeast, invertebrates and vertebrates (Figure 2-8c-d). We did not identify carriers of this variant by sequencing exon 2 from 295 neurologically normal Caucasian controls The observed allele frequencies were 0/590 in controls and 4/190 in CMT patients (p=0.003). The four patients carry I41T on the same 15 kb haplotype, defined by SNPs rs3799845 (G), rs2025249 (C) and rs7764711 (G) (haplotype frequency 0.29), consistent with inheritance of a common ancestral mutant allele (Figure 2-9). The evidence suggests that I41T is a partial loss of function allele with population frequency below 0.005 that is pathogenic only in combination with a null allele of FIG4.

To assess the functional effect of the I41T allele, we tested the corresponding mutation (I59T) in yeast. Wildtype and mutant cDNAs were transformed into Fig4 null yeast strain lacking functional Fig4 (Duex et al., 2006a). Transformation with vector only did not correct the enlarged vacuoles in Fig4 null cells which reflect the slightly reduced levels of PI(3,5)P2 that result from the absence of Fig4 (Duex et al., 2006a) (Figure 2-10a). Vacuolar enlargement was corrected to a comparable extent by WT and mutant Fig4, indicating that under basal conditions cells expressing $Fig4^{I59T}$ produce normal levels of PI(3,5)P2 (Figure 2-10a). The ability of the mutant to activate

Fab4/PIKfyve kinase was tested by treatment with hyperosmotic shock as previously described (Duex et al., 2006a; Duex et al., 2006b). In cells expressing wildtype Fig4, hyperosmotic shock produces a transient 10-fold increase in intracellular PI(3,5)P2 concentration due to activation of Fab1/PIKfyve kinase (Figure 2-10b). In cells expressing the mutant, a partial increase of 4-fold was observed, demonstrating impaired activation of Fab1/PIKfyve kinase. It is not clear whether the phosphatase activity of the mutant is also impaired, due to the low levels of PI(3,5)P2.

The data presented here demonstrate that mutation of FIG4 is responsible for peripheral neuronopathy in human patients. We propose the designation CMT4J for this disorder, based on the recessive inheritance pattern. Phosphoinositide signaling has previously been implicated in Charcot Marie Tooth type 4B1, 4B2 and 4H (Begley et al., 2006; Bolino et al., 2004; Bolino et al., 2000; Bonneick et al., 2005; Senderek et al., 2003; Stendel et al., 2007a). Other genes that function in vesicle trafficking, such as Rab7 and dynamin 2 in human (Verhoeven et al., 2003; Zuchner et al., 2005) and Vps54 in mouse (Schmitt-John et al., 2005), are associated with inherited neuropathies.

The *plt* mutant provides the first evidence regarding the functional role of mammalian *Fig4*. The results demonstrate a conserved biochemical function in metabolism of PI(3,5)P2, a conserved cellular role in regulation of endosomal vesicles, and an unexpected role in neuronal survival. The molecular basis for

the differential sensitivity of neuronal subtypes to loss of this widely expressed gene is unclear. The key role of PI(3,5)P2 in differential neuronal sensitivity is supported by the observation of a very similar pattern of neuronal loss in a mouse mutant of Vac14 (Zhang et al., 2007). Vac14 is the homolog of a yeast protein that complexes with and activates Fig4p (Duex et al., 2006a). Mammalian Vac14 is located in synaptic microsomal membrane fractions and interacts with neuronal nitric oxide synthase (Lemaire and McPherson, 2006). Neuronal dependence on FIG4 may be related to the role of endosomal vesicles in delivering membrane components to dendritic spines during long-term potentiation (Park et al., 2006). The *pale tremor* mouse will be useful for investigation of PI(3,5)P2 signaling in neurons and as a model for CMT and related human neuropathies.

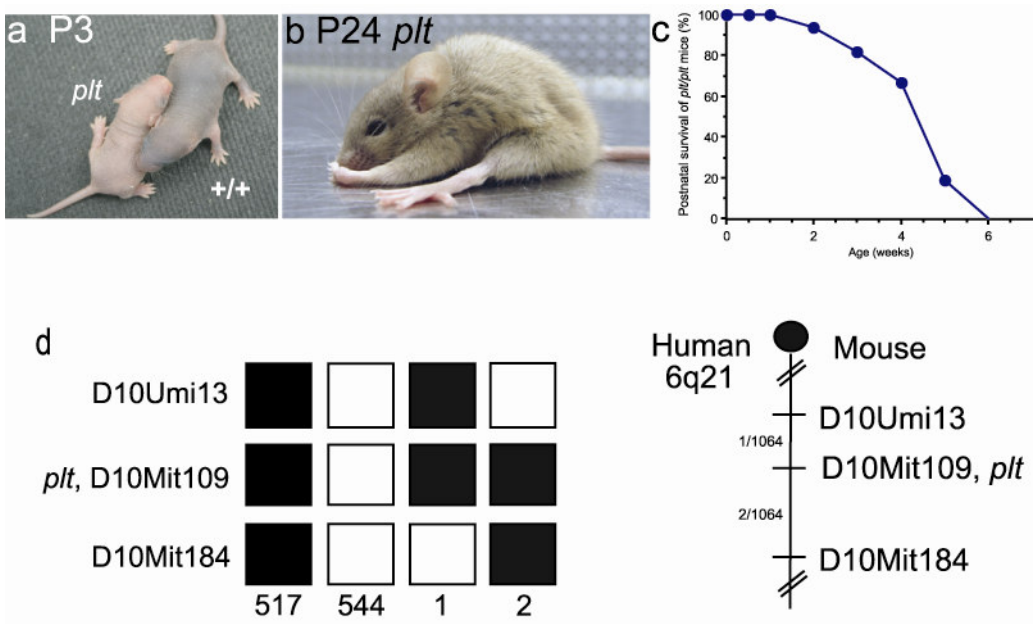

Figure 2-1. Phenotypes and genetic mapping of *pale tremor* mice. **a**. Diluted pigmentation at postnatal day 3 (P3). **b.** Abnormal limb postures at P24. **c.** Juvenile lethality of F2 mice from the CAST/Ei cross (n= 50). **d.** Genetic mapping of *plt* on mouse chromosome 10. The haplotypes of 3 recombinant chromosomes and 1,061 nonrecombinant chromosomes are indicated; solid symbols represent alleles from inbred strains; open symbols represent CAST alleles. The 2 Mb nonrecombinant interval of mouse chromosome 10 between D10Umi13 and D10Mit184 is shown at the right.

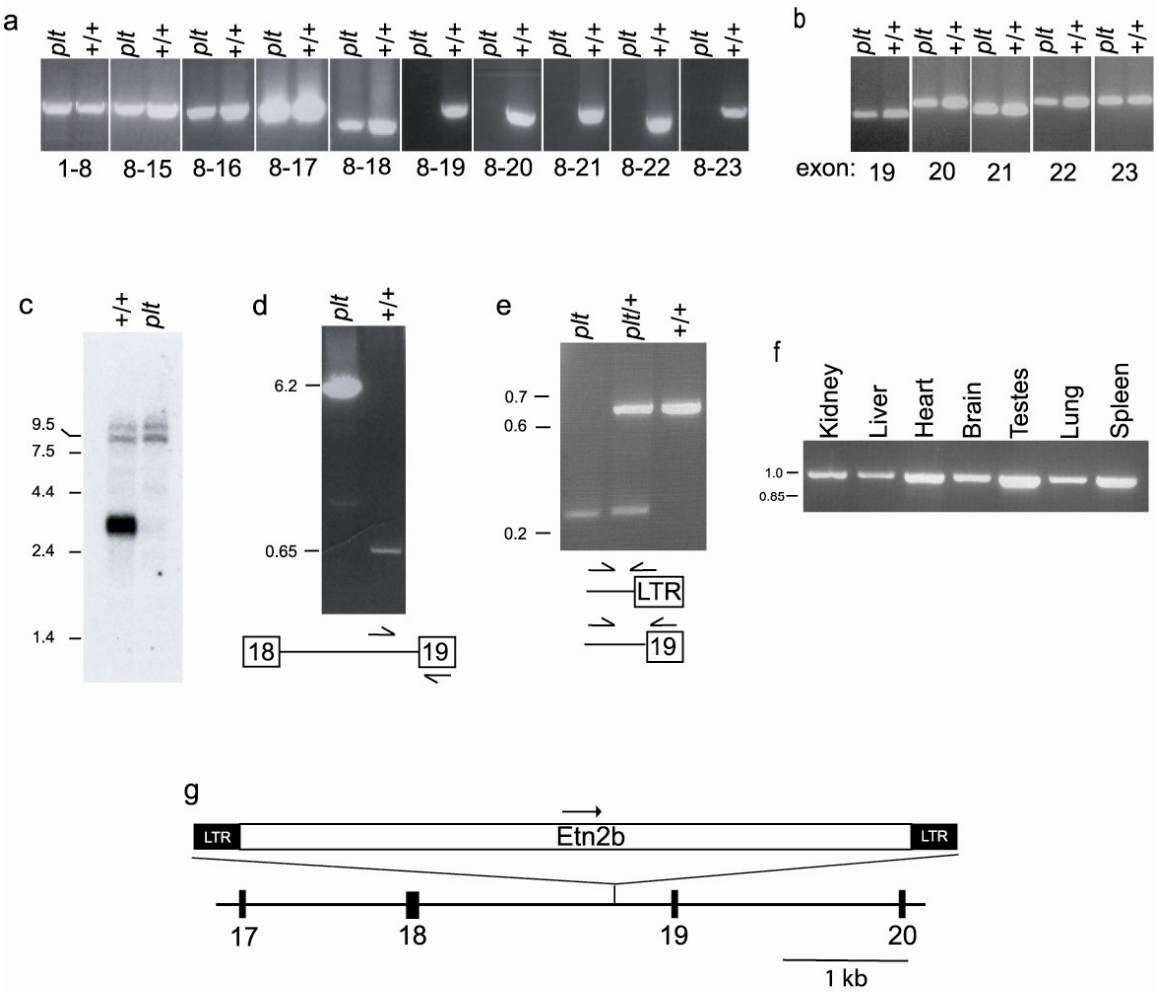

Figure 2-2. *Fig4* is mutated in the *pale tremor* mice. **a.** RT-PCR of the *Fig4* transcript from wildtype tissues with primers in the indicated exons. **b.** PCR of genomic DNA using primers flanking exons 19 through 23. **c.** Northern blot containing 3 ug of brain polyA+ RNA, isolated at P7 prior to extensive neurodegeneration, hybridized with 1 kb *Fig4* cDNA probe (exons 8 to 15). RNA integrity and equal loading of samples indicated by the intensity of minor bands (9-10 kb). **d.** Long-range PCR of genomic DNA using the indicated primers in intron 18 and exon 19. **e.** Three-primer genotyping assay for the Fig4^{plt} allele with Etn2β insertion produces a 646 bp wildtype product and a 245 bp *plt* fragment; MW markers at left (kb). **f.** RT-PCR of the *Fig4* transcript from wildtype tissues; primers located in exon 8 and exon 15. **g**. Etn2β retrotransposon in intron 18 of *Fig4*.

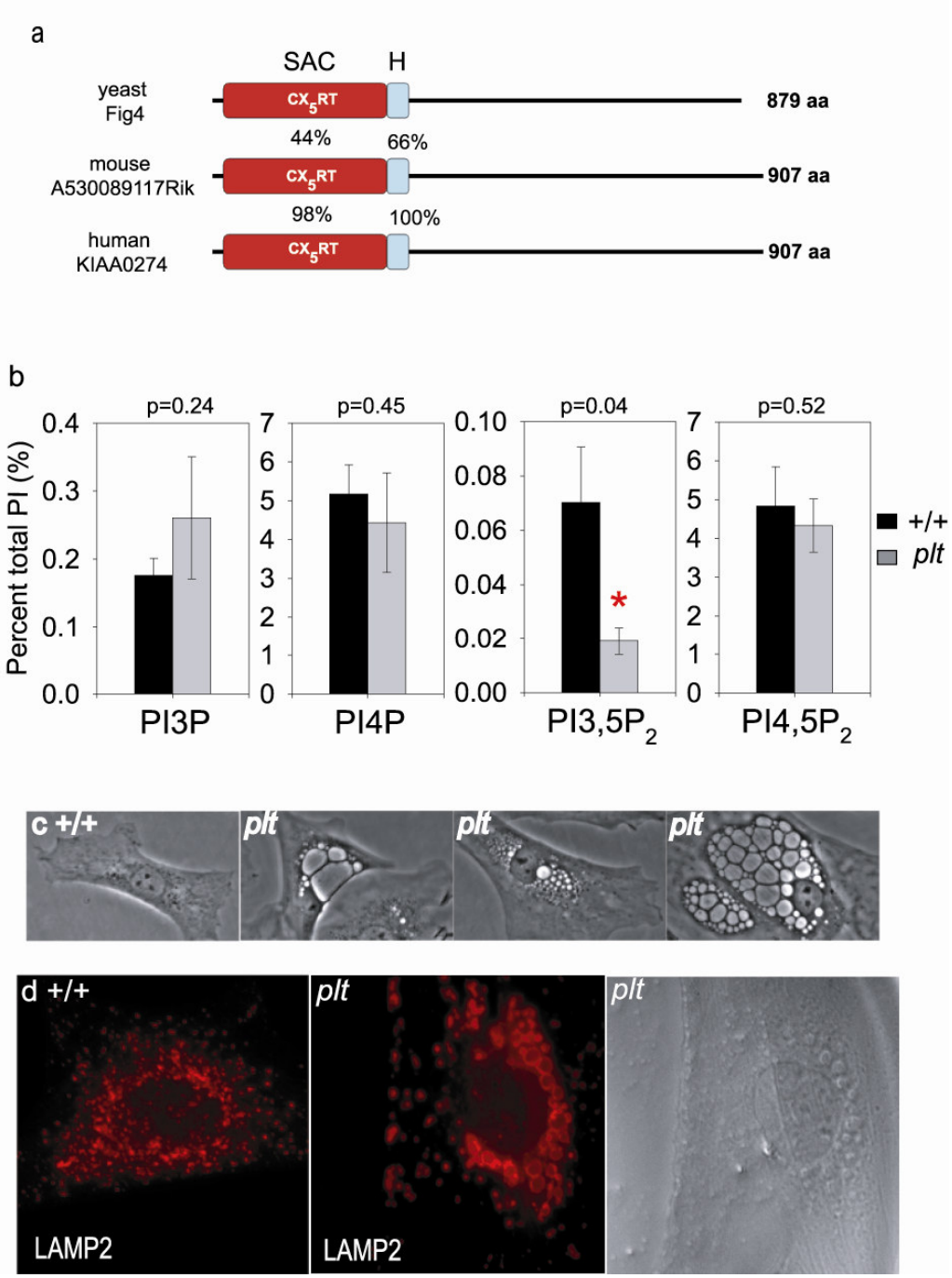

Figure 2-3. Mouse *Fig4* has conserved function. **a.** Protein domains of yeast Fig4p and mammalian homologs. See text for description of the SAC phosphatase domain. **b.** Altered abundance of the phosphoinositide PI(3,5)P2 in cultured fibroblasts from mutant mice. mean ± SD (n=6). **c.** Mutant fibroblasts are filled with vacuoles. **d.** Membranes of large cytoplasmic vesicles stain with antiserum to LAMP2, a lysosomal membrane protein.

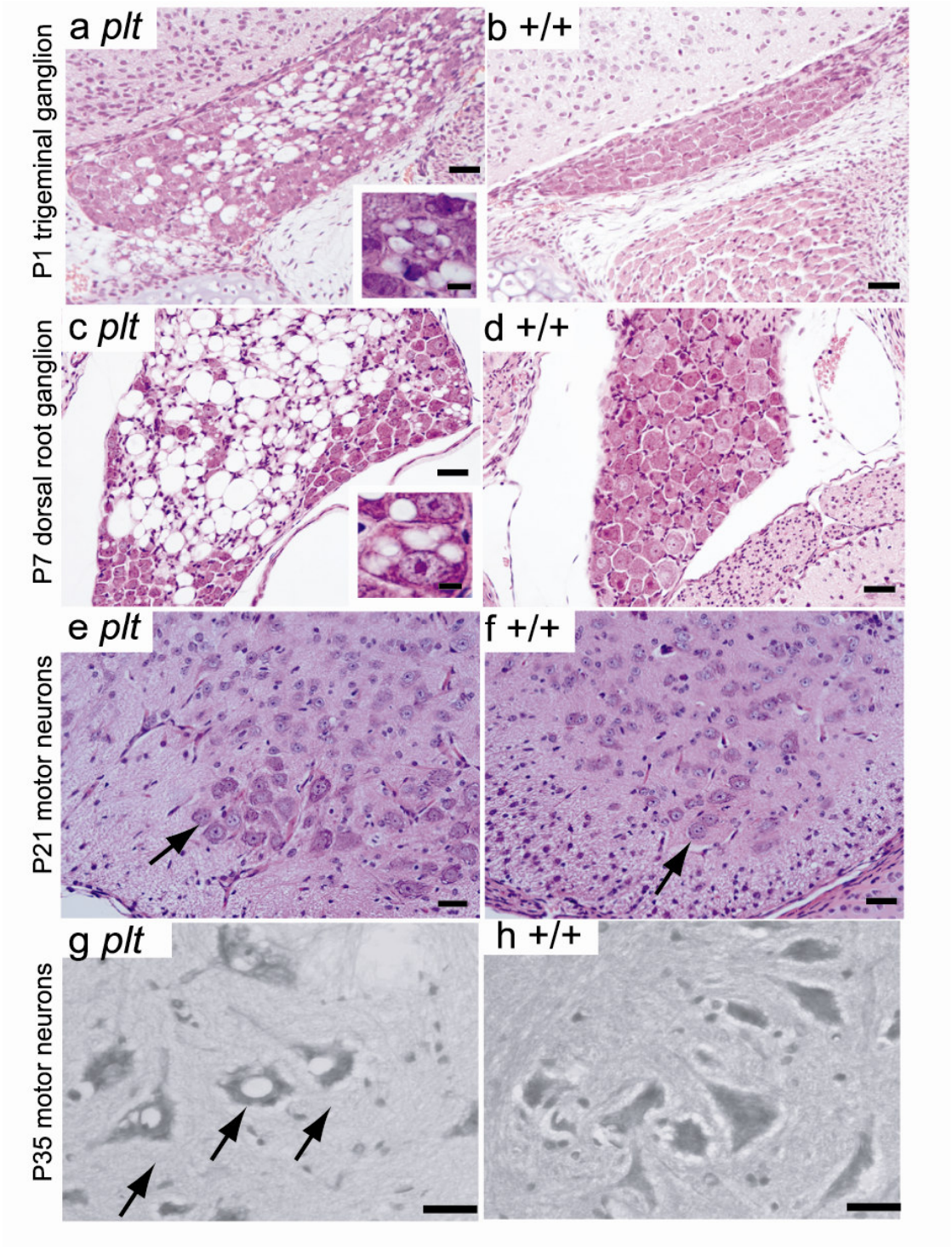

Figure 2-4. Neuropathology in *pale tremor* mice. a-b. trigeminal ganglia, **c-d.** dorsal root ganglia from lumbar region. Insets reveal cytoplasmic vacuoles. Superior cervical ganglia have a similar appearance. **e-h.** Spinal cord ventral horn. arrow, motor neuron cell body. Scale bars: 25 microns for panels a-g, 12.5 microns for insets a-d.

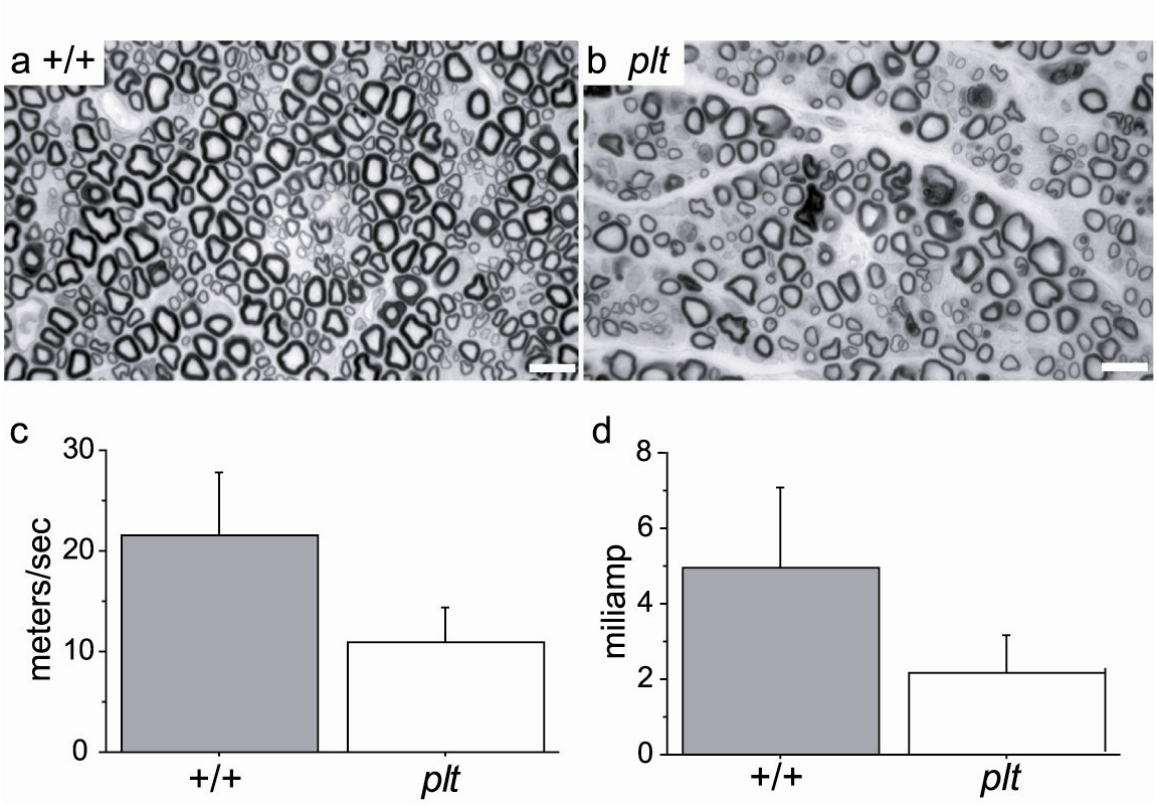

Figure 2-5. Pathological abnormalities in peripheral nerves. a-b. Semi-thin sections of sciatic nerve prepared as described(Li et al., 2006) demonstrating reduced density of large diameter myelinated axons in *plt* mutant. Scale bars: 10 microns. **c-d**. Reduced sciatic nerve conduction velocity (mutant = 11.0 ± 3.4 m/sec, wildtype = 21.5 ± 6.3) and reduced amplitude of compound muscle action potentials (mutant = 2.2 ± 1.0 mA; wildtype = 5.0 ± 2.1) (mean ± SD, n=6).

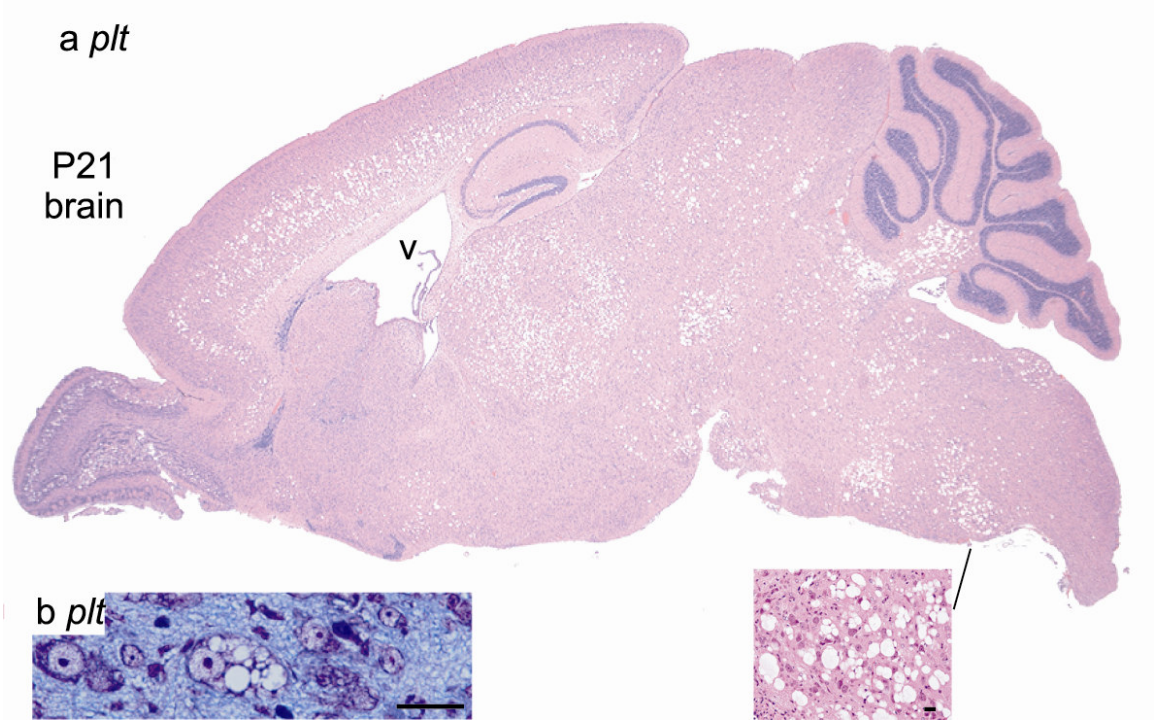

Figure 2-6. Brain degeneration in *pale tremor* mice. **a.** Sagittal section of the brain of a *pale tremor* mouse. V, enlarged ventricle. **b.** Neuronal cell bodies from regions of a degeneration P7 brain. Scale bars: 25 microns.

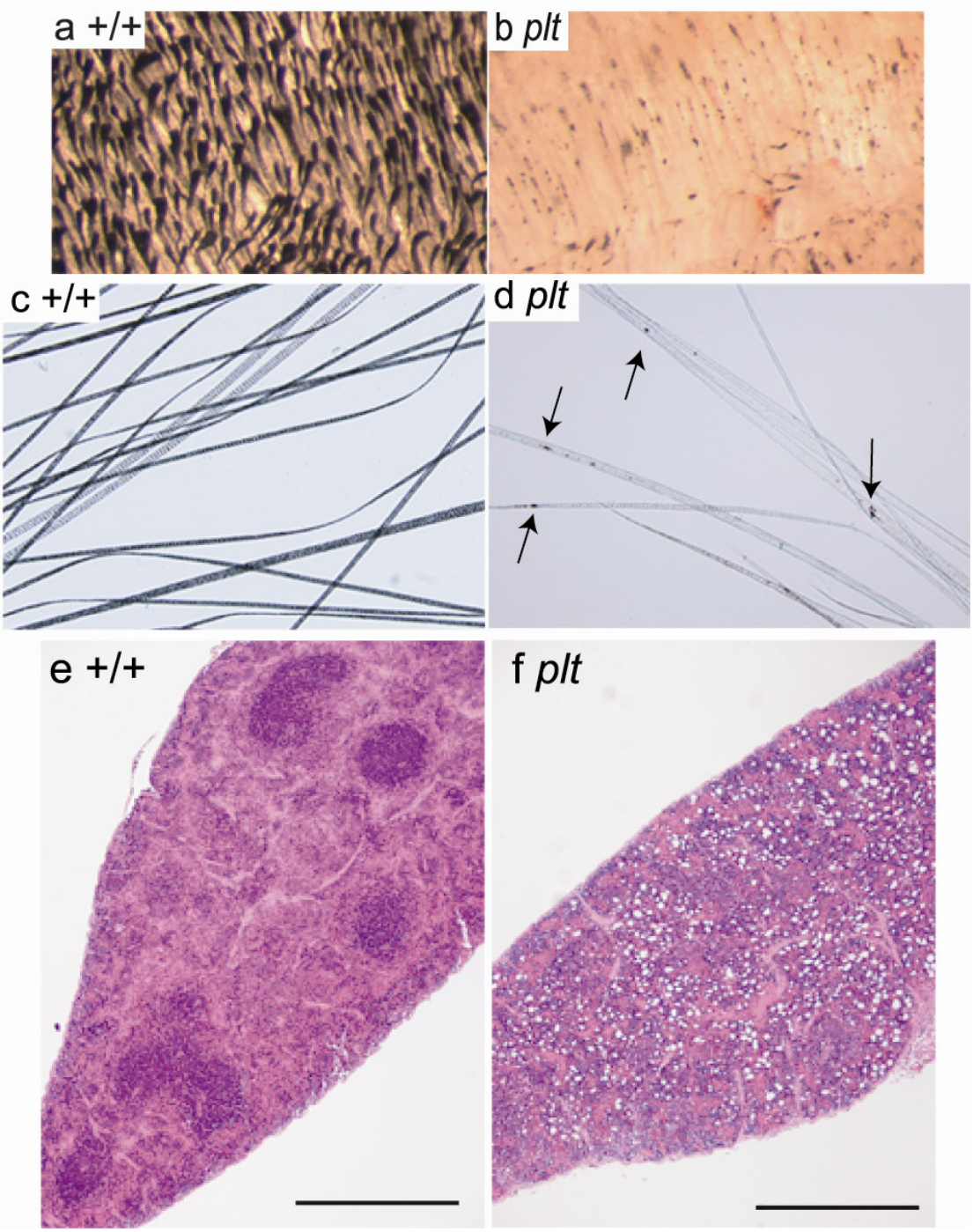

Figure 2-7. Pigment and spleen abnormalities in *pale tremor* mice. a-b. Skin wholemounts from P10 mice demonstrating pigment-containing hair follicles. Original magnification: 8.5X. **c-d.** Melanosome clumping in mutant hair shafts (arrows). Original magnification: 10X. *plt* (**e**) and wt (**f**) spleens from 3 week old animals. H&E. scale bar: 250 microns.

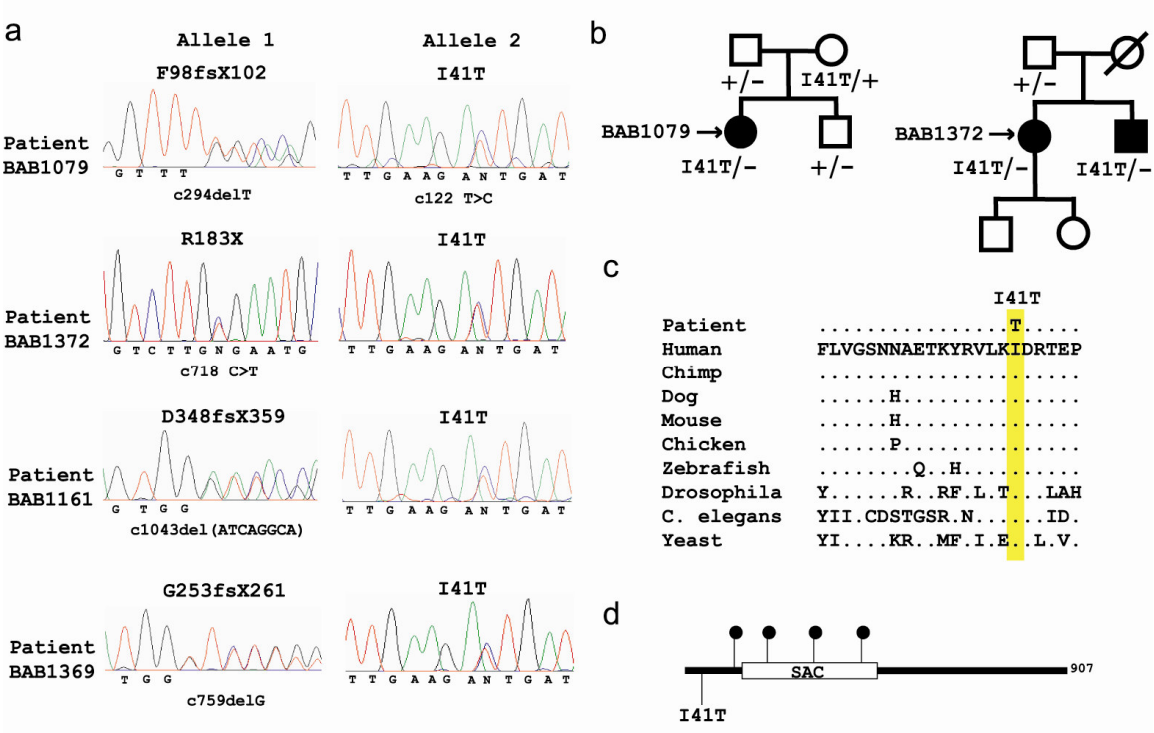

Figure 2-8. Mutations of *FIG4* in patients with Charcot-Marie-Tooth disease. **a.** Sequencing chromatographs for four unrelated patients with Charcot-Marie-Tooth disease. **b.** Inheritance of mutant alleles in two pedigrees. BAB1079 is a compound heterozygote for protein truncation mutation F98fsX102 and missense mutation I41T. BAB1372 and BAB1373 are compound heterozygotes for nonsense mutation R183X and missense mutation I41T. **c.** Residue isoleucine 41 is evolutionarily invariant in FIG4 from vertebrates, invertebrates and yeast. **d.** Location of CMT mutations in the FIG4 protein. Solid circles, protein truncation mutations.

a

		1372	1373	2587	1079	2588	2589	2590	1161	1363
intron 1	rs829811	G/A	G/A	G/A	G/A	G/A	G/A	G/A	G/G	G/A
intron 1	rs3799845	G/G	G/G	G/A	G/G	G/A	G/G	G/A	G/G	G/G
intron 1	rs2025149	C/T	C/T	T/T	C/T	C/T	T/C	T/T	C/C	C/T
exon 2		I41T	I41T		I41T	I41T			I41T	I41T
intron 2	rs3799849	C/A	C/A	C/A	C/A	C/A	C/A	C/A	C/A	C/A
intron 3	rs7764711	G/C	G/C	C/C	G/C	G/C	C/G	C/C	G/G	G/C
intron22		G/G	G/G	G/G	G/G	G/G	G/G	G/G	G/G	G/G
intron 22	rs4330563	T/T	T/T	T/G	G/T	G/G	T/G	T/G	G/G	G/T
intron 22	rs4947022	G/G	G/G	G/C	C/G	C/C	G/C	G/C	C/C	C/G

b

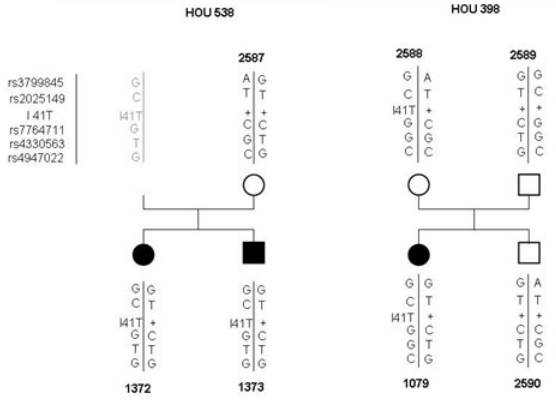

Figure 2-9. Haplotypes of CMT patients with mutations in FIG4.
a. Genotypes. Seven SNPs from the HapMap database, and the Ile41Thr mutation (c.122T>C) were genotyped for patients and family members. **b.** Haplotypes. The five SNPs shown in black were informative in the two available pedigrees and permitted reconstruction of the haplotypes. The Ile41Thr (c.122T>C) allele is carried by the same haplotype in all four patients. The Ile41Thr allele has a calculated LD coefficient D' equal to 1 for rs3799845, rs2025149 and rs7764711. D' equals 0.11 for rs4330563 and rs4947022.

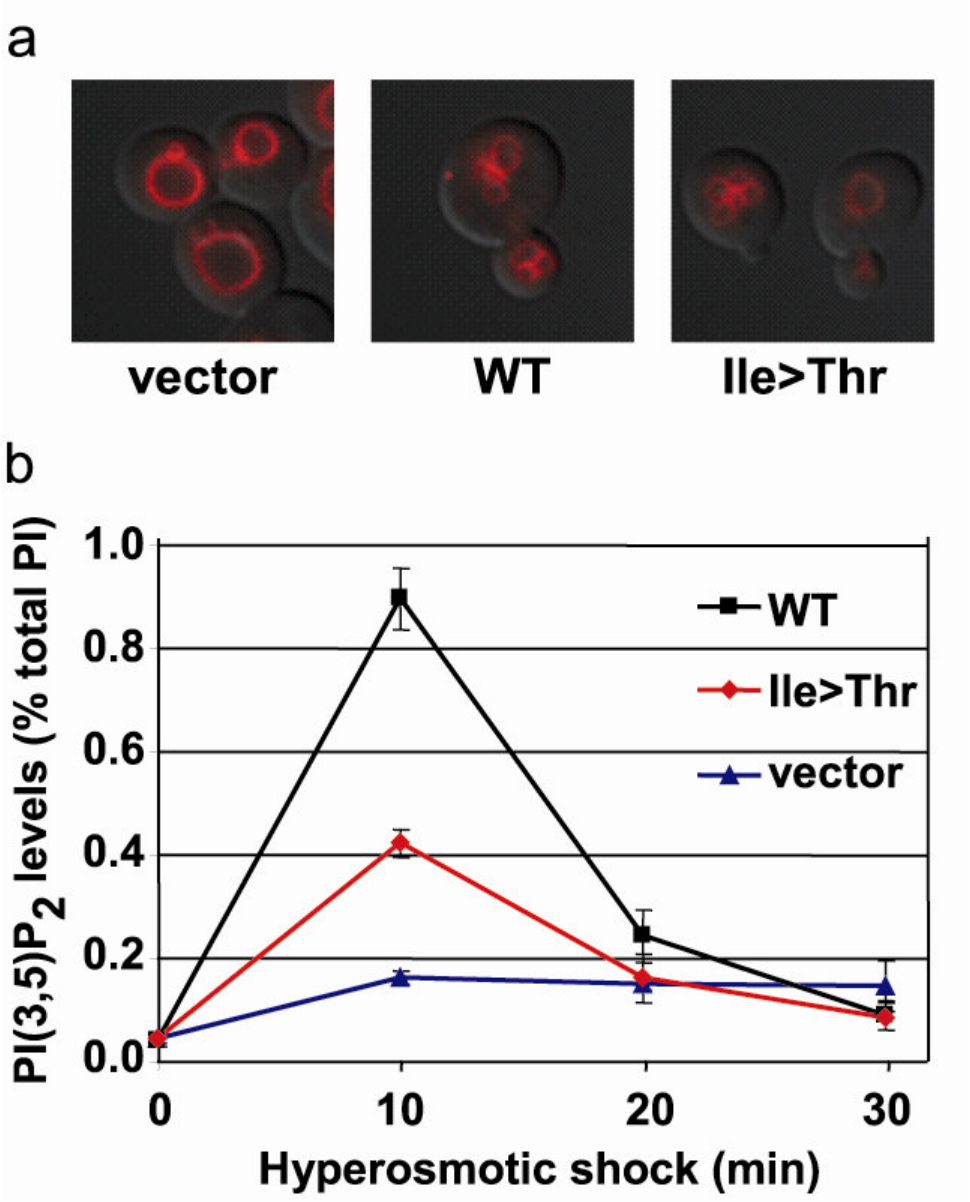

Figure 2-10. Yeast Fig4$^{Ile>Thr}$ is defective in activation of kinase Fab1/PIKfyve. The fig4 null yeast strain lacking endogenous Fig4p (Duex et al., 2006a; Duex et al., 2006b) was transformed with empty vector (vector), wildtype myc-Fig4 (WT), or myc-Fig4 containing I59T corresponding to human I41T (mutant). **a.** Yeast were labeled with FM4-64 to assess vacuole volume, an indicator of basal levels of PI(3,5)P2. **b.** Time course of PI(3,5)P2 levels after hyperosmotic shock reflects activation of Fab1 kinase. Compared with wildtype, the mutant protein exhibits impaired activation at 10 min ($p=0.004$) (mean ± SD, $n = 3$).

Materials and Methods

Animals

The *plt* mutation arose on a mixed background derived from inbred strains 129/Ola, C57BL/6J, C3H, and SJL (Adamska et al., 2005). For genetic mapping, *plt/+* heterozygotes were crossed with strain CAST/Ei (Jackson Laboratory, Bar Harbor, ME). This research was approved by the University of Michigan Committee on Use and Care of Animals. Animals were housed and cared for in accordance with NIH guidelines.

Genotyping and Markers

Genotyping was carried out using microsatellite markers from public databases as well as novel microsatellite markers designed from mouse genomic sequence (www.ensemble.org). D10Umi13 was amplified with the forward primer 5'-CCACC ACATC AACAG GCTCA CAGG and reverse primer 5'-AATGCAACCG TGACA CAAGT ACAC. PCR was carried out with the PCR core kit (Qiagen). PCR products were separated on 6% acrylamide gels and stained with ethidium bromide. The *plt* mutation is genotyped by PCR with a forward primer in intron 18 (5' CGTAT GAATT GAGTA GTTTT GATG) and two reverse primers, one in the proximal LTR of the inserted Etn2β element (5' GCTGG GGGAG GGGAG ACTAC ACAG) and one in exon 19 (5' ATGGA CTTGG ATCAA TGCCA ACAG).

RT-PCR

Total RNA was isolated from brain of P7 mice, prior to extensive neurodegeneration. cDNA was synthesized using the First Strand cDNA Synthesis Kit (Invitrogen Corp.). RT-PCR was carried out with the PCR Core Kit (Qiagen). Long range PCR was performed with the Expand Long Template PCR System (Roche).

Northern blot

The Northern blot with 3 ug of polyA+ RNA was prepared as previously described (Kohrman et al., 1996). The hybridization probe, a 1 kb RT-PCR product containing exons 8 to 15, was labeled with two radiolabeled nucleotide triphosphates.

Histology

Tissues were sectioned and stained at HistoServ (Germantown, MD). Fast blue/eosin staining was carried out in the Department of Pathology, University of Michigan. Light microscopy was performed on an Olympus BX-51 microscope and DP50 camera. Sciatic and femoral nerves were sectioned and stained with osmium for electron microscopy as previously described (Li et al., 2006). Skin whole mounts were prepared from P10 mice with the guidance of Dr. Andrzej Dlugosz, Department of Dermatology, University of Michigan. The commercial depilatory Nair was applied to the dorsal surface for five minutes followed by washing with warm water to remove hair. The skin was dissected

and superficial fascia removed. Follicles were visualized on a standard dissecting microscope with transmitted light.

Neurophysiology

Nerve conduction velocities were recorded from affected *pale tremor* mice and littermate controls. Mice were anesthetized with ketamine/zylazine and placed under a heating lamp to maintain body temperature at 32^{o}C. Recordings were obtained using a Nicolet VikingQuest portable system and Nicolet disposable EEG needles. Tail sensory responses were obtained by stimulating proximally over a 3 cm region. Sciatic nerve motor velocities were obtained by stimulating distally at the sciatic notch and proximally at the knee.

Cell culture and immunoflouresence

Primary fibroblasts were cultured from mouse tail biopsies treated with collagenase. Cells were plated in Dulbecco's modified Eagle medium (DMEM) with fetal bovine serum (FBS) and maintained at 37^{o} C with 5% CO_2 for up to 3 passages. For immunoflouresence, 100,000 cells were seeded on polylysine-coated cover slips in 35 mm dishes. We thank Dr. Thomas August and the Developmental Studies Hybridoma Bank (University of Iowa, IA) for mAbs LAMP-2, developed under the auspices of the NICHD and maintained by the Department of Biological Sciences, University of Iowa, Iowa City, IA 52242. For labeling with antibody, cells were fixed with ice cold methanol at -20^{o} C for 5 min. and blocked with 2% goat serum. Antibodies were applied for 1 hour in PBS with

2% serum at room temperature and detected with Alexa fluor 488 donkey anti-rabbit or Alexa fluor 594 goat anti-rat (Molecular Probes). Cells were visualized on a DeltaVision Deconvolution microscope system (Applied Precision).

Hippocampal neurons were cultured with glial conditioned media. Neurons were visualized with a Nikon TE2000 microscope.

Phosphoinositide assays

Fibroblast phosphoinositides were labeled with myo-[2-^{3}H] inositol, extracted, and quantitated by HPLC. Mouse fibroblasts from the first passage were grown in 100 mm dishes to 60%-70% confluency. The culture was rinsed with PBS and starved for 12 hours in inositol-free DMEM (Tissue culture support center, Washington University, MO) supplemented with 5 ug/ml transferrin, 5 ug/ml insulin and 10% dialyzed fetal bovine serum. The medium was replaced with labeling medium (inositol-free DMEM containing 5 ug/ml transferrin, 20 mM Hepes, and 50 uCi myo-[2-^{3}H] inositol (GE Healthcare, Piscatway, NJ)). After 24 hours, the culture was treated with 0.6 ml of 4.5% (v/v) perchloric acid for 15 min, scraped off the plate, and spun down at 12,000xg for 10 min at 4℃. The pellet was washed with 0.1 M EDTA once and resuspended in 50 ul deionized water. To deacylate the lipids, samples were transferred to a glass vial, mixed with 1 ml methanol/40% methylamine/n-butanol (4:4:1, v/v) and incubated at 55℃ for 1 hour. The resulting samples were vacuum dried, resuspended in 0.3 ml water

and extracted twice with an equal volume of butanol/ethyl ether/formate (20:4:1, v/v). The aqueous phase was vacuum dried and resuspended in 20 ul water.

For separation of all isoforms of the glycerophosphoinositides by HPLC, two different elution gradients were used at 1 ml/min flow rate. (pump A: H_2O; pump B: 1M $(NH_4)_2HPO_4$, pH3.8). Gradient 1: 0% B for 5 min; 0 – 2% B over 15 min; 2% B for 80 min; 2 -12% B over 20 min; 12% B for 20 min; 12 - 80% B over 40 min; 80% B for 20 min; 80 – 0% B over 5 min. To separate GroPIns(3,4)P_2 from GroPIns(3,5)P_2, a longer gradient was used: 0% B for 5 min; 0 – 2% B over 15 min; 2% B for 80 min; 2 -10% B over 20 min; 10% B for 65 min; 10 - 80% B over 40 min; 80% B for 20 min; 80 – 0% B over 5 min, The positions of GroPIns(3)P, GroPIns(3,5)P_2, GroPIns(3,4)P_2 and GroPIns(3,4,5)$_3$ were determined by ^{32}P labeled standards received as gifts from Dr. Lucia Rameh (Boston Biomedical Research Institute, MA). The positions of GroPIns(4)P and GroPIns(4,5)P_2 were confirmed with yeast glycerophosphoinositide extracts.

Human mutation detection

The cohort of unrelated patients with CMT was previously described (Szigeti et al., 2006). The clinical diagnosis was based on clinical examination, electrophysiological studies, and in a few cases, nerve biopsy. All patients received appropriate counseling and gave informed consent approved by the institutional review board. For the initial screen of *FIG4*, each coding exon was amplified and examined by heteroduplex analysis as previously described

(Escayg et al., 2000). The patient mutations were identified by sequencing products exhibiting abnormal mobility. Subsequently, the 23 exons of *FIG4* were completely sequenced from the four individuals carrying variants. Genomic DNA from neurological normal control individuals was obtained from the Coriell Institute (panels NDPT006 and NDPT009, 96 samples each) and from a collection of 111 subjects older than 60 years of age without personal or family history of neurological disease (Rainier et al., 2006).

Acknowledgements

For valuable discussions, we are grateful to A. Dlugosz, E. Feldman, D. Goldowitz, J. Hammond, L. Isom, J. M. Jones, A. Lieberman, M. Khajavi, J. Swanson, K. Verhey, and S. H. Yang. S. Cheek and M. Hancock provided expert technical assistance. Supported by NIH R01 grants GM24872 (MHM), GM50403 (LW) and NS27042 (JRL) and predoctoral training grant GM007544 (CYC).

Notes

*This chapter was previously published as:

Chow, C. Y., Zhang, Y., Dowling, J. J., Jin, N., Adamska, M., Shiga, K., Szigeti, K., Shy, M. E., Li, J., Zhang, X.*, et al.* (2007). Mutation of FIG4 causes neurodegeneration in the pale tremor mouse and patients with CMT4J. Nature *448*, 68-72.

CHAPTER III

A TRANSGENIC MOUSE MODEL OF CMT4J

Introduction

The *pale tremor* mouse is a null allele of *Fig4* (referred to as *Fig4*$^{-/-}$). *pale tremor* displays severe peripheral neuropathy, neurodegeneration in the CNS and pale coat color. Study of *pale tremor* led to identification of CMT4J patients with mutations in FIG4 (Chow et al., 2007). All four CMT4J families have one protein truncating, null mutation and the missense mutation I41T (genotype *FIG4*$^{I41T/-}$).

In yeast, the I41T allele has partial function and results in reduced levels of PI(3,5)P2 (Chow et al., 2007). Yeast carrying I41T also have an enlarged vacuole phenotype similar to Fig4 null cells (Chow CY, unpublished results). *Fig4*$^{-/-}$ mice die by six weeks of age. CMT4J patients are less severely affected and one family has adult onset disease. CMT4J patients do not have pigment abnormalities or develop CNS dysfunction (Chow et al., 2007). The phenotypic difference between *Fig4*$^{-/-}$ mice and CMT4J patients suggests that I41T may be a partially functioning allele.

To test this hypothesis, I sought to make a transgenic mouse model of CMT4J. I hypothesized that the CMT4J mouse model would closely mimic CMT4J disease with severe peripheral neuropathy without any CNS involvement or pigment abnormalities.

Results

Generation of I41T transgenic mice

Fig4 is a ubiquitous protein (Chow et al., 2007), thus I sought to match the expression of the transgene to endogenous *Fig4*. The I41T transgene consists of the mouse *Fig4* cDNA cloned downstream of a CMV enhancer and β-actin promoter (Figure 3-1). The CMV enhancer and β-actin promoter provide broad expression (Buchner et al., 2003; Niwa et al., 1991). However, expression of transgenes can be highly insertion site dependent. Site directed mutagenesis was performed to insert the I41T mutation into the mouse cDNA. The I41T transgene was injected by the University of Michigan Transgenic Animal Model Core. Genotyping of the transgene was performed with a forward primer in the β-actin promoter and a reverse primer in the cDNA (Figure 3-1). This amplifies the transgene and not the endogenous locus. Sixty nine potential founders were born. Eleven transgenic founders were identified by PCR genotyping. Five transgenic founders transmitted to the next generation. Three lines, Tg721, Tg716, and Tg705, were chosen for analysis.

RT-PCR was performed on brain cDNA to evaluate expression of *Fig4*. To distinguish transgene expression from endogenous expression, analysis was conducted on *Fig4*$^{-/-}$, Tg^{+} mice (see below). *Fig4*$^{-/-}$ mice do not express endogenous *Fig4* mRNA (Figure 3-2) (Chow et al., 2007). *Fig4*$^{-/-}$, Tg^{+} animals only express *Fig4* from the transgene. Tg716 *Fig4* transcript levels were close to those of the endogenous gene, while Tg721 and Tg705 are expressed at approximately twice the level of endogenous *Fig4* (Figure 3-2).

Due to variability in the phenotype of the Tg716 line, it was discarded and not included in the study. *Fig4*$^{-/-}$, *Tg716+* mice exhibited two different phenotypes. 50% of the *Fig4*$^{-/-}$, *Tg716+* survived past 4 months of age and appeared to be unaffected. However, the other half of the *Fig4*$^{-/-}$, *Tg716+* mice died by five weeks age and were identical in phenotype to the original *Fig4*$^{-/-}$ mice. This data is consistent with two independent transgene insertions where one site is not being expressed and does not recue the null phenotype.

Tg721 and Tg705 transmitted in Mendelian ratios consistent with one insertion site (Table 3-1). Transgene positive mice from both lines are indistinguishable from wildtype littermates at all ages, indicating no detectable insertion related phenotypes.

The I41T transgene rescues the *Fig4*$^{-/-}$ lethal phenotype

Tg721 and Tg705 were both bred onto the *Fig4*$^{-/-}$ background (Figure 3-3). Because no endogenous FIG4 protein is expressed (Chow et al., 2007), the *Fig4*$^{-/-}$, Tg^{+} mice are similar to CMT4J patients expressing only the I41T protein. Results are similar from both transgene lines and will not be differentiated. *Fig4*$^{-/-}$, Tg^{+} mice develop and grow similar to wildtype littermates (Figure 3-4), and have normal neuromuscular function as measured by the hanging wire test (Figure 3-5). *Fig4*$^{-/-}$, Tg^{-} mice quickly develop a movement disorder and die by six weeks of age (Figure 3-6). At seven months of age, there is still no sign of neurological disorder or lethality in the *Fig4*$^{-/-}$, Tg^{+} mice (Figure 3-4, 3-5, and 3-6). One mouse from the Tg721 line died at 4 months of age (1/12) and appeared to have severe hydrocephalus, but no other mice have become sick.

While the neurological and early lethality phenotypes are rescued by the I41T transgene, all *Fig4*$^{-/-}$, Tg^{+} mice have diluted coat color similar to *Fig4*$^{-/-}$, Tg^{-} mice (Figure 3-7). *Fig4*$^{-/-}$, Tg^{+} mice are easily identifiable at 3 days of age, as they are lighter in pigmentation than wildtype littermates. *Fig4*$^{-/-}$, Tg+ mice continue to be diluted as they age, but are otherwise indistinguishable from wildtype mice.

The *Fig4* variant R905C in mouse strain WSB/EiJ and a human patient with CMT.

In the course of the CMT screen for *FIG4* mutations (Chapter II), I identified a novel missense variant in patient BAB1591. The variant, c2713 C>T, is in exon 23 and results in the amino acid substitution R905C, three residues from the end of the protein (Figure 3-8a,b). Arginine 905 is evolutionarily invariant in all vertebrates (Figure 3-8c), but the carboxy terminus of FIG4 is not conserved between human and yeast. Patient BAB1591 has autosomal recessive CMT with spinocerebellar ataxia (CMT+SCA). Sequencing of all *FIG4* coding exons from patient BAB1591 did not identify a second mutation. R905C was not identified in 363 neurologically normal controls.

To find nonsynonymous variants in mouse, I searched the NCBI Entrez SNP database (http://www.ncbi.nlm.nih.gov/sites/entrez?db=snp). Mouse SNPs identified in the Perlegen resequencing project have been deposited in this database (Frazer et al., 2004). The mouse strain WSB/EiJ was one of the resequenced mouse strains and carries the same nonsynonymous SNP, R905C, in *Fig4*. WSB/EiJ genomic DNA was ordered from the Jackson Lab and sequenced to confirm the presence of R905C (Figure 3-9a). WSB/EiJ mice have a very subtle pale agouti coat color (a^w/ a^w) and no obvious neurological deficits. I imported these mice and performed a complementation test with the *Fig4* null allele (Figure 3-9b). Compound heterozygous mice $Fig4^{R905C/-}$ do not have a neurological phenotype. The original pale coat is subtle and it is unclear if

compound heterozygous mice have the same subtle pale agouti coat color. These mice will be aged and monitored for neurological phenotypes. The *Fig4*^{R905C} allele is currently being bred onto a black coat color (a/a) (Figure 3-9c), because this might make the pale coat phenotype more evident than on a^{w}/ a^{w}. Fibroblasts have also been cultured from *Fig4*$^{R905C/-}$ mice. The fibroblasts have a similar fraction of vacuolated cells compared to control fibroblasts (*Fig4*$^{R905C/-}$ cells, 24% vacuolated; *Fig4*$^{R905C/+}$ cells, 26% vacuolated).

Discussion

Charcot-Marie-Tooth disease type 4J is caused by mutations in *FIG4*. Here I report a transgenic mouse that may be a new model of CMT4J (CMT4J mice). The I41T transgene rescues early lethality and neurological disease observed in the *Fig4*$^{-/-}$ mouse. Despite having normal growth and neurological function, CMT4J mice have a pale coat color. The I41T transgene fails to rescue the pigment defect. The data presented in this report indicates that the I41T allele retains enough activity for nervous system function and survival.

It is evident at P3 that the CMT4J mice have a dilute coat color similar to the original *Fig4*$^{-/-}$ mice. It is unknown why loss of FIG4 function results in diluted pigment. Melanosomes are specialized organelles synthesized by melanocytes, pigment cells in the skin (Marks, 2008). Melanosomes originate from late endosomes (Marks, 2008; Raposo and Marks, 2007). Endosome and lysosome trafficking is abnormal is *Fig4*$^{-/-}$ fibroblast and neurons (Chow et al., 2007).

Perhaps a similar defect in endosome/lysosome trafficking is present in melanocytes, preventing synthesis and delivery of pigment to the hair.

Careful analysis of melanocytes and pigment biogenesis in CMT4J mice and *Fig4*$^{-/-}$ mice is warranted. I have not analyzed I41T transgene expression in melanocytes in the CMT4J mice. If the transgene is not expressed, then the pigment phenotype is simply identical to *Fig4*$^{-/-}$ and not being rescued because I41T is not expressed in the appropriate cell type. Pale coat color was observed in three independent lines. It is likely that I41T is a partial functioning allele and does not retain the necessary function for the production of pigment in mice. Studies involving the role of *Fig4* and pigmentation are underway.

The CMT4J mouse demonstrates that the mouse pigment pathway may be more sensitive than the nervous system to the loss of *Fig4* function. This is interesting, as the opposite is observed in CMT4J patients. The patients have no known pigment abnormalities, but have a very severe peripheral neuropathy (Chow et al., 2007). This may result from species differences in the peripheral nervous system. Peripheral nerves in mouse are shorter than in human. Vesicle trafficking through axons is most likely less of a burden in the shorter axons of mouse peripheral nerves. This may make mouse peripheral nerves less sensitive to improper *Fig4* function.

As of this report, CMT4J mice from both lines are >7 months old and are unaffected as indicated by normal body weight and performance on neuromuscular tests. These data indicate that the I41T allele still retains enough function to produce an intact, functioning nervous system in the mouse. It remains to be seen if older CMT4J mice will develop neuropathy. Other CMT mouse models are also much less severely affected than the human disease. For example, mouse models of CMT4B1 and CMT4B2 display only minor dysmyelination after one year of age (Bolis et al., 2007; Previtali et al., 2007). If CMT4J mice develop late onset disease, study of these mice may facilitate in understanding the disease and development of a therapy.

A thorough study is needed to properly characterize any subtle neurological defects. Since CMT4J is a peripheral nerve disease, nerve conduction velocity (NCV) measurements should be taken from the CMT4J mice as they age. Subtle NCV abnormalities are likely to be present before any movement disorder is displayed, signaling the onset of disease. If there are no NCV abnormalities, then as the mice age, they should also be subjected to a battery of behavioral tests to monitor them for subtle neurological disorder. Mice should be tested for neuromuscular abnormalities with the rotarod, hanging wire tests, and grip strength measurements. Several mice at each time point should be evaluated histologically. Subtle demyelination and axonal degeneration could be present in the peripheral nerves. Neurons in the brain and motor neurons in the spinal cord should be monitored for signs of vacuolization, like those

observed in the *Fig4*$^{-/-}$ mice. Though CMT4J patients do not display any brain degeneration, the *Fig4*$^{-/-}$ mice display severe brain degeneration. To test for CNS function, mice should also be evaluated with cognitive tests, such as the Morris Water Maze. This would determine if there is subtle brain degeneration in the CMT4J mice that might be missed by gross histology.

Two independent transgenic lines were studied and both displayed no neurological deficits, but retained a pale coat color. Analysis of multiple transgenic lines ensures that the results reported here are not due to insertional effects. Expression of the transgene can vary between transgenic lines and further analysis of line Tg705 and Tg721 is needed to establish whether expression differences are present. Quantitative gene expression such as real time PCR should be used to determine the levels of *Fig4* expression in the nervous system and skin of CMT4J mice. It is possible that over expression of the transgene in the nervous system is protecting CMT4J mice from degeneration. This might not represent the human disease where only one copy of I41T is being expressed. *in situ* hybridization analysis can be used to determine the spatial expression pattern of the transgene in brain and other somatic tissues.

The CMT4J mouse is a partial rescue of *Fig4*$^{-/-}$. The CMT4J mouse has demonstrated that the I41T allele retains enough function to protect the mouse from early lethality and neurodegeneration in the context of these transgene

expression levels. The pigmentation defect suggests that the I41T mutation disrupts PI(3,5)P2-related interactions that are essential for pigmentation. Further analysis of the CMT4J mouse will determine if it will be a good model of CMT4J pathogenesis in humans.

It remains to be seen if the missense variant Fig4^{R905C} has functional consequences in mouse and human. The occurrence of the same mutation in two different species is not often observed. In this case, the explanation probably lies in the fact that conversion of the arginine codon CGU to the cysteine codon UGU can occur by demethylation of the CpG dinucleotide in positions 1 and 2 of this codon. CpG demethylation is a common molecular mechanism for mammalian mutations, and recurrent independent mutations are observed in unrelated patients with similar disorders, e.g. epilepsy patients with CGA (arginine) to TGA (stop codon) mutations in SCN1A (Kearney et al., 2006). There is no evidence of neurological disorder in WSB/EiJ mice. Our cross with the *Fig4* null allele also suggests that R905C does not affect neurological function or vacuolation of cells. R905C cannot be tested in yeast because the C-terminus of Fig4 is not well conserved between mouse and yeast. Ongoing analysis will determine if R905C affects pigmentation.

Here I have presented initial analysis of mouse models of two human *FIG4* variants. Both transgenic mice and naturally occurring variants could be useful in studying functional effects of variants in *FIG4*.

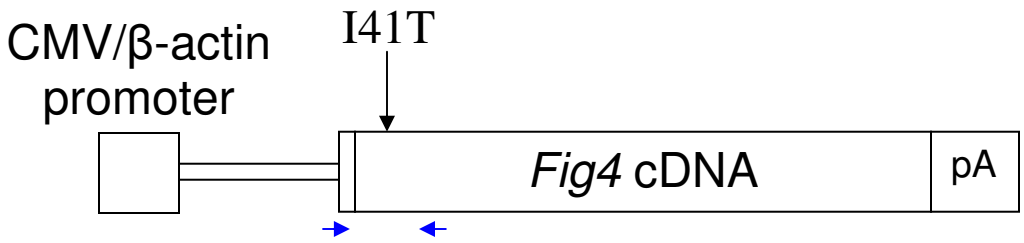

Figure 3-1. Structure of I41T transgene. The mouse *Fig4* cDNA with the I41T mutation was cloned upstream of a CMV/ β-actin promoter. Arrows, genotyping primers. pA, poly-A.

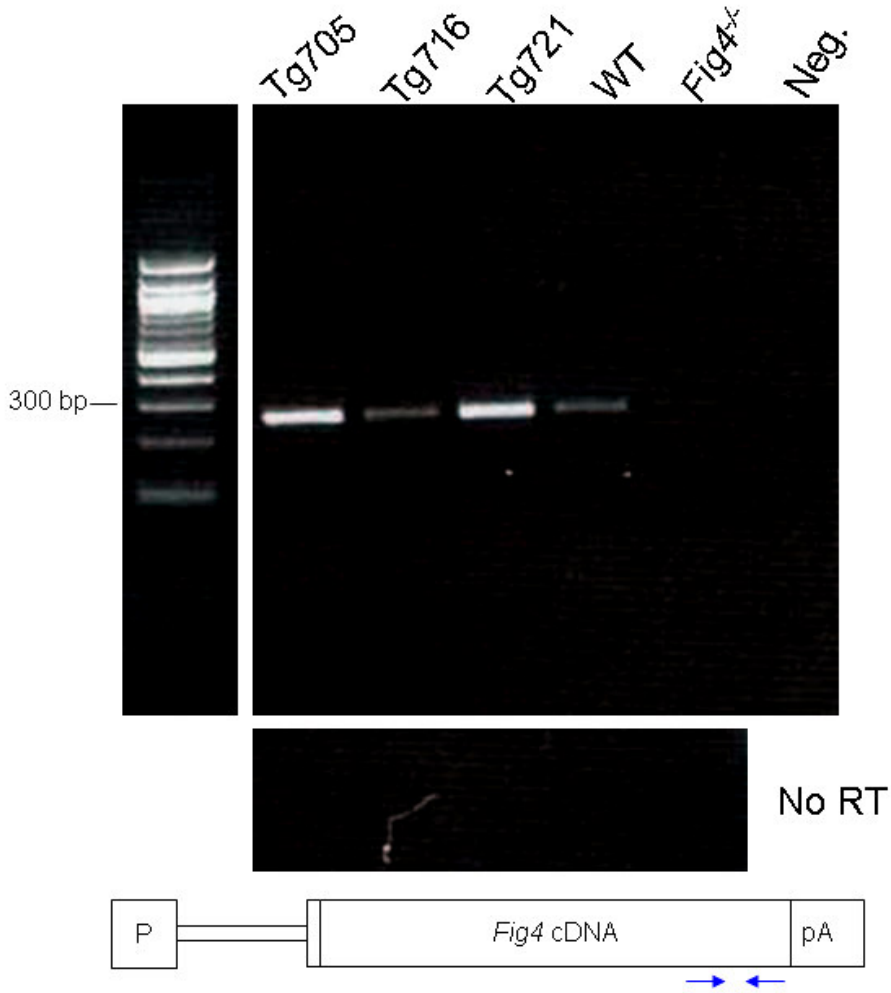

Figure 3-2. Expression of *Fig4* in transgenic lines. RT-PCR analysis of transgene expression in brain RNA with 25 cycles. Line Tg716 is similar in expression to wildtype (WT). Tg705 and Tg721 have equal expression, but more than wildtype. *Fig4*$^{-/-}$ has little to no expression. Transgenic samples are from *Fig4*$^{-/-}$, *Tg*$^{+}$ mice. Amplification was not due to genomic DNA contamination, as indicated by lack of amplification in 'No RT' gel below. Reverse transcriptase was excluded from the 'No RT' reactions, any amplification would be from genomic DNA. Arrows on transgene diagram indicate primers used for expression analysis. Neg., negative control reaction lacking template. P, promoter. pA, poly-A.

Table 3-1. Inheritance of transgene in Tg705 and Tg721 is consistent with one insertion site

	Tg+ (%)	Tg- (%)
Tg705 (n=130)	50	50
Tg721 (n=108)	55	45
expected for 1 insertion site	50	50
expected for 2 insertion sites	75	25

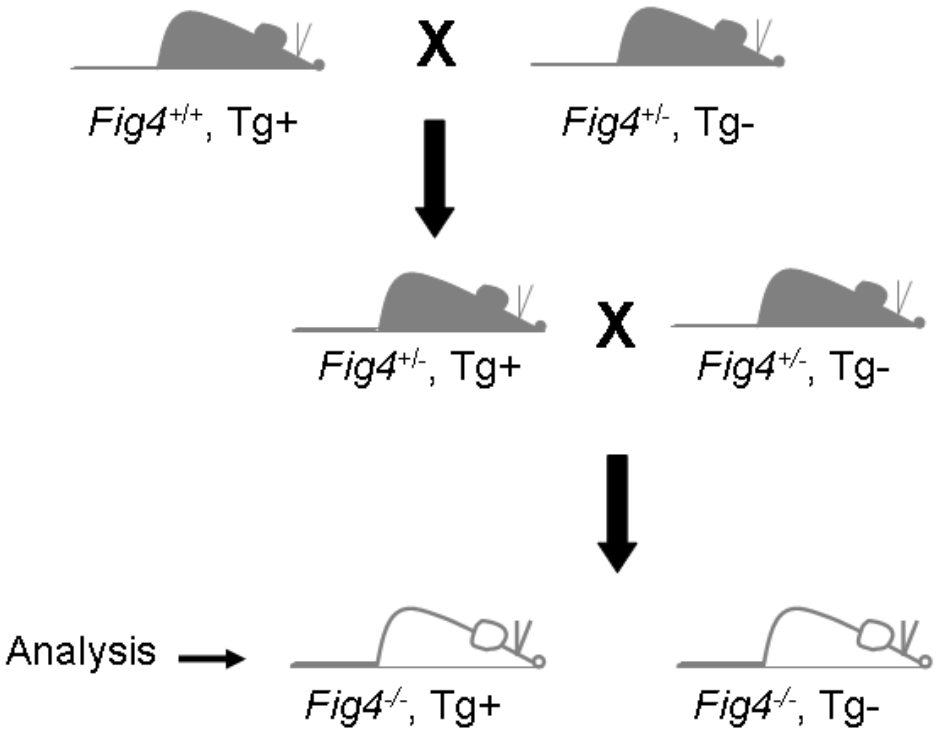

Figure 3-3. I41T transgene experimental breeding scheme. Two generation breeding scheme to produce the experimental CMT4J mice. *Fig4*$^{-/-}$ mice without the transgene were compared to *Fig4*$^{-/-}$ mice carrying the transgene.

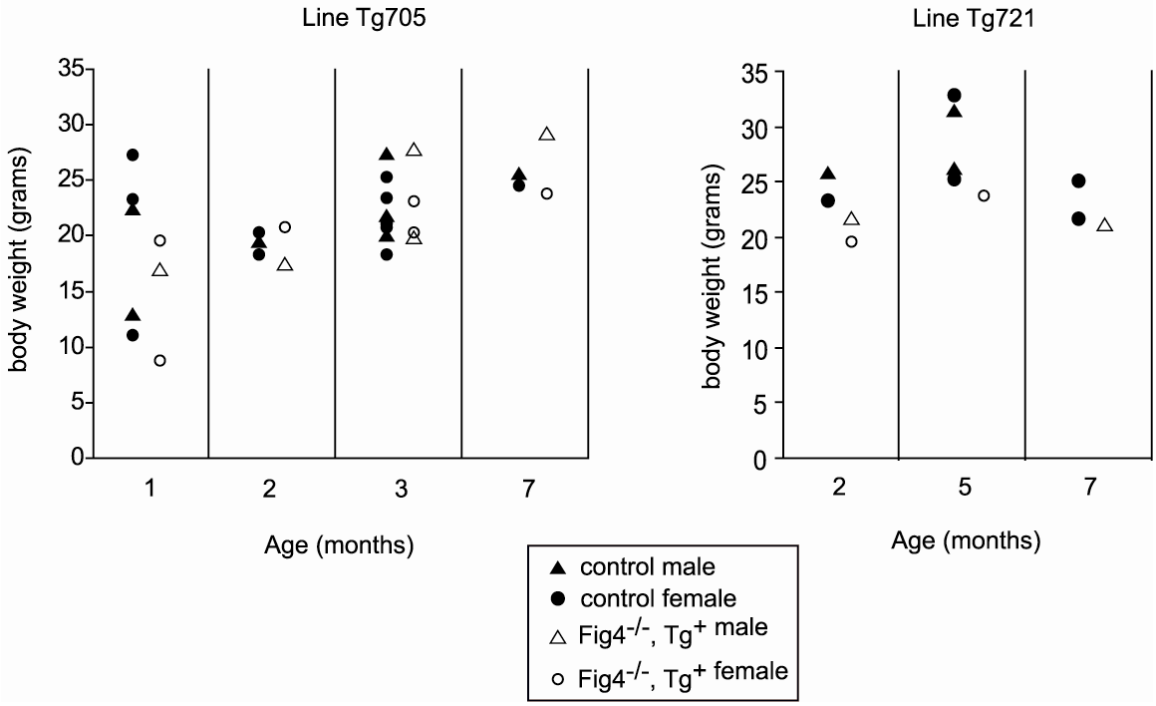

Figure 3-4. Reduced body weight of Fig4$^{-/-}$ mice is rescued by the I41T transgene. Rescue of body weight is evident in line Tg705 and Tg721. There is no difference in body weight between control and *Fig4$^{-/-}$, Tg^{+}* mice. Control mice consisted of littermates with the following genotypes: Fig4$^{+/+}$, Tg^{-}, Fig4$^{+/-}$, Tg^{-}, Fig4$^{+/+}$, Tg^{+} and Fig4$^{+/-}$, Tg^{+}. Each symbol represents one mouse.

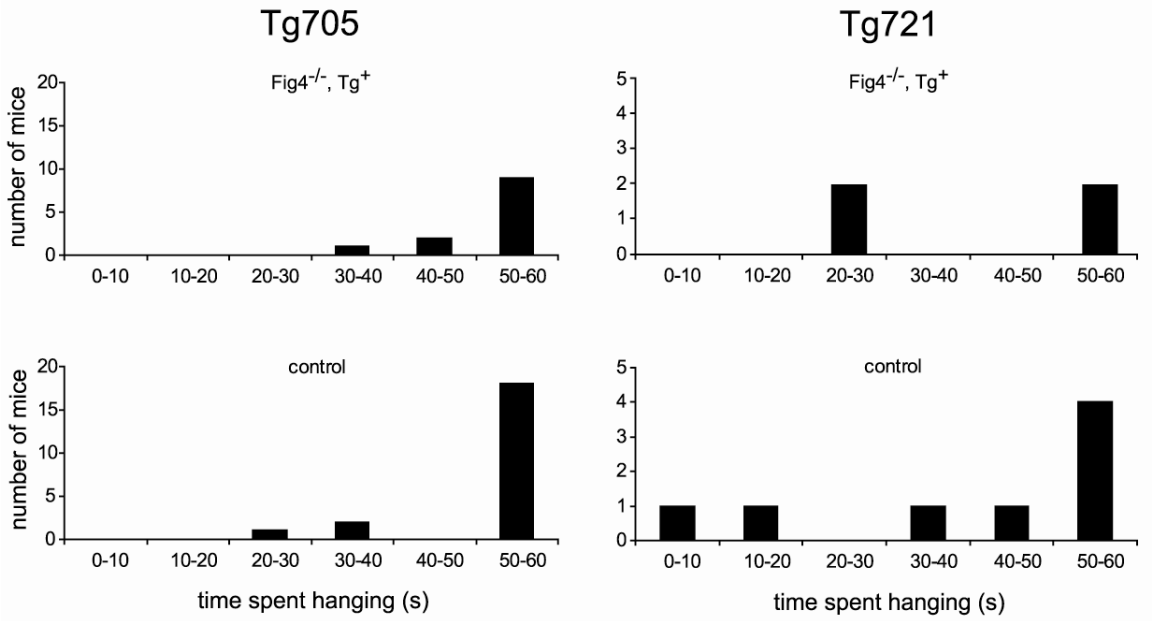

Figure 3-5. Normal neuromuscular ability of *Fig4$^{-/-}$, Tg^{+}* mice. Mice were subjected to the wire hang test for neuromuscular ability. The time spent hanging was recorded (0-60 seconds). *Fig4$^{-/-}$, Tg^{+}* mice were identical in ability to littermate controls. Note the low number of animals from line Tg721. (Line Tg705: *Fig4$^{-/-}$, Tg^{+}*: n=13; controls: n=21. Line Tg721: *Fig4$^{-/-}$, Tg^{+}*: n=4; controls: n=8). Mice of different ages (1-7 months of age) and sex were combined for this analysis. Control mice consisted of littermates with the following genotypes: Fig4$^{+/+}$, Tg^{-}, Fig4$^{+/-}$, Tg^{-}, Fig4$^{+/+}$, Tg^{+} and Fig4$^{+/-}$, Tg^{+}.

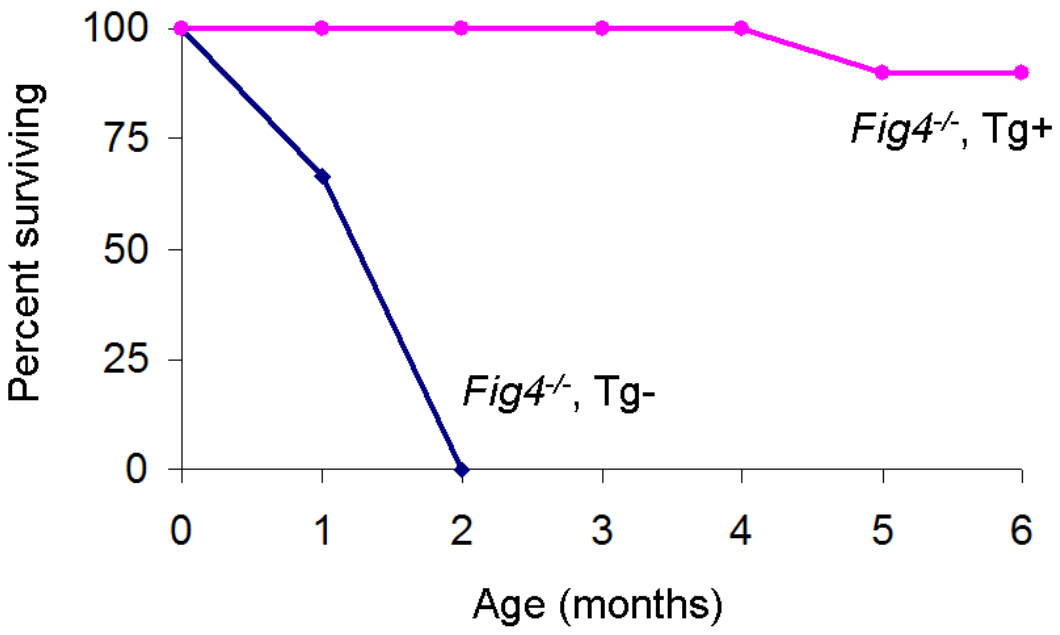

Figure 3-6. Lethality of *Fig4*$^{-/-}$ is rescued by I41T transgene. The survival of *Fig4*$^{-/-}$*, Tg+* (n=8) and *Fig4*$^{-/-}$*, Tg-* (n=6) mice.

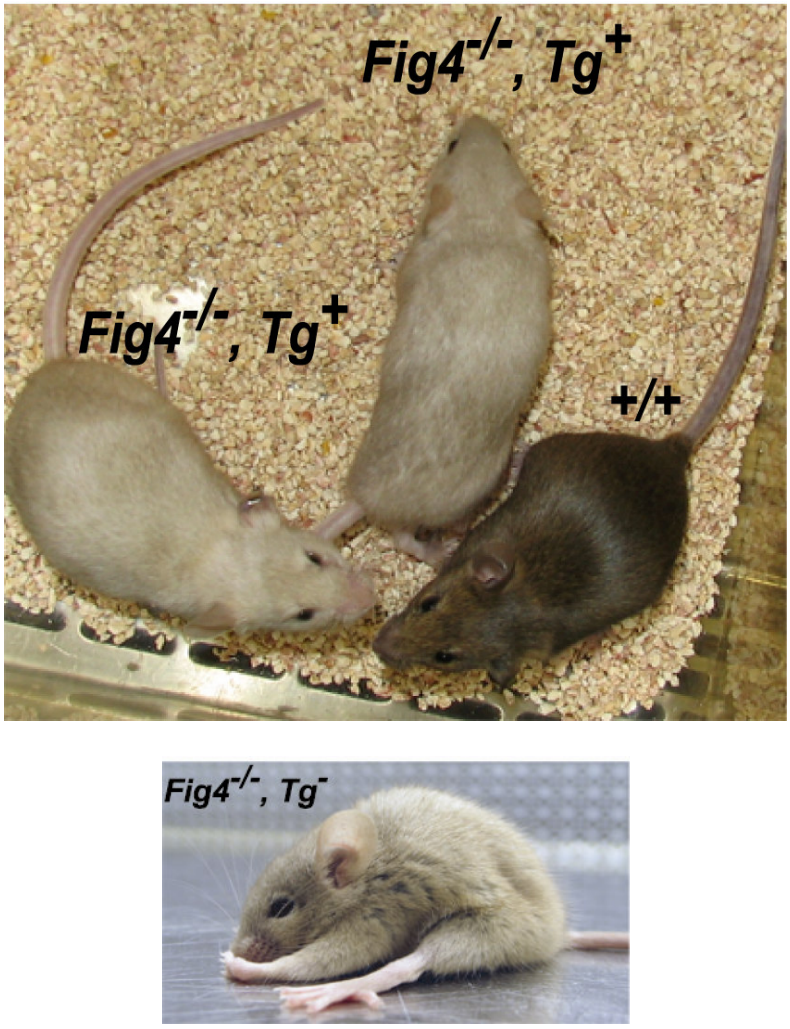

Figure 3-7. *Fig4*$^{-/-}$*, Tg*$^{+}$ mice have pale coat color. 4 month old *Fig4*$^{-/-}$*, Tg*$^{+}$ mice and a wildtype littermate. *Fig4*$^{-/-}$*, Tg*$^{+}$ mice have dilute coat color similar to the original *Fig4*$^{-/-}$*, Tg*$^{-}$, below. Picture of *Fig4*$^{-/-}$*, Tg*$^{-}$ mouse taken from (Chow et al., 2007).

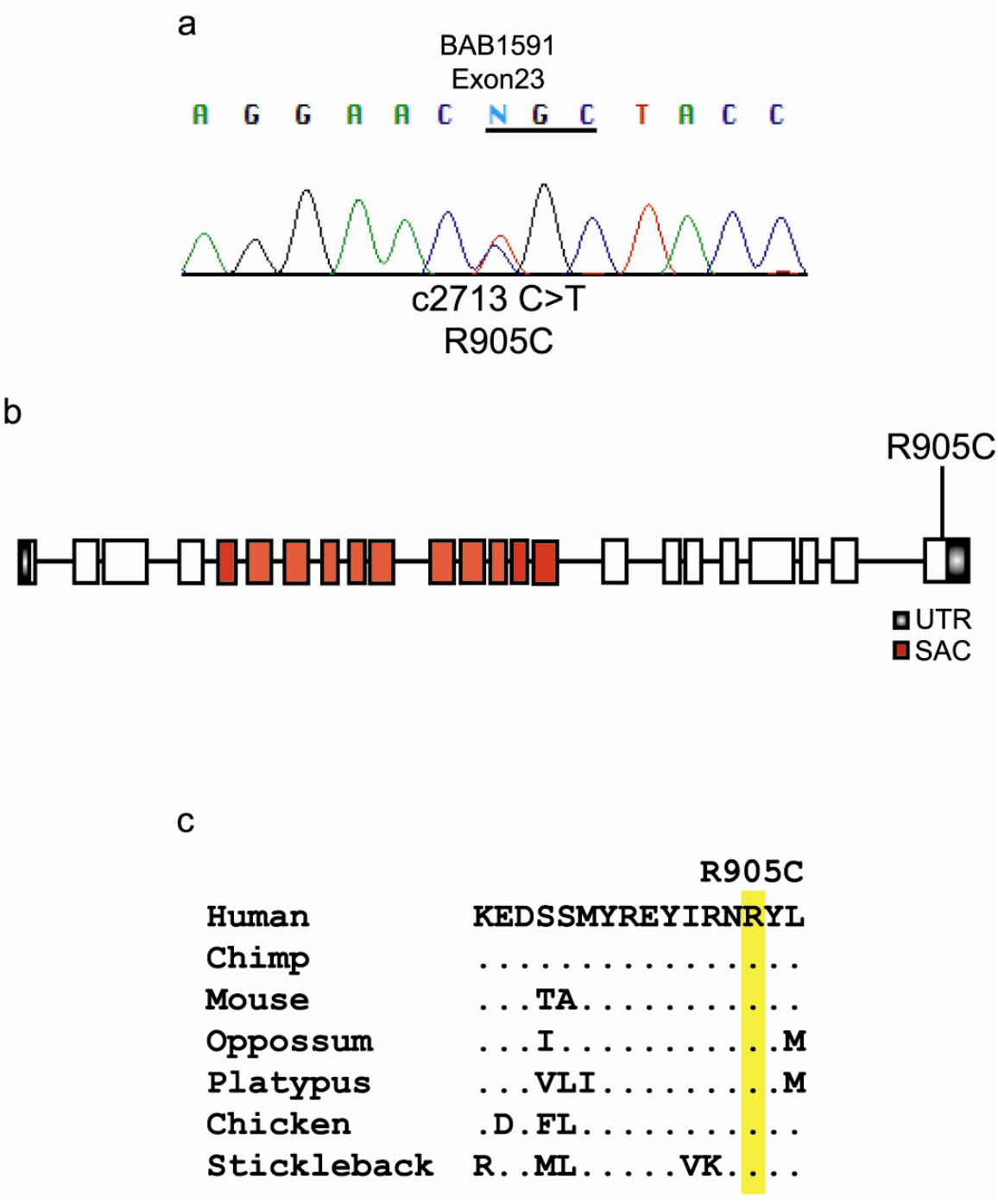

Figure 3-8. A *FIG4* missense variant in a CMT patient. **a.** Sequencing of exon 23 from patient BAB1591 reveals the missense variant R905C. **c.** R905C, in exon 23, is three residues from the c-terminus. **b.** Residue arginine 905 is evolutionarily invariant in vertebrates.

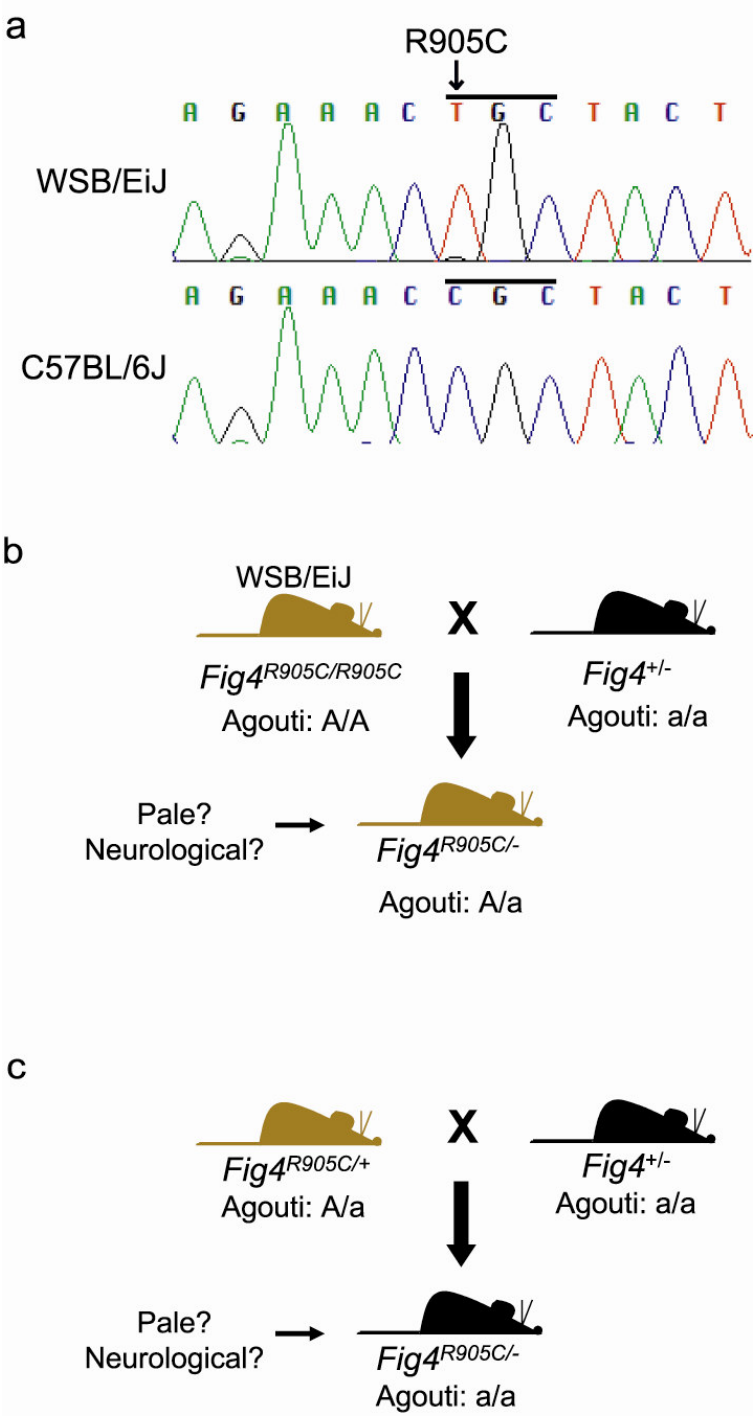

Figure 3-9. R905C is a SNP in mouse train WSB/EiJ. a. Sequencing of exon 23 from WSB/EiJ and C57Bl/6J mice. **b.** Complementation test with the null allele of *Fig4* on agouti coat color (agouti genotype, A/a). **c.** Complementation test with null allele of *Fig4* on black coat color (agouti genotype, a/a).

Materials and Methods

Animals

Fig4$^{-/-}$ mice were previously described (Chow et al., 2007) and are maintained on a mixed background comprised of 50% CAST/Ei and a mix of C57BL/6J, SJL, C3H and 129. Transgenic founders were C57BL/6J/SJL F2. Transgenic founders were bred directly to *Fig4*$^{+/-}$ heterozygous mice (Figure 3-3). WSB/EiJ mice were ordered from the Jackson Lab (Bar Harbor, ME). This research was approved by the University of Michigan Committee on Use and Care of Animals. Animals were housed and cared for in accordance with NIH guidelines.

cDNA construct

The *Fig4* cDNA was amplified by PCR from C57BL/6J brain cDNA using forward primer 5' ACGCATGCTATGTGTCTGGTGTGCTGGAGGTCTG 3' and reverse primer 5' TCGCATGCAGTCCTTTACCAATGAGCTGCATC 3'. These primers added *Sph1* sites upstream and downstream of the cDNA. PCR product was digested with *Sph1* and cloned into the *Sph1* site of the pCAG3z vector. The I41T mutation was inserted by site-directed mutagenesis of the pCAG3z-FIG4 vector. Sequencing confirmed the presence of I41T as well as the absence of PCR induced errors.

Generation of transgenic mice

DNA from pCAG3z-FIG4 was isolated according to the Qiagen Maxi Prep Kit. The vector was digested with *BamH*I. The purified fragment containing the

cDNA construct was microinjected into (C57BL/6 X SJL)F2 mouse eggs and transferred to recipients by the University of Michigan Transgenic Animal Model Core. Founders were identified by genomic PCR of tail DNA with a transgene specific forward primer, 5' TGCTGGTTATTGTGCTGTCTCATC 3', and reverse primer in the coding sequence, 5' CTTCGTTTCTGCATGATTGCTCCC 3'.

Genotyping

Genotyping was performed on genomic DNA from tail biopsies. *pale tremor* mice were genotyped as previously described (Chow et al., 2007). Transgenic mice were genotyped using the same primers described for founder identification. WSBEi/J genomic DNA was ordered form the Jackson Lab. Sequencing was performed at the University of Michigan Sequencing Core. WSB/EiJ mice are genotyped with forward primer, 5' GAGGTTGCCCTTGGTTGGTGAAGC, and reverse primer, 5' ACAAAATCTGGAAGACAACACTGG. PCR product is subsequently digested by *Alu*I endonuclease.

RT-PCR

RNA was prepared from brain, subjected to DNAse treatment, and synthesized into first-strand cDNA. Transgene expression was assessed with a forward primer in exon 18 and a reverse primer in exon 19 of *Fig4*. RT-PCR was performed with various numbers of cycles to establish linear amplification. The results 25 cycles of amplification are shown in Figure 3-2.

Wire hang

Neuromuscular strength was tested with the wire hang test (McKinney et al., 2008). Mice were placed on a wire mesh and gently shaken so that the mouse firmly griped the wire. The mesh was turned upside down and the trial ends when the mouse falls off or 60 seconds has elapsed. Time spent hanging was measured. Mice were weighed at the end of the trial.

Acknowledgements

I thank Sarah Bergren for her assistance in preparing the RNA from brain and performing the expression experiments. I thank Adrienne Grant for her expertise and assistance in genotyping all the mice described in this chapter. I thank the University of Michigan Transgenic Core for their advice in designing the transgene described.

CHAPTER IV

MUTATION OF THE PI(3,5)P2 REGULATOR VAC14 CAUSES A LETHAL NEUROLOGICAL DISORDER IN THE *INGLS* MOUSE MUTANT*

Introduction

Missense mutations offer a unique opportunity to determine the function of genes. A single amino acid substitution often does not result in complete loss-of-function. Study of multiple amino acid substitutions can define multiple functions of a gene (Oliver et al., 2007). An allelic series is a collection of organisms with different mutations in the same gene and can reveal unexpected function and phenotypes, as it is often difficult to predict, *a priori,* what a single amino acid change will do.

Fab1, Vac14, and Fig4 regulate the levels of PI(3,5)P2. PI(3,5)P2 is synthesized from PI3P by the kinase Fab1 (Cooke et al., 1998; Gary et al., 1998). Fig4 dephosphorylates PI(3,5)P2 to make PI3P. Vac14 does not have enzymatic activity, but functions as a scaffolding protein and activator of Fab1 activity (Bonangelino et al., 2002; Dove et al., 2002). Loss of Vac14 results in large yeast vacuoles and abnormal PI(3,5)P2 levels. Under basal conditions, Vac14 null yeast cells have undetectable levels of PI(3,5)P2. Vac14 null cells

are also defective in hyperosmotic shock induced elevation of PI(3,5)P2 (Duex et al., 2006b). Loss of Fig4 produces a phenotype that is similar to, but less severe than loss of Vac14.

Complete loss of *Vac14* in mouse results in severe neurodegeneration and perinatal lethality (Zhang et al., 2007). *Vac14* null mice display severe degeneration in the brain and peripheral ganglia, including the dorsal root ganglia (DRG) and trigeminal ganglia. Hydrocephalus is also apparent in brains from *Vac14* null mice. Neurons and cultured fibroblasts from *Vac14* null mice accumulate large cytoplasmic vacuoles of late endosome or lysosome origin. Importantly, *Vac14* null fibroblasts display decreased levels of PI(3,5)P2 (Zhang et al., 2007).

Loss of *Vac14* in mammalian cells is similar to loss of Vac14 in yeast. Both result in abnormal enlargement of late endosome/lysosome compartments as well as decreased production of PI(3,5)P2. Loss of *Fig4*, the PI(3,5)P2 5-phosphatase, in mouse closely resembles loss of *Vac14*, with similar neurodegeneration and cellular phenotypes. These results suggest that Vac14 and Fig4 function are well conserved between yeast and mammals.

Fab1, Fig4 and Vac14 form a multi-protein complex in mammalian cells (Sbrissa et al., 2007), but little is known as to how these proteins interact and whether there are other components of this complex. These interactions are very

intricate. The presence of all of these proteins is required for proper functioning of the entire complex (Chow et al., 2007; Duex et al., 2006a; Duex et al., 2006b; Zhang et al., 2007). Analysis of other mouse mutants in this pathway would further our understanding of these interactions, as well as the role of PI(3,5)P2 in the nervous system.

To identify other mouse mutants of *Fab1*, *Vac14*, and *Fig4*, I searched the Neuromice database (http://www.neuromice.org) and the Jackson Lab Mutant Mouse Resource (JAX MMR, http://mousemutant.jax.org) for mutants with neurological and/or coat color defects. I limited my search to the three chromosomes containing *Fab1* (chr. 1), *Vac14* (chr. 8), and *Fig4* (chr. 10). The mouse mutant *infantile gliosis (ingls*) was identified on mouse chromosome 8 from the Jackson Lab Mutant Mouse Resource (http://mousemutant.jax.org/gliosis_paper.html). *ingls* mice have pale coat color (Figure 4-1a), severe movement disorder, and lethality by 3 weeks of age. *ingls* mice display severe hydrocephalus and vacuolization throughout the brain, including the cortex, thalamus, and brainstem. Prior to the striking neurodegeneration, profound astrogliosis is apparent in the brain. Interestingly, no degeneration in the spinal cord or dorsal root ganglia (DRG) is observed. All other organs appeared to be unaffected (see results and http://mousemutant.jax.org/gliosis_paper.html). These features are similar to those observed in null mutants of *Fig4* and *Vac14* (Chow et al., 2007; Zhang et al., 2007).

ingls is a recessive mutation and was previously linked to mouse chromosome 8 between microsatellite markers *D8Mit33* (98.6 Mb) and *D8Mit200* (117.2 Mb) (http://mousemutant.jax.org/gliosis_paper.html). *Vac14* lies within this 18.6 Mb nonrecombinant interval at 113.1 Mb. The phenotype of *ingls* and presence of *Vac14* within the nonrecombinant region led me to hypothesize that *ingls* is an allele of *Vac14*.

Identification of additional mutant alleles of *Fig4* and *Vac14* will further our understanding of the role of these proteins and PI(3,5)P2 in the nervous system. Here I report the mouse mutant *ingls* is a new allele of *Vac14*.

Results

Identification of a *Vac14* mutation in *ingls*

Homozygous *ingls* DNA was ordered from the Jackson Lab. Sequencing of all 19 exons of *Vac14* revealed a missense mutation (c467 T>G) resulting in the amino acid substitution L156R (Figure 4-1b). *ingls* arose on the DBA/2J inbred mouse line. L156R is not present in DBA/2J mice (not shown), indicating that L156R is most likely the pathogenic mutation in *ingls* mice. The L156R mutation is distinguished by genomic PCR and subsequent digest by the *Sac*I endonuclease (Figure 4-1c). Leucine 156 is evolutionarily invariant in vertebrates, invertebrates and yeast (Figure 4-1d).

Noncomplementation of *Vac14*$^{-/-}$ and *ingls*

To provide additional evidence that *Vac14* ^{L156R} is the mutation responsible for *ingls*, I performed a complementation test with a null allele of *Vac14* (Vac14$^{-/-}$) (Zhang et al., 2007). Unaffected *ingls/+* heterozygous mice were mated with unaffected *Vac14*$^{+/-}$ heterozygous mice. All mice born with genotype *Vac14*$^{L156R/-}$ (25%) were severely affected, dying before 14 days of age. Several mice died on P1, and the survivors were runted, diluted in color (Figure 4-2) and had a severe movement disorder. All other genotypes were unaffected and appeared at the expected Mendelian ratio (Figure 4-2b). *ingls* failed to complement the *Vac14* null allele, confirming that the *Vac14*^{L156R} allele is the pathogenic mutation.

Phenotypic characterization of *ingls* (*Vac14*$^{L156R/L156R}$) and *Vac14*$^{L156R/-}$ mice

Homozygous *ingls* mice (referred to as *Vac14*$^{L156R/L156R}$) and *Vac14*$^{L156R/-}$ mice display severe tremor and movement disorder. Severe hydrocephalus was suggested by the domed heads of the mice. This was confirmed with sagittal sections of brain from *Vac14*$^{L156R/L156R}$ and *Vac14*$^{L156R/-}$ mice (Figure 4-3). Similar to *Vac14*$^{L156R/L156R}$ mice (Figure 4-4), *Vac14*$^{L156R/-}$ mice displayed vacuolization throughout the brain (Figure 4-5), including the cortex, thalamus, cerebellar nuclei, and brainstem. No degeneration was observed in DRGs or motor neurons in either mouse (Figure 4-6). It should be noted that half the *Vac14*$^{L156R/-}$ mice born were dead on P1. The analysis presented here is

representative of mice that survived past P1. It is possible that mice dying on P1 have much more severe neurodegeneration.

Vac14$^{L156R/L156R}$ fibroblasts display lowered PI(3,5)P2 levels

Vac14$^{L156R/L156R}$ brain extracts were probed for Vac14 protein expression. Homozygous *Vac14*$^{L156R/L156R}$ mice had equal amounts of Vac14 as their wildtype littermates (Figure 4-7a). The *Vac14*^{L156R} mutation does not result in unstable protein and may have altered function.

To determine the functional consequences of the *Vac14*^{L156R} mutation, fibroblasts were cultured from *Vac14*$^{L156R/L156R}$ and wildtype littermates. The fibroblasts accumulated numerous large cytoplasmic vacuoles (Figure 4-7b, top right panel) similar to the *Vac14* and *Fig4* null fibroblasts (Chow et al., 2007; Zhang et al., 2007). The abnormal vacuole phenotype was rescued by transfection with wildtype *Vac14*, further indicating that *Vac14*^{L156R} is loss-of-function. (Figure 4-7b). Large cytoplasmic vacuoles are a consequence of abnormal PI(3,5)P2 levels (Ikonomov et al., 2002a; Ikonomov et al., 2001; Rutherford et al., 2006). *Vac14* null fibroblasts have significantly lower PI(3,5)P2 levels (Zhang et al., 2007). To test if *Vac14*^{L156R} alters PI(3,5)P2 levels, phosphoinositides were measured from *Vac14*$^{L156R/L156R}$ and wildtype littermate fibroblasts. *Vac14*$^{L156R/L156R}$ fibroblasts showed a significant decrease in PI(3,5)P2 levels as compared to wildtype cells (Figure 4-7c). There was no

change in other phosphoinositide levels. These results demonstrate that *Vac14*^{L156R} and the *Vac14* null allele have similar cellular phenotypes.

Vac14^{L156R} disrupts protein interaction in yeast

To probe yeast Vac14 protein interactions with yeast Fab1 and Fig4, a directed yeast two-hybrid assay was undertaken. Wildtype Vac14 interacted with itself. Wildtype Vac14 also strongly interacted with Fig4 and Fab1 (Figure 4-8). To test if the Vac14^{L156R} mutation affected these interactions, the same directed yeast two-hybrid was performed on the mutant Vac14 protein. The homologous amino acid change in yeast is L149R. Vac14^{L149R} strongly interacted with wildtype Vac14 and Vac14^{L149R}. Interestingly, Vac14^{L149R} failed to interact with Fab1. Interaction with Fig4 was preserved (Figure 4-8). These data indicate that the *Vac14*^{L156R} mutation directly affects the assembly of the core protein complex that regulates PI(3,5)P2, by disrupting interaction with Fab1.

Discussion

I identified a new spontaneous missense mutation of *Vac14* in the mouse mutant *infantile gliosis* (*ingls*). Sequencing identified the amino acid substitution, L156R. A complementation test with the *Vac14* null allele confirmed that *Vac14*^{L156R} is the pathogenic mutation in *ingls (Vac14*$^{L156R/L156R}$).

The phenotype of the *ingls* mouse is very similar to the *Vac14* null mouse (Zhang et al., 2007). Both display hydrocephalus and vacuolization throughout

the brain. Interestingly, no degeneration is observed in *ingls* DRGs. Severe degeneration of the DRGs is observed in the *Vac14* null mouse (Table 4-1) (Zhang et al., 2007). The difference in DRG degeneration suggests peripheral neurons are less sensitive to the loss of *Vac14* function, while the CNS is highly dependent on *Vac14* function.

The compound heterozygous *Vac14*$^{L156R/-}$ mouse allows us to evaluate whether gene dosage is important to *Vac14* function. *Vac14*$^{L156R/-}$ mice carry the null mutation and the *Vac14*^{L156R} mutation, expressing 50% partial functioning protein. Compound heterozygous mice display hydrocephalus and vacuolization throughout the brain. No degeneration is detected in motor neurons and DRGs. Fifty percent partially functioning *Vac14* has a similar effect as 100% partially functioning *Vac14* on the central and peripheral nervous system.

The degeneration in the nervous system of *Vac14*$^{-/-}$, *Vac14*$^{L156R/\ L156R}$, and *Vac14*$^{L156R/-}$ mice suggests that the CNS is very sensitive to loss of *Vac14* function (Table 4-1). The DRGs are only affected by complete loss of *Vac14*. Despite the qualitative similarity of the CNS degeneration, the onset of neurodegeneration in the mutant mice varies. *Vac14*$^{-/-}$ mice die on P1 and CNS degeneration begins during embryogenesis (Zhang et al., 2007). *Vac14*$^{L156R/\ L156R}$ and *Vac14*$^{L156R/-}$ mice both begin to develop hydrocephalus during the first week of age. This demonstrates that the *Vac14*^{L156R} protein retains some function.

While null mice die on P1, *Vac14*$^{L156R/\ L156R}$ and *Vac14*$^{L156R/\ -}$ mice have a range of survival from P1 to P21. The range of survival time may be due to stochastic variation during development. There may be a small developmental window when Vac14 is essential and the Vac14^{L156R} protein may have enough function some of the time. The variation could also be due to modifier genes. The *Vac14*$^{L156R/L156R}$ mice are congenic C57BL/6J, but the compound heterozygous mice are on a mixed background. Evidence from studies with the *Fig4* and *Vac14* null mice suggests that modifier genes may affect survival (Chow CY, unpublished data). Further analysis of the time course of degeneration in each of these mutant mice will shed light on this question.

The milder phenotype of the *ingls* mice indicate that the *Vac14*^{L156R} protein still has residual function and is not a null allele. However, *Vac14* null cells and *Vac14*$^{L156R/L156R}$ fibroblasts show 50% decrease in PI(3,5)P2 levels. This demonstrates that the *Vac14*^{L156R} mutation results in decreased PI(3,5)P2 synthesis, most likely caused by loss of Fab1activation. The decrease in PI(3,5)P2 levels is confirmed by the presence of large cytoplasmic vacuoles in *Vac14*$^{L156R/L156R}$ fibroblasts.

Leucine 156 is evolutionarily invariant, suggesting that it is crucial for normal *Vac14* function. Because *Vac14*^{L156R} does not destabilize the protein, I hypothesized that it may affect critical protein-protein interactions. Leucine 156 is part of a dileucine pair (Figure 4-1d and 4-9). There are seven total conserved

dileucine pairs in *Vac14* (Figure 4-9) (Dove et al., 2002). Dileucine repeats have been shown to be involved in adaptor protein binding during clathrin-coated vesicle formation (Liu et al., 1998; Vowels and Payne, 1998). Further analysis of the wildtype and *Vac14*^{L156R} proteins is needed to determine if clathrin coated vesicle transport is abnormal in these mice.

Dileucine motifs are also important for protein-protein interactions that are involved in sorting proteins to the endosome and lysosome (Bonifacino and Traub, 2003). Directed yeast two-hybrid results suggest that L156R disrupts interaction within the PI(3,5)P2 complex. Fab1 phosphorylates PI3P to make PI(3,5)P2 and the function of Fab1 requires Vac14 and Fig4. Fig4 dephosphorylates PI(3,5)P2 to make PI(3)P. These three proteins have been shown to be in a complex in mammalian cells (Sbrissa et al., 2007) as well as in yeast (Rudge et al., 2004). We show that wildtype yeast Vac14 interacts with yeast Fig4 and Fab1. Vac14 also interacts with itself, confirming previous results (Dove et al., 2002). When yeast Vac14^{L156R} was tested for these interactions, it interacted with wildtype Vac14 and Fig4, as well as Vac14^{L156R}. Vac14^{L156R} failed to interact with Fab1. These data suggests that the pathogenicity of Vac14^{L156R} results from loss of interaction with Fab1. Fab1 may not be fully activated by Vac14^{L156R}. It remains to be seen whether this is also true *in vivo*.

Leucine 156 also lies within a HEAT motif. HEAT motifs are generally composed of two alpha helices which form a helical hairpin and a hydrophobic

core. HEAT repeats are approximately 45 amino acids in length and are repeated in tandem. HEAT repeats are often found in cytoplasmic proteins involved in vesicle transport and mediate protein-protein interactions. Tandem arrays of HEAT motifs can fold into a parallel stack arrangement and proteins have been found to interact in the grooves or outside edges of the alpha helices (Andrade and Bork, 1995; Andrade et al., 2001a; Andrade et al., 2001b). There are nine HEAT motifs in Vac14. Leucine 156 resides in the second repeat (Figure 4-9). It is possible that L156R disrupts the structure of the HEAT repeat and disrupts protein interactions that are critical for endosome to lysosome vesicle transport. Loss of interaction with Fab1 may result from disruption of the dileucine repeat, the HEAT motif, or both.

ingls mice were initially described and deposited in the JAX MMR because of significant astrogliosis. Astrogliosis is often a secondary effect of neurodegeneration (Correa-Cerro and Mandell, 2007). It remains to be seen whether the astrogliosis observed in *ingls* is primary or secondary. Conditional deletion of *Vac14* in astrocytes versus neurons will answer this. Further analysis is needed to determine why the mutation $Vac14^{L156R}$ spares the DRGs, but not the brain. Analysis of protein-protein interactions within the PI(3,5)P2 complex and discovery of other mouse mutants that affect the PI(3,5)P2 complex will further extend structure-function analysis.

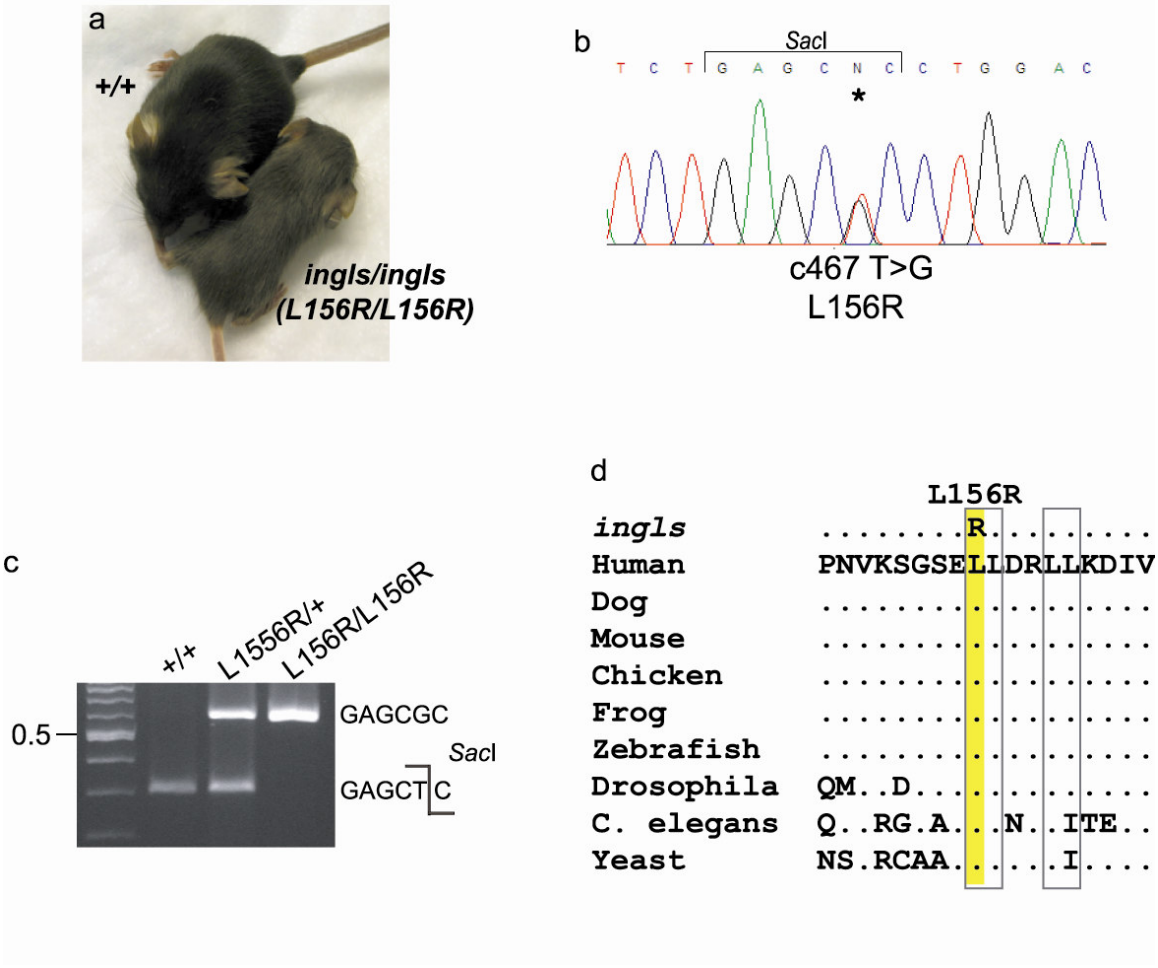

Figure 4-1. A new allele of *Vac14* in the *ingls* mouse. a. *ingls/ingls* homozygous mice (*L156R/L156R*) are diluted in pigment and smaller than wildtype littermates. **b**. Sequence of exon 4 from heterozygous *ingls/+* genomic DNA. **c**. Genotyping assay for the $Vac14^{L156R}$ mutation which destroys a *Sac*I restriction site. **d**. Leucine residue 156 is evolutionarily invariant from mammals to yeast. Boxes mark two dileucine pairs.

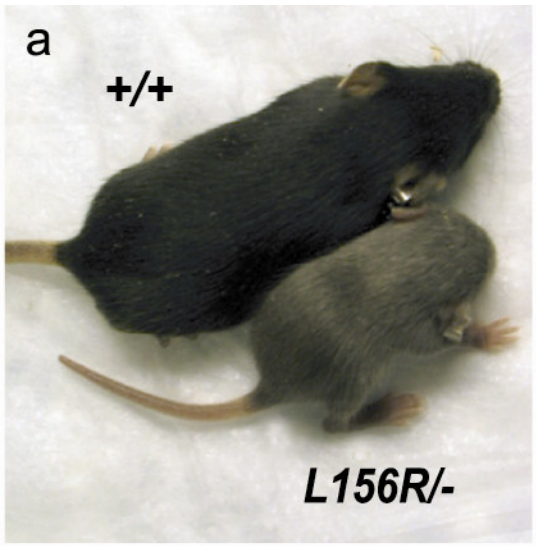

b

	L156R/-	*L156R/+*	*+/-*	*+/+*
number born	5	7	6	6
number at P14	0	7	6	6

Figure 4-2. *ingls (Vac14^{L156R})* does not complement the *Vac14* null allele. A complementation test was performed by crossing *ingls/+* and *Vac14$^{+/-}$* mice. **a.** Compound heterozygotes *Vac14$^{L156R/-}$* exhibit reduced size and diluted pigmentation in comparison with wildtype littermates. **b.** *Vac14$^{L156R/-}$* mice are born at Mendelian ratios, but survive for less than 2 weeks after birth. All other genotypes were unaffected.

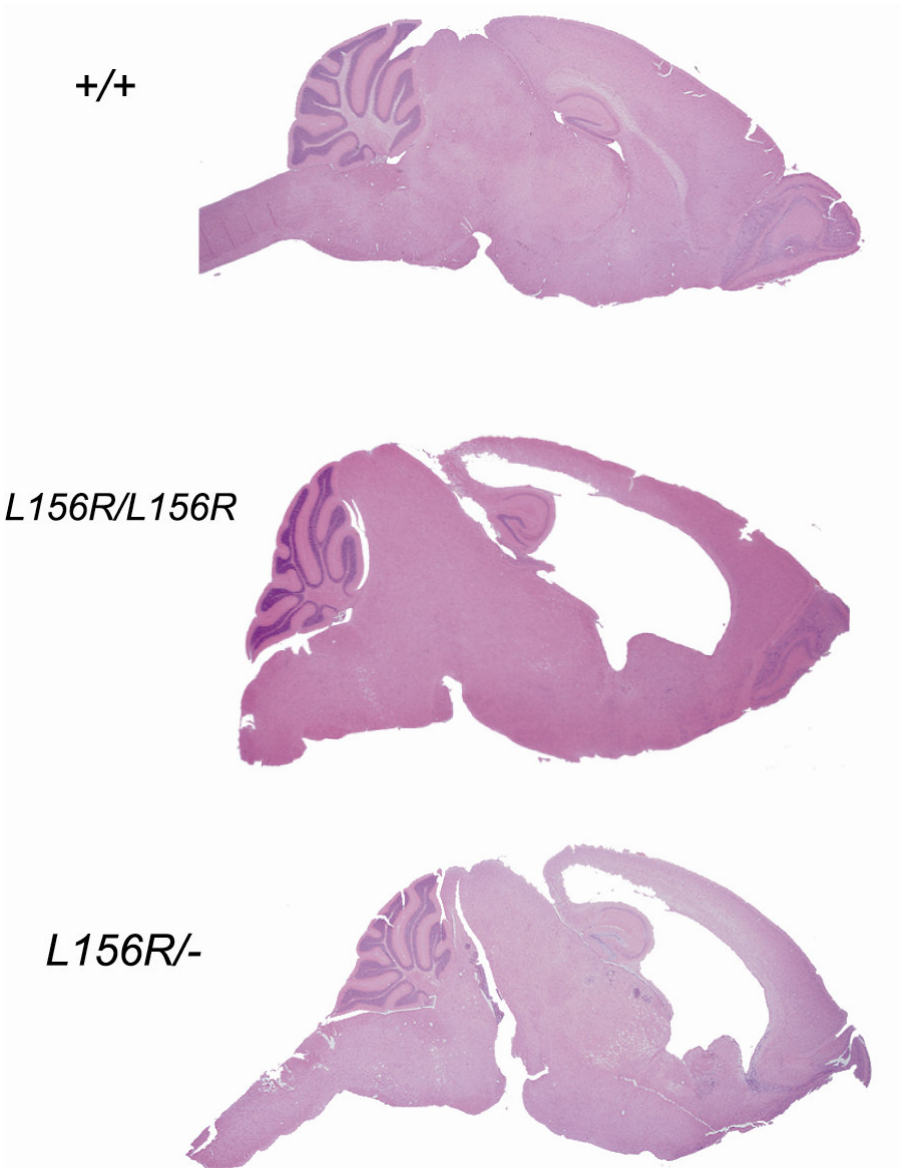

Figure 4-3. Hydrocephalus in *Vac14*$^{L156R/L156R}$ and *Vac14*$^{L156R/-}$ brain. Severe hydrocephalus is observed in *Vac14*$^{L156R/L156R}$ and *Vac14*$^{L156R/-}$ brain as compared to wildtype. Sagittal sections are from P14-P16. H&E.

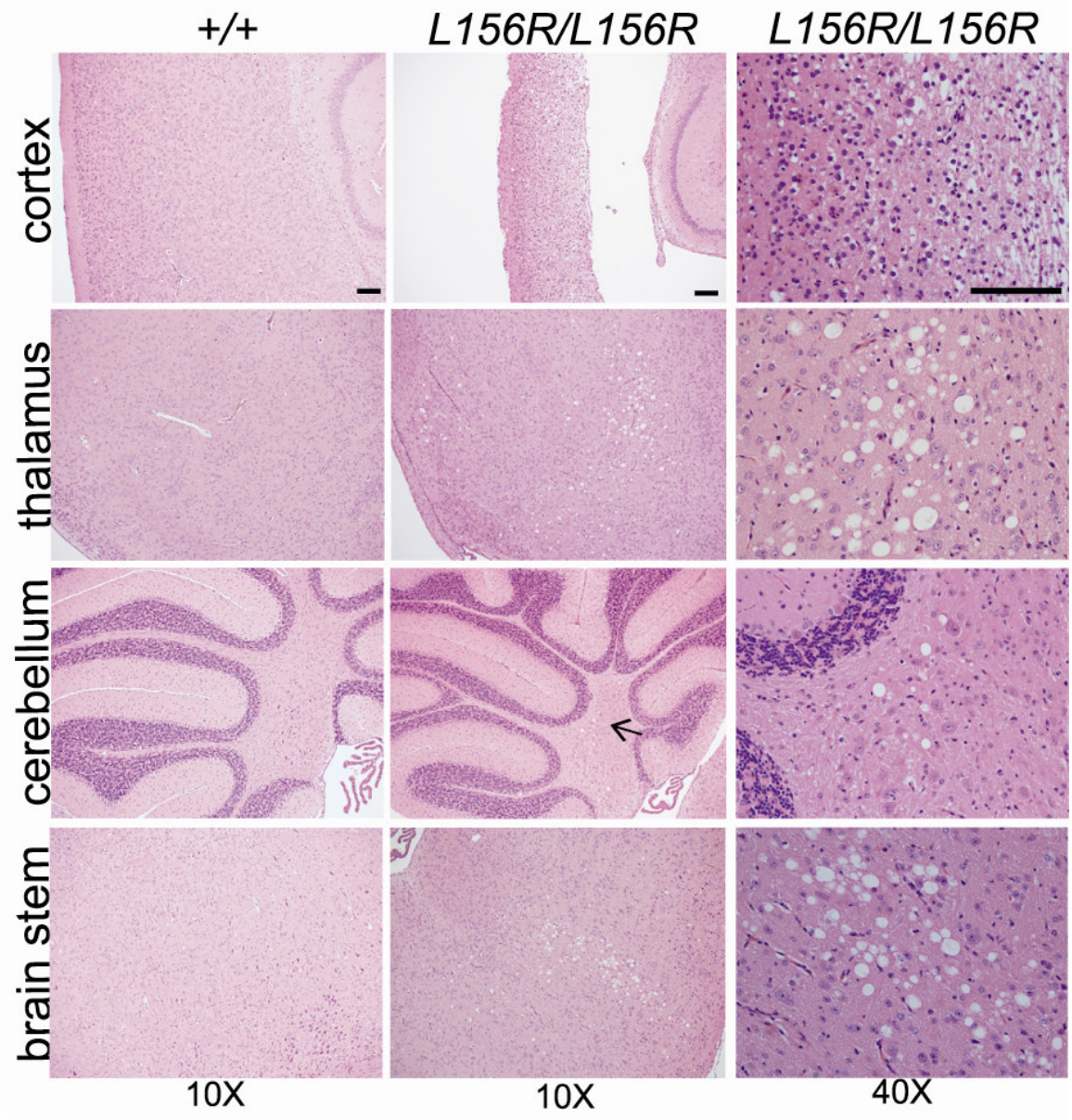

Figure 4-4. Neurodegeneration in brain of *Vac14*$^{L156R/L156R}$ mice. Significant neurodegeneration is observed in *Vac14*$^{L156R/L156R}$ mice. Vacuolation of the brain is evident in regions listed. Lower magnification images (10X) are shown for wildtype and *Vac14*$^{L156R/L156R}$ mice in the left and middle columns. The right column shows higher magnification images (40X) of degenerated regions in *Vac14*$^{L156R/L156R}$ brain. Sections are from P16 mice. Arrow indicates degenerated tissue in cerebellar nuclei. H&E. Scale bars: 100 microns

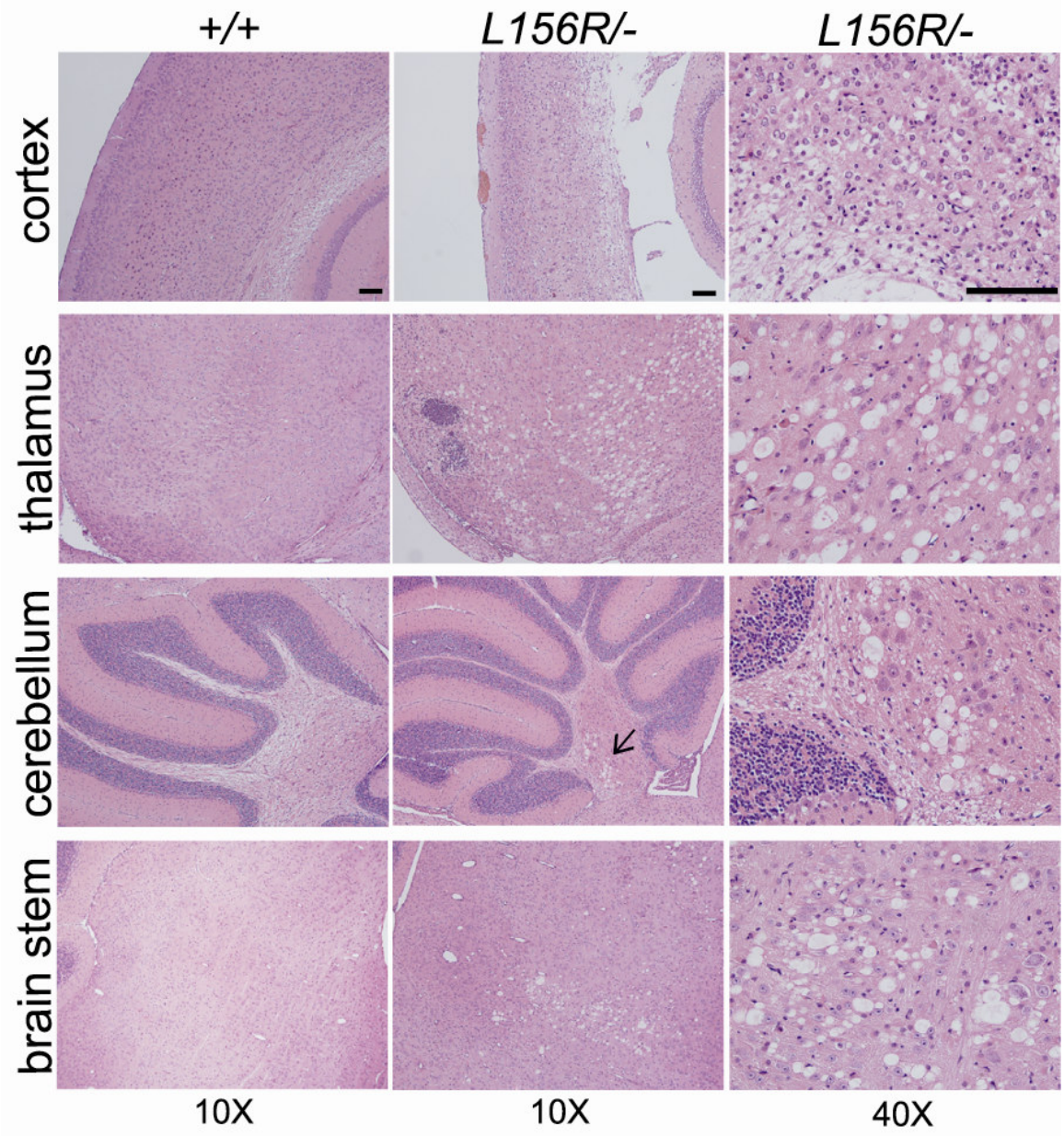

Figure 4-5. Neurodegeneration in brain of *Vac14*$^{L156R/-}$ mice. Significant neurodegeneration is observed in *Vac14*$^{L156R/-}$ mice. Vacuolation of the brain is evident in regions listed. Lower magnification images (10X) are shown for wildtype and *Vac14*$^{L156R/-}$ mice in the left and middle columns. The right column shows higher magnification images (40X) of degenerated regions in *Vac14*$^{L156R/-}$ brain. Sections are from P14 mice. Arrow indicates degenerated tissue in cerebellar nuclei. H&E. Scale bars: 100 microns

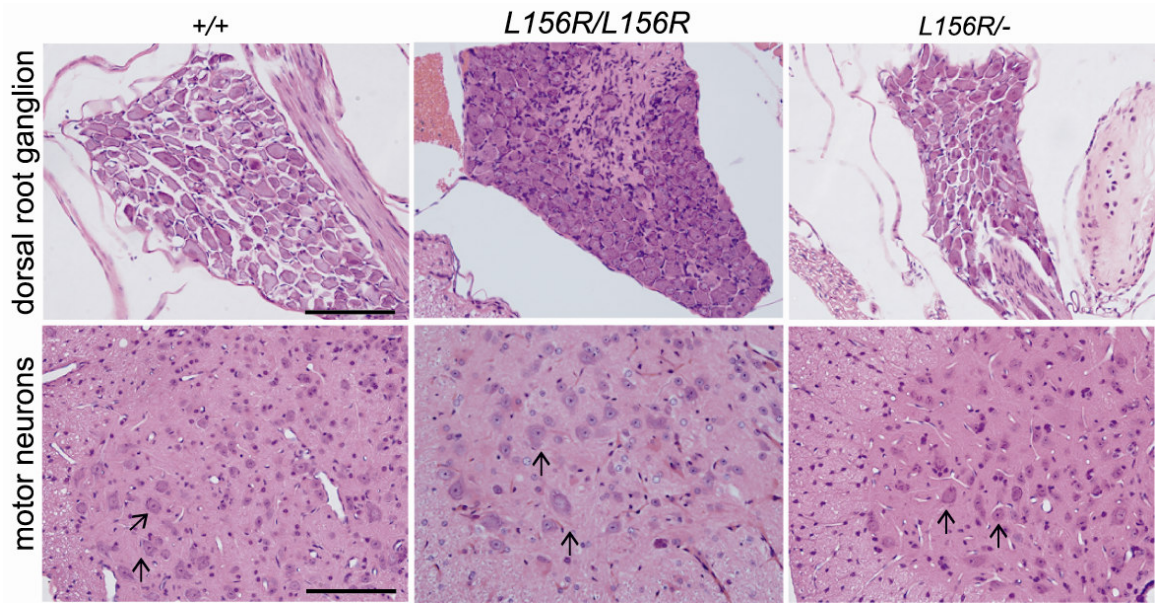

Figure 4-6. No degeneration in DRGs and motor neurons in *Vac14*$^{L156R/L156R}$ *Vac14*$^{L156R/-}$ mice. DRG and spinal motor neurons are shown. No visible degeneration is detected in either tissue. Arrows indicate motor neurons. H&E. Scale bars: 100 microns.

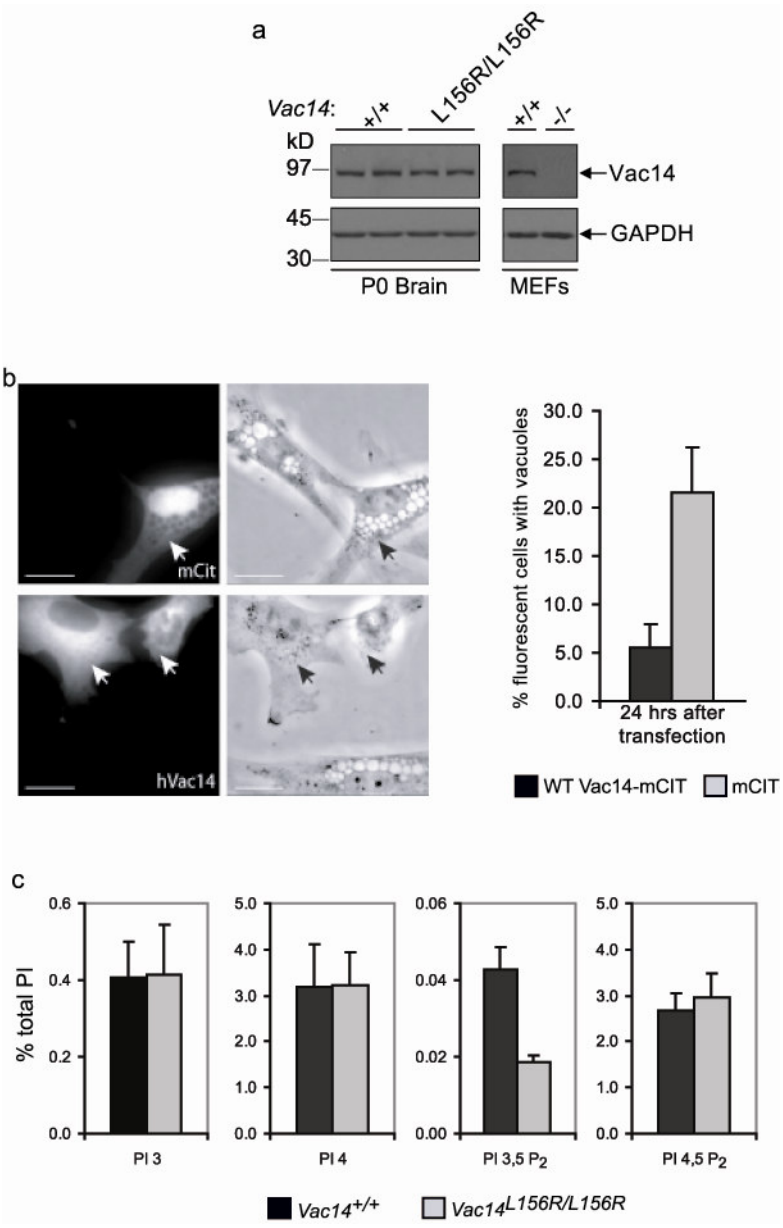

Figure 4-7. *Vac14*^{L156R} causes a defect in the synthesis of PI(3,5)P2. a. *Vac14*$^{L156R/L156R}$ mouse brain extracts have equal amounts of Vac14 protein compared with brain extract of wildtype mice. The specificity of the antiserum is demonstrated by the lack of signal in fibroblasts from Vac14$^{-/-}$ null mice. GAPDH provides a loading control. **b.** *Vac14*$^{L156R/L156R}$ fibroblasts are filled with large cytoplasmic vacuoles. Expression of human Vac14-mCitrine in *Vac14*$^{L156R/L156R}$ fibroblasts rescues vacuolation phenotype. >100 cells were counted. Arrows indicate transfected cells. Scale bars, 20 microns. mCIT, mCitrine **c.** PI(3,5)P2 levels are decreased in *Vac14*$^{L156R/L156R}$ cultured fibroblasts. Other phosphoinositides were unchanged. Error bars represent SD.

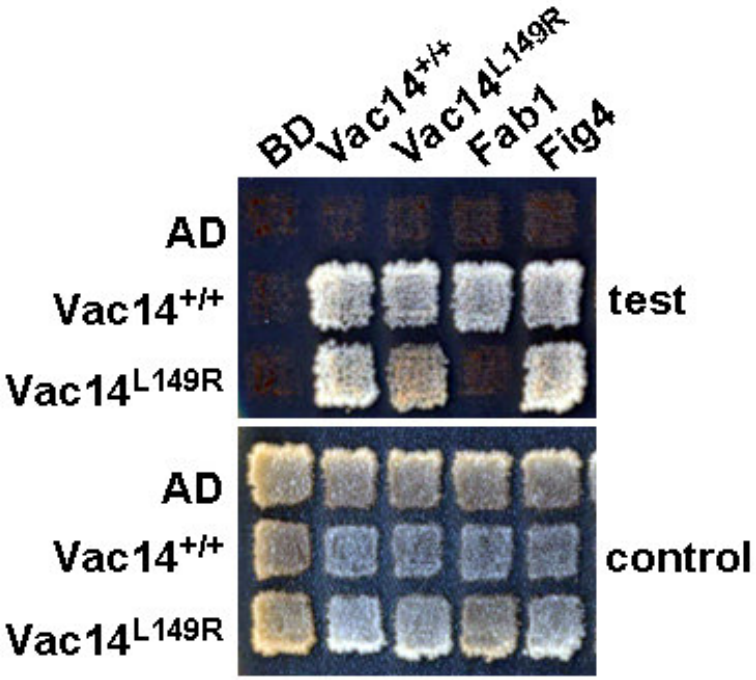

Figure 4-8. Yeast Vac14$^{L>R}$ fails to interact with Fab1. Directed yeast two-hybrid analysis. Wildtype yeast Vac14 and Vac14^{L149R} corresponding to mouse L156R were tested for interaction with wildtype and mutant Vac14, as well as Fab1 and Fig4. Wildtype Vac14 interacts with all proteins tested. Vac14^{L149R} interacts with itself, as well as wildtype Vac14 and Fig4. Vac14^{L149R} fails to interact with Fab1. Top panel is experimental data. Bottom panel is a control indicating that all yeast strains grow well on rich media. The activating domain (AD) and binding domain (BD) do not interact with the proteins tested.

Table 4-1. Comparison of *Fig4* and *Vac14* mutant mice

gene	genotype	survival	coat color	spleen degeneration	HC	neurodegeneration at death		
						brain	DRG	motor neuron
Fig4	*-/-*	prenatal or 3-6 weeks	White to light gray	+	+	cortex thalamus midbrain brainstem	+	+
	-/-, Tg^{I41T}	>7 months	White to light gray	?	?	?	?	?
Vac14	*-/-*	P1	N/A	-	+	cortex thalamus midbrain brainstem	+	-
	L156R/-	P1 to P21	gunmetal	-	+	cortex thalamus midbrain brainstem	-	-
	L156R/L156R	P1 to P21	gunmetal	-	+	cortex thalamus midbrain brainstem	-	-

* data for I41T/plt mice is as of 6 months of age.
+ presence of degeneration
- absence of degeneration
HC - hydrocephalus

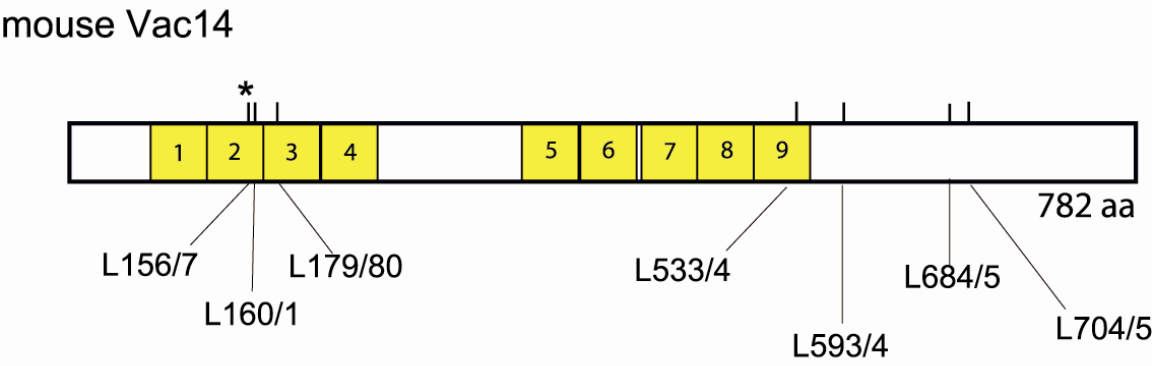

Amino acid position of HEAT repeats in Vac14

	mouse	yeast
1	79-126	81-119
2	129-170	122-160
3	171-208	201-239
4	211-250	242-280
5	355-392	387-425
6	394-428	428-466
7	437-475	475-513
8	478-524	516-553
9	526-562	556-592

Figure 4-9. Vac14 functional protein domains. Vac14 has seven dileucine repeats and nine HEAT repeats. The mouse Vac14 protein is 782 amino acids. Dileucine repeats are indicated by vertical lines and the amino acid position is below. HEAT repeats are indicated by yellow boxes (numbered 1-9). Table shows amino acid position of HEAT repeats in mouse and yeast Vac14. Asterisk (*) indicates position of *Vac14*^{L156R} mutation.

Materials and Methods

Animals

ingls mice were obtained on a C57BL/6J background from the Jackson Lab (stock number: 003095). *Vac14*$^{-/-}$ mice (Vac14$^{\beta\text{-geo}/\beta\text{-geo}}$) were previously described (Zhang et al., 2007). Briefly, *Vac14*$^{-/-}$ mice were created from gene-trap embryonic stem cell line. *Vac14*$^{+/-}$ mice are maintained on a mixed background of strain 129 and C57BL/6J. Complementation test with *Vac14*$^{-/-}$ was performed by mating *Vac14*$^{+/-}$ X *ingls/+*. Mice were genotyped as described below and monitored for phenotypes. P1 is defined as the day of birth. This research was approved by the University of Michigan Committee on Use and Care of Animals. Animals were housed and cared for in accordance with NIH guidelines.

Sequencing and genotyping

ingls genomic DNA was ordered from the Jackson Laboratory. The *Vac14* coding sequence was sequenced with 19 primer pairs flanking the genomic sequence of all 19 exons. PCR was carried out with the PCR Core Kit (Qiagen). PCR products were sequenced by the University of Michigan Sequencing Core. *Vac14*^{L156R} is genotyped by restriction enzyme digest. The *Vac14*^{L156R} mutation destroys a *Sac*I *restriction* site. Genomic PCR is performed (Forward - 5'CAGCCAGTGGGAACAACCGTGTGA and Reverse-5' ACATAGACATGCAAGCAGGCAAAG). PCR product is digested with SAC1. Wildtype mice are indicated by a 300 bp and 296 bp band. Homozygous

Vac14$^{L156R/L156R}$ mice are indicated by a 596 bp band. Heterozygous mice are indicated by the presence of all three bands.

Cell Culture and immunoflouresence

Primary fibroblasts were cultured as previously described (Chow et al., 2007; Zhang et al., 2007). Fibroblasts were obtained from P1 mice. Transfection of fibroblasts and Western blot analysis was performed as previously described (Zhang et al., 2007). Cells were transfected and 24 hours after transfection were fixed with 4% paraformaldehyde in PBS for 10 min at room temperature. Fluorescent cells were scored for the presence of vacuoles. Each data point is a mean of three independent experiments. For each experiment >100 cells were counted. Images of cells were taken on an Axioscope 2 (Carl Zeiss MicroImaging, Jena, Germany) by using a LUCPlanFL N 40×/0.60 Ph2 objective with a DeltaVision microscope system.

Phosphoinositide assays

Levels of phosphoinositides were measured as previously described (Chow et al., 2007; Zhang et al., 2007). Primary fibroblasts were starved in inositol-free DMEM for 12 h and labeled with myo-[2-^{3}H]inositol for 36 h. Lipids were extracted, deacylated, and analyzed by anion-exchange HPLC chromatography.

Histopathology

Mice were dissected and tissues were fixed in 10% buffered formalin. Histology was performed as previously described (Chow et al., 2007).

Yeast two-hybrid analysis

For the pGAD or GBD fused Vac14p (Full length), Full length Vac14 DNA was amplified by PCR and subcloned into XmaI-SalI site. For the pGAD or GBD fused vac14 L149R, CTA(149 aa) was changed to CGA by site directed mutagenesis. For the pGBD fused Fab1p (807-1085 aa), a Fab1p DNA fragment amplified by PCR and subcloned into EcoRI-BglII site. For the pGBD fused Vac7p (394-918 aa), Vac7 DNA fragment was amplified by PCR and subcloned into SmaI-SalI site. For the pGBD fused Atg18p (Full length), Full length Atg18 DNA fragment was amplified by PCR and subcloned into EcoRI-SalI site. For the pGBD fused Fig4p (Full length), Fig4 DNA fragment was amplified by PCR and subcloned into BasmHI-PstI site. Plasmids were cotransformed into the yeast strain PJ69-4A. Transformants were plated onto SC-Leu-Trp, replica-plated onto SC-Leu-Trp-Ade-His + 3AT, and grown for 7 days at 24 ºC.

Websites

Neuromice database (http://www.neuromice.org)

Jackson Lab Mutant Mouse Resource (http://mousemutant.jax.org)

infantile gliosis description (http://mousemutant.jax.org/gliosis_paper.html)

Acknowledgements

I would like to thank the JAX Mouse Mutant Resource for their careful cataloging and description of mutant mice. This project was possible because of their observant eye. I would like to thank Dr. Lois Weisman and her lab for their expertise. They generously provided the *Vac14* null mice. Dr. Sergey Zolov performed the Western blot, the fibroblast cell culture experiments, and the phosphoinositide measurements. Natsuko Jin performed the yeast two-hybrid experiments. Yanling Zhang identified the HEAT elements in Vac14. I would like to thank Adrienne Grant for her assistance in genotyping all the mice described.

Notes

*This chapter is in preparation for submission as a manuscript entitled “A missense mutation of the PI(3,5)P_2 regulatory protein VAC14 disrupts interaction with the lipid kinase FAB1/PIKFYVE and produces a lethal neurological disorder in the *ingls* mouse” by Natsuko Jin[@], Clement Y. Chow[@], Li Liu, Sergey N. Zolov, Rod Bronson, Patricia F. Ward-Bailey, Muriel Davisson, Daniel Goldowitz, Lois S. Weisman[#] and Miriam H. Meisler[#]

@Co-First authors - these authors contributed equally to the work

#Co-Senior authors

CHAPTER V

CONCLUSIONS AND FUTURE DIRECTIONS

In this concluding chapter I will summarize the important findings of my thesis work and explain how these results demonstrate the importance of PI(3,5)P2 function in yeast and mammals. Previous yeast work will be reviewed and I will discuss how yeast data can inform future study of PI(3,5)P2 in mammals. I have shown that mutations in the PI(3,5)P2 pathway cause human neurological disease. I will discuss the different human diseases that I have screened and I will also propose other human diseases that warrant investigation.

PI(3,5)P2 in mammals and yeast

I have described two new mouse mutants in the PI(3,5)P2 pathway, *pale tremor* and *ingls*. *pale tremor* is a null allele of *Fig4* and *ingls* is a missense mutation in *Vac14*. I also contributed to characterization of a third mutant, the *Vac14* null mouse (Zhang et al., 2007). Together, these three mouse mutants provide new information regarding the importance of PI(3,5)P2 to the nervous system. *pale tremor* and *ingls* also demonstrate the importance of PI(3,5)P2 signaling to coat pigmentation. These mutants are the first descriptions of

perturbed PI(3,5)P2 synthesis in an *in vivo* mammalian system and demonstrate that PI(3,5)P2 regulation is critical to mammals.

In yeast, loss of Fab1, Vac14, or Fig4 result in similar phenotypes, with differing severities. The entire complex is important and each individual protein must function within the PI(3,5)P2 complex. Fab1 phosphorylates PI3P to make PI(3,5)P2. Fig4 dephosphorylates PI(3,5)P2 to PI3P. Vac14 activates Fab1 and is required for Fig4 function (Figure 5-1). Loss of any of these three proteins results in an enlarged vacuole, altered basal PI(3,5)P2 levels (except Fig4), and altered PI(3,5)P2 levels in response to hyperosmotic shock (Dove and Johnson, 2007). Loss of Fab1 is the most severe, followed by loss of Vac14. Loss of Fig4 displays the least severe phenotype (Duex et al., 2006b).

pale tremor, ingls and the *Vac14* null mouse mutants show defects in late endosome/lysosome compartments as indicated by fibroblasts that accumulate enlarged cytoplasmic vesicles that are of lysosomal origin. This closely mimics the enlarged vacuole defect in yeast (Dove and Johnson, 2007), as the vacuole is the yeast equivalent of a mammalian lysosome. These mouse mutants also display significant decreases in PI(3,5)P2 levels. This is similar to the yeast phenotype of reduced basal and reduced hyperosmotic shock-induced levels of PI(3,5)P2 (Dove and Johnson, 2007; Duex et al., 2006a).

The *pale tremor* (*Fig4* null) phenotype is the least severe of the three mutant mice, corresponding to the yeast data where loss of Fig4 results in a mild phenotype. *Fig4* null mice survive to six weeks and brain degeneration does not begin until age P7. Only 40% of cultured *Fig4* null fibroblasts vacuolate. On the other hand, the *Vac14* null mouse dies on P1 and brain degeneration begins during embryonic development. The percentage of *Vac14* null fibroblasts that vacuolate approaches 100%. *ingls* is a missense mutation and not a null allele of *Vac14. ingls* neurodegeneration is less severe than the *Vac14* null allele and survival ranges between P1 and 3 weeks of age. The mouse mutants described demonstrate that loss of *Vac14* is more severe than loss of *Fig4*, similar to observations in yeast.

PI(3,5)P2 and the nervous system

The selective importance of PI(3,5)P2 to the nervous system could not have been predicted from previous studies in yeast. All three mutants display severe neurodegeneration. In the *Fig4* null and *Vac14* null mice, degeneration is present in the central and peripheral nervous system. In the dorsal root ganglia (DRG), the majority of neurons accumulate large cytoplasmic vacuoles, similar to the vacuoles in cultured fibroblasts. Interestingly, DRG neurons from *ingls* do not degenerate. Vacuolated neurons are present in the brain of these three mice, but they are rare and can only be found early in disease. Severe degeneration in the CNS is indicated by the spongiform appearance of the brain tissue (empty spaces in the tissue due to loss of neurons). Spinal motor neurons are affected

late in disease in the *pale tremor* mice. *Vac14* null and *ingls* mice do not display vacuolated motor neurons, but this might be due to the shorter life span of these two mutants.

The small number of vacuolated neurons visible in the brain contrast with the large amount of degeneration observed. Vacuolated neurons may be a transient stage prior to cell death. In addition, the spongiform degeneration may result from axon loss due to the death of neurons that project to affected regions. DRG pathways extend from the ganglia, through the spinal cord, brainstem, thalamus and cortex (Wallengren, 2005). Extensive degeneration is observed in all these regions and may be secondary to the loss of DRG neurons.

PI(3,5)P2 is a ubiquitous signaling molecule required for endosome and lysosome trafficking. It is unclear why perturbation of PI(3,5)P2 metabolism specifically affects neurons, while other tissues appear unaffected. Many other neurological diseases result from dysfunction of ubiquitous genes, including many forms of CMT (Niemann et al., 2006), Huntington's disease (Walker, 2007), and Alzheimer's disease (Zhang and Xu, 2007). Neurons are post-mitotic, thus most neurons that die are not replaced, in contrast to other somatic tissues.

Neurons are very metabolically active and require constant protein synthesis to maintain long dendrites and axons (Kennedy and Ehlers, 2006). Sensory neurons in the DRG and motor neurons in the anterior horn of the spinal

cord have long axons, up to a meter in some instances. These long processes require constant turnover of membrane elements and receptors. Vesicle trafficking is critical to this process. Proteins and lipids are synthesized in the soma and packaged into cytoplasmic vesicles which are delivered through the axon to the target, so-called anterograde vesicle trafficking. Proteins and lipids are recycled as well. Receptors and surface proteins are endocytosed and delivered back into the soma, where they are degraded. Signaling receptors and growth factors are also endocytosed and delivered to the soma to induce signaling that ultimately results in gene expression and growth of an axon. Retrograde trafficking moves cargo from the distal processes and nerve terminals to the soma. Perturbed neuronal trafficking is implicated in several forms of CMT (Niemann et al., 2006) and ALS (Pasinelli and Brown, 2006; Schymick et al., 2007).

The three mouse mutants described allow us to investigate whether PI(3,5)P2 signaling is required for anterograde or retrograde trafficking. We hypothesized that because PI(3,5)P2 controls trafficking between endosomes and lysosomes, neurodegeneration in the *pale tremor* mouse may be a result of perturbed axon trafficking. Two tests of this hypothesis have been carried out. Localization of sodium channel Nav1.6 involves anterograde trafficking of newly synthesized channels to the nodes of Ranvier. Localization of Nav1.6 in sciatic nerve appears normal in *pale tremor* mice (L. Sharkey, unpublished observations). Dr. Michael Q. Kemp (Michigan State University) observed that

the rate of retrograde axonal transport in sciatic nerve is also normal in *pale tremor* mouse, as assessed by transport of horseradish peroxidase from injected muscle to motor neuron soma in the ventral spinal cord (personal communication). Enlarged cytoplasmic vacuoles do not accumulate in the axons of DRG and motor neurons (Zhang et al., 2008). Enlarged vesicles are restricted to the soma. This preliminary data suggests that there are no major defects in anterograde or retrograde trafficking. Additional measurements of neuron-specific processes might reveal the basis for the particular sensitivity of neurons to abnormal PI(3,5)P2 levels.

The disease in the *pale tremor* mouse is classified as a neuronopathy. The neuron soma is first affected and axon loss is secondary. It is clear that neurons are primarily affected because they accumulate large cytoplasmic vacuoles. However, as in many neurodegenerative diseases, it is unclear whether astrocytes are also dysfunctional and contribute to disease. Mutations in MTMR2 cause CMT4B1, a peripheral neuropathy. Conditional deletion of *Mtmr2* revealed that dysfunction of astrocytes was both necessary and sufficient to recapitulate the disease (Bolis et al., 2005). Furthermore, astrocytes have been shown to modulate disease severity in ALS caused by mutations in SOD1, despite being a primary motor neuron disease. SOD1 mutant astrocytes secrete an unknown toxic factor that kills wildtype motor neurons. Wildtype astrocytes protect SOD1 mutant mice and prolong survival (Cassina et al., 2008; Di Giorgio et al., 2007; Nagai et al., 2007; Yamanaka et al., 2008).

The *ingls* mouse was first identified because of extensive astrogliosis. It remains to be seen whether this is primary or secondary to neurodegeneration. Conditional deletion of *Fig4* or *Vac14* in neurons and astrocytes will define the role of astrocytes in PI(3,5)P2-related neurodegeneration.

PI(3,5)P2 and other tissues

The *pale tremor* mouse displays diluted pigment and cell loss in the spleen. Both of these issues merit further investigation. Fibroblasts vacuolate in culture, but do not appear to vacuolate *in vivo*. Macrophages also vacuolate in culture (S. Yoshi and J. Swanson, unpublished observations). Hippocampal neurons, which are unaffected *in vivo,* vacuolate when cultured, as well (Chow et al., 2007). These observations suggest that latent endosomal/lysosomal dysfunction exists in all cells. Culture conditions may lack growth factors or nutrients that prevent vacuolation *in vivo*. Further analysis of cellular phenotypes due to loss of PI(3,5)P2 may be facilitated by using easily cultured cells, like fibroblasts, rather than neurons.

The mouse as a tool to study PI(3,5)P2

Both loss-of-function *Fig4* and *Vac14* mutations demonstrate the importance of PI(3,5)P2 in the mammalian nervous system. However, these mutations do not provide information about the intricacies of the interactions of PI(3,5)P2 regulatory proteins. To find other mutations in this pathway, I searched for mouse mutants similar to *pale tremor*. I searched mouse mutant databases

(http://neuromice.org/ and http://mousemutant.jax.org/) for mutants with neurological and coat color abnormalities. The unique pattern of neurodegeneration in *pale tremor,* combined with diluted coat color, made the overall phenotypic description good search criteria. I identified *ingls* using this phenotypic information. *ingls* was first observed at the Jackson Lab in 1991, but remained uncloned for >15 years. The description of *ingls* was nearly identical to *pale tremor*, suggesting that it might have a mutation affecting PI(3,5)P2 metabolism. By careful analysis, I identified *Vac14* in the nonrecombinant region. Together, all this suggested to me that *ingls* might be an allele of *Vac14*. Experimental analysis confirmed this.

Many mouse mutants have been phenotypically characterized, but have not been genetically mapped. Both spontaneous and chemical induced mutants are described in various databases such as at the Jackson Lab and Neuromice (see above). By adopting a phenotype driven approach, one is guaranteed to find gene mutations that affect the phenotype of interest. Careful phenotypic analysis of cloned mouse mutants is important for identifying new mutants. This strategy has already proven to be successful and may continue to yield new mouse mutants involved in PI(3,5)P2 metabolism.

There has been more than a decade of research in the yeast PI(3,5)P2 pathway. This work is a rich resource for understanding the role of PI(3,5)P2 in the mammalian nervous system and human disease. Structure and function

studies have been carried out for many of the yeast proteins. This knowledge can be directly translated to study of the mammalian system. These studies and how they may inform the study of PI(3,5)P2 in mouse will be discussed.

Homologs of several yeast PI(3,5)P2-related proteins exist in mammals (Figure 5-1). There is one homolog for Fab1, Vac14, and Fig4 in mammals. In yeast, Vac7 is the major activator of Fab1. Vac7 is crucial for Fab1 function and loss of Vac7 results in a similar phenotype as loss of Fab1. There is no recognizable homologue of Vac7 in mammals (Gary et al., 2002). It remains to be seen whether another mammalian protein replaces Vac7, or if the Vac14/Fig4 complex is the main Fab1 activator. Atg18 modulates PI(3,5)P2 levels and is a PI(3,5)P2 effector in yeast. There are at least four mammalian homologs of Atg18, WIPI1-4 (Dove et al., 2004).

Mutagenesis in yeast has identified important amino acid residues in several of these proteins. Both gain-of-function and loss-of-function mutations have been described. Fig4 is the PI(3,5)P2 5-phosphatase, yet null Fig4 yeast cells have a net decrease in PI(3,5)P2 (Duex et al., 2006a). This surprising finding suggests that Fig4 also functions as a regulator of Fab1. It has been hypothesized that Fig4 dephosphorylates Fab1 in addition to PI(3,5)P2 (Duex et al., 2006a). These predictions were validated with a mutation in Fig4. The mutation *Fig4*^{G519R} is located 44 amino acids downstream of the catalytic site (yeast: $^{467}Cx_5RT$) in the SAC phosphatase domain (Table 5-1)(Gary et al., 2002).

This mutation resulted in increased basal levels of PI(3,5)P2, indicating it has reduced PI(3,5)P2 phosphatase activity. In response to hyperosmotic shock, wildtype yeast display a 20 fold increase in PI(3,5)P2 by 10 minutes. This high level of PI(3,5)P2 is quickly returned to basal levels over the next 10 minutes. In response to hyperosmotic shock, the *Fig4*^{G519R} strain displayed deficits in the initial increase of PI(3,5)P2 (phosphorylation) and failed to completely return to basal levels (dephosphorylation) (Duex et al., 2006b). This demonstrates that the SAC phosphatase activity is crucial for both production and turnover of PI(3,5)P2. A second mutation in the catalytic site of the SAC domain, *Fig4*^{D469N}, has a similar phenotype (Table 5-1) (Duex et al., 2006b).

Another mutation in yeast Fig4 identified a domain that is required for localization of the protein to the vacuole. A truncated form of Fig4 was expressed in yeast by deleting the last 118 amino acids (Table 5-1). This protein did not localize to the vacuole and was completely cytoplasmic (Rudge et al., 2004). Further analysis was not conducted, but this observation indicates that an interaction at the carboxyl terminus with a protein or a lipid is responsible for subcellular localization of Fig4.

The majority of mutations in Fab1 affect the kinase domain and kinase activity. Fab1 also has a FYVE domain that binds PI3P and a CCT chaperone domain thought to be involved in protein-protein interactions. Mutants with reduced or no kinase activity are similar to Fab1 null yeast (Table 5-2). These

mutations are located in kinase-specific catalytic motifs. They display reduced or undetectable levels of PI(3,5)P2 levels and grossly enlarged vacuoles (Gary et al., 1998; Michell et al., 2006).

In yeast, Fab1 cannot function without Vac7, Vac14, and Fig4. This suggests that Fab1 is not constitutively active. A study to find Fab1 mutants that bypass the need for Vac14 or Vac7 yielded many mutations with constitutive kinase activity (Table 5-2) (Duex et al., 2006b). These mutants rescued the enlarged vacuole phenotype and fell into two categories. One group of mutations rescued Vac14 null yeast cells. The second group rescued both Vac7 null and Vac14 null cells. Both groups of mutations display elevated basal PI(3,5)P2, but hyperosmotic shock-induced PI(3,5)P2 levels were not affected (Duex et al., 2006b). This demonstrates that the regulation of basal and stress-induced levels of PI(3,5)P2 differs. Mutations that rescued Vac7 null and Vac14 null cells had higher basal levels of PI(3,5)P2 as compared to those that could only rescue Vac14 null cells (Duex et al., 2006b), consistent with more severe phenotypes observed in Vac7 null yeast. All the mutations that can bypass Vac14 or Vac7 reside in amino acids that are not directly related to kinase activity. Several mutations are outside of the kinase domain, suggesting these mutations activate kinase activity via protein interactions.

The yeast mutations in Tables 5-1 and 5-2 may shed light on PI(3,5)P2 function in mammals. Loss-of-phosphatase mutations in *Fig4* should resemble

pale tremor (*Fig4* null). These mutations may reveal other *Fig4* functions because the protein would still be intact and expressed. The SAC domain is the only recognizable domain in *Fig4* and is highly conserved between mouse and yeast. It is likely that other mutations in the SAC domain would resemble null alleles.

The lack of additional recognizable domains in Fig4 makes it difficult to predict what kind of mutations would cause disease. The SAC domain comprises 50% of the Fig4 protein. The N-terminal ~150 amino acids upstream of the SAC domain are well conserved, containing stretches of invariant or nearly invariant residues between yeast and mouse. Mutations in this region might be instructive to identify new protein-protein interactions. I performed a yeast two-hybrid experiment with the N-terminus of Fig4 and identified several relevant protein interactions involved in vesicle transport (data not shown). These are in the process of being validated. Mutations in the N-terminus may disrupt these interactions.

The C-terminal ~400 amino acids downstream of the SAC domain are less conserved. Nonetheless, the last 118 amino acids in yeast are critical for subcellular localization to the vacuole (Rudge et al., 2004). It may be instructive to construct hybrid proteins in which the C-terminus of the mouse and yeast Fig4 proteins is switched. This may indicate whether the interactions required for localization are conserved. Finally, human Fig4 contains several motifs known to

interact with endosomal proteins (^{49}LVIID ^{351}DPF, and ^{656}F*X*D*X*F) (Sbrissa et al., 2007). Mutations in these motifs may reveal new protein-protein interactions. This could be tested with wildtype and mutated Fig4. Loss of interaction and abnormal cellular phenotype would establish the importance of these motifs to Fig4 function.

Mouse mutants of *Fab1* have not been reported and analysis has been limited to *in vitro* cell culture studies utilizing siRNA knockdown or over expression of a kinase-dead mutant. These studies revealed defects in the late endosome/lysosome pathways as well as reduced PI(3,5)P2 levels, as predicted from the yeast work. These experiments also suggested that Fab1 and PI(3,5)P2 may affect insulin signaling by perturbing insulin receptor trafficking (Ikonomov et al., 2002b) and osmotic response (Sbrissa et al., 2002). Knockouts of Fab1 have been reported in *C. elegans* (Nicot et al., 2006) and *drosophila* (Rusten et al., 2006). Both result in embryonic lethality, enlarged vesicles, and abnormalities in the endosome/lysosome pathway.

Heterozygous mutations of human *FAB1* cause François-Neetens mouchetée fleck corneal dystrophy (CFD) (Li et al., 2005b). CFD is an autosomal dominant disease and the majority of mutations are protein truncating. Reported mutations in *FAB1* reside in or around the CCT chaperone domain (Li et al., 2005b). It is unclear as to the significance of the location of these mutations, as studies in yeast and mammalian cells have focused on the kinase

domain of Fab1. Yeast two-hybrid experiments should be carried out to establish protein-protein interactions that the CCT domain might facilitate.

The *FAB1* mutation, K1103R, is the only missense mutation reported in CFD (Li et al., 2005b). Lysine 1103 is 39 amino acids downstream of the CCT domain and is evolutionarily invariant in vertebrates and yeast. The yeast mutation Fab1-1 (G864E) resides in an invariant residue in the CCT domain (Table 5-2) (Michell et al., 2006). G864E causes inability to activate in response to hyperosmotic shock, suggesting that it is disrupting a protein interaction that is required for activation, but not kinase activity (Michell et al., 2006). Studying K1103R and G864E in mammalian cells or transgenic mice could identify protein interactions that are essential for Fab1 activation in mammals. These mutations may be similar to Vac14 or Fig4 mutants, where Fab1 is not activated.

A mouse with a null allele of *Fab1* is predicted to be similar to, but more severely affected than, *Fig4* and *Vac14* null mice since the net result of loss of *Vac14* or *Fig4* is decreased PI(3,5)P2. *Fab1* null mice and cells would demonstrate the effect of complete loss of PI(3,5)P2. *Fab1* null cells would be expected to vacuolate and null mice would be embryonic lethal, as no PI(3,5)P2 would be synthesized. Reduced kinase activity mutants may establish a minimal amount of PI(3,5)P2 that is required for normal *in vivo* function.

Hyperactive Fab1 mutations present an interesting opportunity. It is unknown what the consequence is of increased levels of PI(3,5)P2 in the mammalian nervous system. Increased levels could result in perturbed vesicle trafficking and lead to human disease. It is difficult, *a priori,* to predict what kind of disease a hyperactive *Fab1* mutation would cause. Hyperactive Fab1 mutations have been studied in yeast (described above and Table 5-2) and these mutations can be engineered into a mouse *Fab1* transgene. Transgenic mice expressing a hyperactive *Fab1* mutation would model the dominant nature of constitutive activity. These mice would inform the search for human diseases that are caused by hyperactive *FAB1* mutations.

Hyperactive Fab1 mutants could determine if reduction in PI(3,5)P2, *per se*, is responsible for phenotypes observed in *Fig4*$^{-/-}$, *Vac14*$^{-/-}$, and *Vac14*$^{L156R/L156R}$ mice. All three mutants display reduced levels of PI(3,5)P2 in cultured fibroblasts, but this may be secondary to another unidentified function of this pathway. Some phenotypes observed in the mutant mice may be due to loss of protein interactions rather than loss of PI(3,5)P2. A transgenic mouse expressing a hyperactive Fab1 protein could be bred onto the background of *Fig4*$^{-/-}$, *Vac14*$^{-/-}$, and *Vac14*$^{L156R/L156R}$ mutant mice. If this rescues the mouse phenotypes, then it would be clear that lower levels of PI(3,5)P2 are responsible for the disease observed in these three mouse mutants. If certain phenotypes remain, it would indicate that other unknown functions or interactions of this complex contribute to the disease phenotype.

Two *Vac14* mutants have been studied in mice, the null and the *ingls* mutation, $Vac14^{L156R}$. *Vac14* does not have well defined protein functional domains. $Vac14^{L156R}$ changes a dileucine repeat and may disrupt a HEAT motif. We have already established that $Vac14^{L156R}$ disrupts interaction with Fab1 in a directed yeast two-hybrid analysis. Other yeast two-hybrid studies comparing wildtype and mutated Vac14 may yield other interactions that $Vac14^{L156R}$ may have interrupted. Seven dileucine repeats are found in *Vac14*. Dileucine repeats are involved in protein interactions important for endocytic vesicle trafficking (Bonifacino and Traub, 2003; Liu et al., 1998; Vowels and Payne, 1998). Perhaps additional mutations in these residues would reveal new protein interactions as well. The *ingls* mouse demonstrates that missense mutations in *Vac14* can affect certain, but not all phenotypes observed in the null mouse. DRGs are severely degenerated in the null, but not in the *ingls* mouse. Since it is difficult to predict which amino acids would be most important to Vac14 function, spontaneous mouse mutants of *Vac14* may be the most useful. New alleles of *Vac14* can be identified by screening ENU mutagenized ES cell lines (http://www.mmrrc.org/distribution/UNC_Library.html).

The PI(3,5)P2 pathway and human disease

I established that dysfunction in the PI(3,5)P2 pathway results in severe neurodegeneration in the mouse and hypothesized that a human disease with severe degeneration of the CNS and PNS observed in the *pale tremor* mouse, would be prenatal or perinatal lethal. We therefore focused on the peripheral

neuropathy. The *pale tremor* peripheral neuropathy closely mimics severe forms of Charcot-Marie-Tooth disease (Bernard et al., 2006; Dubourg et al., 2006). I identified four CMT patients with recessive mutations in *FIG4*. Four percent of the patients I screened carried mutations in *FIG4*, suggesting that a significant number of CMT patients carry *FIG4* mutations (Chow et al., 2007). Continued screening of CMT patients will establish the contribution of *FIG4* mutations to CMT.

Because *FIG4* was found to contribute to CMT, we hypothesized that mutations in *VAC14* would also result in CMT. We screened the same 95 CMT patients for mutations in *VAC14*, however, no mutations were identified (Table 5-3). Further screening is needed to establish whether *VAC14* contributes to CMT. Mutations in *FAB1* might also cause CMT. Haploinsufficiency for *FAB1* results in François-Neetens mouchetée fleck corneal dystrophy (Li et al., 2005b). This suggests that *FAB1* CMT would be recessive. We have not yet screened CMT patients for mutations in *FAB1*.

My mutation screens have yielded human *FIG4* missense variants that warrant further study (Table 5-4 and 5-5). The I41T mutation was identified in four CMT patients and I have developed a mouse model carrying I41T. It remains to be seen if this will be an accurate model of CMT4J. In addition to this, I have identified several other missense mutations in CMT patients and in a screen of patients with motor neuron disease (Chow CY, unpublished results)

(Table 5-4). The N-terminus and SAC domains of yeast and human FIG4 are well conserved, indicating that these protein domains are important for function. Yeast is a good model for evaluating the functional effects of missense variants identified in human *FIG4*. We have tested several human N-terminal and SAC domain missense variants in yeast (Table 5-4). Fig4 null yeast cells display an enlarged vacuole phenotype. The vacuole appears swollen and is easily visualized when labeled with the lipiphilic dye FM4-64. A construct carrying the yeast Fig4 gene with the corresponding missense mutation was tested for its ability to rescue Fig4 null yeast cells. A rescued cell has a normal wildtype-sized vacuole. Many cells are counted and the number of rescued and non-rescued cells was compared to Fig4 null cells and cells rescued with a wildtype construct. Populations of Fig4 null cells rescued with a wildtype construct have ~90% cells with normal, small vacuoles, while FIG4 null populations have ~5% cells with normal, small vacuoles. PI(3,5)P2 levels should also be measured from these cells, but this has not been done. Several of the missense mutations identified in patients have been shown to rescue the null phenotype (data not shown) indicating that they retain wildtype levels of function.

C-terminus mutations are more difficult to test because it is not well conserved between human and yeast. Due to lack of conservation, they will likely require testing in a mammalian system. Mutant *Vac14* fibroblasts can be rescued by transfection with a wildtype *Vac14* construct (Zhang et al., 2007). This suggests that *Fig4* null fibroblasts can also be rescued by transfection of

wildtype *Fig4*. Mutant *Fig4* constructs can be transfected into *Fig4* null cells to assess the ability of the mutant protein to rescue the vacuolization phenotype. This technique warrants further development.

I identified a *FIG4* C-terminal missense variant, R905C, in one CMT patient and in the mouse strain WSB/EiJ (Chapter III). Experiments are underway to establish if R905C is a partial functioning allele in WSB/EiJ mice. R905C does not seem to affect the nervous system or cellular vacuolation, but it remains to be seen if it affects pigmentation.

To extend our knowledge of PI(3,5)P2 related diseases, it will be important to continue to screen for mutations in *FIG4*, *VAC14* and *FAB1*. Besides CMT, I have screened several other diseases (Table 5-3 and 5-4). Centronuclear Myopathy (CNM) results in hypotonia, weakness and early lethality. CNM is characterized by hypotrophic muscle fibers and centrally placed nuclei in muscle cells (Pierson et al., 2005). The most common form of CNM is caused by mutations in myotubularin (*MTM1*), a PI3P and PI(3,5)P2 3-phosphatase (Pierson et al., 2005). *MTM1* is related to *MTMR2* and *MTMR13* which cause CMT4B1 and CMT4B2, respectively (Robinson and Dixon, 2006). Mutations in *DNM2*, a phosphoinositide binding protein, cause both CNM and CMT1DB (discussed in Chapter I). These data suggests that dysfunction of *FIG4* may cause CNM as well. I obtained nine CNM samples from Dr. Jim Dowling (University of Michigan) to screen. No new variants were identified in this small

group of patients (Table 5-3). A more comprehensive screen is needed to establish whether mutations in *FIG4* contribute to CNM. *VAC14* and *FAB1* should also be screened in these samples.

The CMT disease in one of the patients with *FIG4* mutations is primarily motor in origin (Zhang et al., 2008). While there is degeneration of the sensory nerves, the clinical disease primarily affects motor abilities and degeneration of the motor nerves is present (Zhang et al., 2008). Degeneration in both motor nerves and motor neurons is observed in the *pale tremor* mouse (Chow et al., 2007). This prompted me to obtain samples from 26 CMT patients with a primarily motor disease from Dr. Michael Shy (Wayne State University). I screened these 26 samples, but found no mutations (Table 5-3). Further screening of motor-specific CMT is warranted.

To date, we have not identified a human disease that completely recapitulates the neurological disease and pigment abnormalities of the *pale tremor* mouse. A literature search identified two reports of patients with a neurocutaneous syndrome (Buoni et al., 2006; Zannolli et al., 2008). These patients have many neurological defects, including speech delay, mental retardation, and epilepsy. They also displayed pigmentation abnormalities and vacuolation within melanocytes, keratinocytes, Langerhans cells, and fibroblasts, similar to the *pale tremor* and *Vac14* null fibroblasts. I sequenced *FIG4* in both patients, but did not identify any mutations. We also sequenced *VAC14* and no

mutations were found (Table 5-3). This indicates that coding mutations do not cause this unique syndrome, but does not rule out regulatory mutations in *FIG4* or *VAC14*. *FAB1* has not been screened in these samples.

I searched the OMIM database (Online Mendelian Inheritance in Man) for human diseases that mapped to the chromosome regions that contain *FIG4* (chr. 6q21), *VAC14* (chr. 16q22.1), and *FAB1* (chr. 2q33.3). The search identified spinocerebellar ataxia 4 (SCA4). The SCA4 nonrecombinant region spans chromosome 16q22.1 and includes *VAC14*. SCA4 presents with ataxia and peripheral sensory axonal neuropathy (Flanigan et al., 1996). The sensory neuropathy resembles CMT. We obtained a sample from the SCA4 family from Dr. Louis Ptacek (UCSF) and I sequenced the *VAC14* coding exons, but did not identify a *VAC14* mutation (Table 5-3). Again, a *VAC14* regulatory mutation would have been missed.

Further screening will establish whether mutations in the PI(3,5)P2 pathway contribute to these diseases. CMT is a peripheral neuropathy that can affect sensory neurons, motor neurons, or both. CMT is a spectrum of diseases. Related diseases include Hereditary Spastic Paraplegia (HSP), Amylateral Sclerosis (ALS), Distal Hereditary Motor Neuronopathy (dHMN), Hereditary Sensory Neuropathy (HSN), and Spinal Muscular Atrophy (SMA). These diseases resemble CMT as they are genetically heterogeneous, overlap phenotypically with CMT, and can be caused by mutations in the same genes as

identified in CMT. HSP is characterized by progressive, severe lower extremity spasticity caused by degeneration of the motor neurons in the corticospinal tracts (Fink et al., 1996). ALS is characterized by loss of motor neurons in the brain, brainstem, and spinal cord, ultimately leading to paralysis (Pasinelli and Brown, 2006). dHMN is clinically similar to CMT, but results from degeneration of only spinal motor neurons (Irobi et al., 2006). HSN is also similar to CMT, but is limited to sensory neuron degeneration with no motor involvement (Auer-Grumbach et al., 2006). SMA is characterized by muscle atrophy and degeneration of spinal motor neurons (Monani, 2005). All of these diseases display phenotypes that are observed in the *pale tremor* mouse. Phosphoinositide signaling pathways have been implicated in several of these diseases.

Heterozygous mutations in *FAB1* cause François-Neetens mouchetée fleck corneal dystrophy. This suggests that heterozygous mutations in *FIG4* and *VAC14* may also cause a similar corneal dystrophy. Heterozygous and homozygous *Fig4* null mice do not display any corneal defects (Chow CY, unpublished observations). Furthermore, there is no evidence of corneal dystrophy in the CMT4J patients. To date, we have not screened any patients with corneal dystrophy.

Massive neurodegeneration is observed in the *pale tremor*, *Vac14* null, and *ingls* brain, indicating the importance of PI(3,5)P2 signaling in the CNS as

well as the PNS. The *ingls* mouse has demonstrated that certain mutations in this pathway only affect brain function. The PNS may be less sensitive to abnormal PI(3,5)P2 signaling. Human neurodegenerative diseases that affect only the brain should be screened as well. Diseases that include hydrocephalus and vacuolation of brain tissue (spongiform appearance) should be considered. Frontal Temporal Dementia (FTD) is the second most common form of dementia. FTD is characterized by spongiform degeneration of cortical regions and ventricle dilation (hydrocephalus) (Bugiani, 2007). FTD is genetically heterogeneous and may be caused by mutations in the PI(3,5)P2 pathway.

Concluding remarks

The discovery of several spontaneous mouse mutants in PI(3,5)P2 signaling has established the importance of PI(3,5)P2 in mammals. Study of these mouse mutants led to identification of a new form of CMT caused by mutations in *FIG4*. The future of PI(3,5)P2 research should utilize mouse and human genetics. Both phenotype and genotype driven approaches will contribute to understanding the regulation and interactions of this pathway. Work in the mouse will be accelerated if it is informed by the body of knowledge gained from yeast. Continuing to screen human diseases for mutations in the PI(3,5)P2 pathway will identify new mutations and crucial functions of these genes. As we understand more about PI(3,5)P2 signaling, and identify more patients, we will hopefully be able to use the knowledge gained to develop therapies.

Yeast	Mammals
Fab1	FAB1(PIKfyve / PIP5K3)
Vac14	VAC14 (ArPIKfyve)
Fig4	FIG4 (SAC3)
Vac7	--
Atg18/Svp1	WIPI1, WIPI2, WIPI3, WIPI4

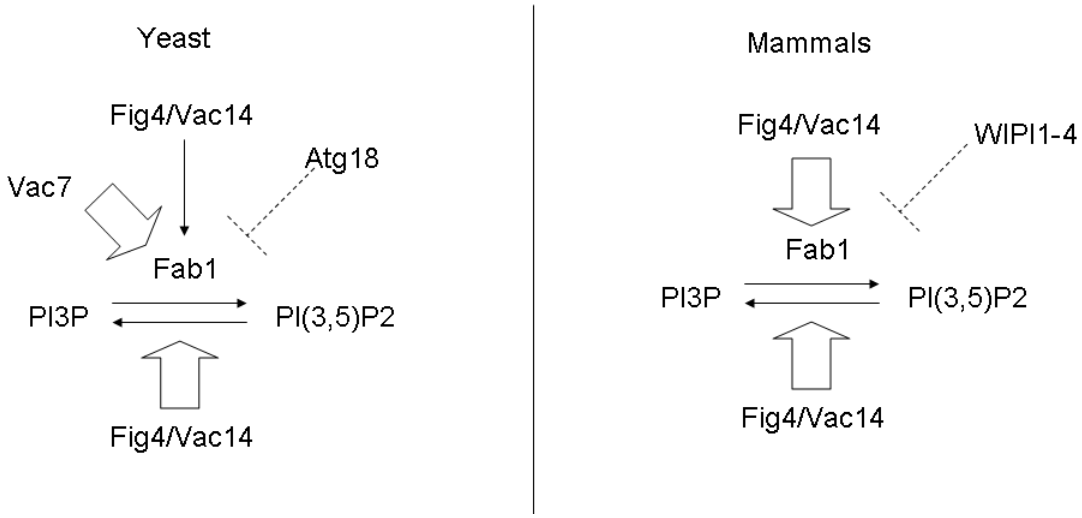

Figure 5-1. PI(3,5)P2 pathway in yeast and mammals. The PI(3,5)P2 pathway is well conserved in yeast and mammals. Vac7 is a yeast specific activator of Fab1. WIPI1-4 are mammalian homologs of Atg18. it is unknown which if any of these play the same role as Atg18. Dotted lines indicate hypothesized function.

Table 5-1. Missense mutations of yeast Fig4.

yeast mutation	equivalent human residue	domain	phenotype	reference
G519R	G538	SAC	phosphatase activity reduced increased steady state levels of PI(3,5)P2 decreased production and turnover of PI(3,5)P2 during osmotic stress	Gary et al., 2002 Duex et al., 2006
D469N	D488	SAC	phosphatase activity reduced increased steady state levels of PI(3,5)P2 decreased production and turnover of PI(3,5)P2 during osmotic stress	Duex et al., 2006
Δ761-879	14% identical 55% similar to human C-term	C-term.	cytoplasmic localization	Rudge et al., 2004

Table 5-2. Missense mutations of yeast Fab1

yeast mutation	equivalent human residue	domain	phenotype	reference
G864E	G683	CCT	loss of hyperosmotic induced activation	Mitchell, 2006
G2042V G2045V	G1863 G1860	kinase	nearly kinase dead - 9-fold lower (PI(3,5)P2 levels	Gary et al., 1998
D2134R	D1951	kinase	kinase dead - no detectable levels of PI(3,5)P2	Gary et al., 1998
T2250A	S2068	kinase	FAB1-6 8 fold higher than WT basal levels of PI(3,5)P2* rescues Vac14 null cells	Duex et al., 2006
G2238W	G2058	kinase	FAB1-7 rescues Vac14 null cells	Duex et al., 2006
E1822K N1832Y	E1620 N1630	--	FAB1-8 rescues Vac14 null cells	Duex et al., 2006
T2250A E1822A F1833L	S2068 E1620 L1631	kinase and other	FAB1-14 17 fold higher WT basal levels of PI(3,5)P2* rescues Vac14 null and Vac17 null cells	Duex et al., 2006

* PI(3,5)P2 levels in response to hyperosmotic stress is normal if Vac7, Vac14 and Fig4 are present. Without them, this response is destroyed.

Table 5-3. Mutation screens with negative results

disease	number of samples	genes screened	source
CMT	95	*VAC14*	Jim Lupski (Baylor)
Centronuclear Myopathy	9	*FIG4*	Jim Dowling (U of M)
Motor CMT	26	*FIG4*	Michael Shy (Wayne State)
Neurocutaneous syndrome	2	*FIG4* *VAC14*	Raffaella Zannolli (UNISI)
SCA4	1	*VAC14*	Louis Ptacek (UCSF)

*With the exception of SCA4, all these disease should be screened for *FAB1* and the other genes in the PI(3,5)P2 pathway.

Table 5-4. Novel nonsynonymous and protein truncating variants identified in human *FIG4*

	protein truncating	missense
CMT#	F98fsX102 R183X D348fsX359 G253fsX261	I41T* Y58C R244C R905C**
motor neuron disease##	R183X Q403X Exon2-1 G>T	D48G D53Y R388G I902T N494N (changes ESE)
controls	--	K278N T282A Y400C S853L

missense variants not included in (Chow et al., 2007) except I41T

unpublished study

* I41T transgenic mouse is being studied (Chapter III)

**R905C is the same variant found in mouse strain WSB/EiJ (Chapter III)

Underlined variants have been tested in yeast vacuole assay

Table 5-5. Common nonsynonymous variants identified in human *FIG4*

variant	rs#	minor allele freq
c1090 A>T (M364L)	rs2295837	0.04
c1961 T>C (V654A)	rs9885672	0.14

These have not been functionally tested.

REFERENCES

Adamska, M., Billi, A. C., Cheek, S., and Meisler, M. H. (2005). Genetic interaction between Wnt7a and Lrp6 during patterning of dorsal and posterior structures of the mouse limb. Dev Dyn *233*, 368-372.

Andrade, M. A., and Bork, P. (1995). HEAT repeats in the Huntington's disease protein. Nat Genet *11*, 115-116.

Andrade, M. A., Perez-Iratxeta, C., and Ponting, C. P. (2001a). Protein repeats: structures, functions, and evolution. J Struct Biol *134*, 117-131.

Andrade, M. A., Petosa, C., O'Donoghue, S. I., Muller, C. W., and Bork, P. (2001b). Comparison of ARM and HEAT protein repeats. J Mol Biol *309*, 1-18.

Auer-Grumbach, M., Mauko, B., Auer-Grumbach, P., and Pieber, T. R. (2006). Molecular genetics of hereditary sensory neuropathies. Neuromolecular Med *8*, 147-158.

Begley, M. J., Taylor, G. S., Brock, M. A., Ghosh, P., Woods, V. L., and Dixon, J. E. (2006). Molecular basis for substrate recognition by MTMR2, a myotubularin family phosphoinositide phosphatase. Proc Natl Acad Sci U S A *103*, 927-932.

Berger, P., Berger, I., Schaffitzel, C., Tersar, K., Volkmer, B., and Suter, U. (2006). Multi-level regulation of myotubularin-related protein-2 phosphatase activity by myotubularin-related protein-13/set-binding factor-2. Hum Mol Genet *15*, 569-579.

Berger, P., Bonneick, S., Willi, S., Wymann, M., and Suter, U. (2002). Loss of phosphatase activity in myotubularin-related protein 2 is associated with Charcot-Marie-Tooth disease type 4B1. Hum Mol Genet *11*, 1569-1579.

Bernard, R., De Sandre-Giovannoli, A., Delague, V., and Levy, N. (2006). Molecular genetics of autosomal-recessive axonal Charcot-Marie-Tooth neuropathies. Neuromolecular Med *8*, 87-106.

Berti, C., Nodari, A., Wrabetz, L., and Feltri, M. L. (2006). Role of integrins in peripheral nerves and hereditary neuropathies. Neuromolecular Med *8*, 191-204.

Bolino, A., Bolis, A., Previtali, S. C., Dina, G., Bussini, S., Dati, G., Amadio, S., Del Carro, U., Mruk, D. D., Feltri, M. L.*, et al.* (2004). Disruption of Mtmr2 produces CMT4B1-like neuropathy with myelin outfolding and impaired spermatogenesis. J Cell Biol *167*, 711-721.

Bolino, A., Muglia, M., Conforti, F. L., LeGuern, E., Salih, M. A., Georgiou, D. M., Christodoulou, K., Hausmanowa-Petrusewicz, I., Mandich, P., Schenone, A.*, et al.* (2000). Charcot-Marie-Tooth type 4B is caused by mutations in the gene encoding myotubularin-related protein-2. Nat Genet *25*, 17-19.

Bolis, A., Coviello, S., Bussini, S., Dina, G., Pardini, C., Previtali, S. C., Malaguti, M., Morana, P., Del Carro, U., Feltri, M. L.*, et al.* (2005). Loss of Mtmr2 phosphatase in Schwann cells but not in motor neurons causes Charcot-Marie-Tooth type 4B1 neuropathy with myelin outfoldings. J Neurosci *25*, 8567-8577.

Bolis, A., Zordan, P., Coviello, S., and Bolino, A. (2007). Myotubularin-related (MTMR) phospholipid phosphatase proteins in the peripheral nervous system. Mol Neurobiol *35*, 308-316.

Bonangelino, C. J., Nau, J. J., Duex, J. E., Brinkman, M., Wurmser, A. E., Gary, J. D., Emr, S. D., and Weisman, L. S. (2002). Osmotic stress-induced increase of phosphatidylinositol 3,5-bisphosphate requires Vac14p, an activator of the lipid kinase Fab1p. J Cell Biol *156*, 1015-1028.

Bonifacino, J. S., and Traub, L. M. (2003). Signals for sorting of transmembrane proteins to endosomes and lysosomes. Annu Rev Biochem *72*, 395-447.

Bonneick, S., Boentert, M., Berger, P., Atanasoski, S., Mantei, N., Wessig, C., Toyka, K. V., Young, P., and Suter, U. (2005). An animal model for Charcot-Marie-Tooth disease type 4B1. Hum Mol Genet *14*, 3685-3695.

Buchner, D. A., Trudeau, M., and Meisler, M. H. (2003). SCNM1, a putative RNA splicing factor that modifies disease severity in mice. Science *301*, 967-969.

Bugiani, O. (2007). The many ways to frontotemporal degeneration and beyond. Neurol Sci *28*, 241-244.

Buoni, S., Zannolli, R., de Santi, M., Macucci, F., Hayek, J., Orsi, A., Scarinci, R., Buscalferri, A., Cuccia, A., Zappella, M., and Miracco, C. (2006). Neurocutaneous syndrome with mental delay, autism, blockage in intracellular vescicular trafficking and melanosome defects. Eur J Neurol *13*, 842-851.

Cassina, P., Cassina, A., Pehar, M., Castellanos, R., Gandelman, M., de Leon, A., Robinson, K. M., Mason, R. P., Beckman, J. S., Barbeito, L., and Radi, R. (2008). Mitochondrial dysfunction in SOD1G93A-bearing astrocytes promotes motor neuron degeneration: prevention by mitochondrial-targeted antioxidants. J Neurosci *28*, 4115-4122.

Chow, C. Y., Zhang, Y., Dowling, J. J., Jin, N., Adamska, M., Shiga, K., Szigeti, K., Shy, M. E., Li, J., Zhang, X.*, et al.* (2007). Mutation of FIG4 causes neurodegeneration in the pale tremor mouse and patients with CMT4J. Nature *448*, 68-72.

Cooke, F. T., Dove, S. K., McEwen, R. K., Painter, G., Holmes, A. B., Hall, M. N., Michell, R. H., and Parker, P. J. (1998). The stress-activated phosphatidylinositol 3-phosphate 5-kinase Fab1p is essential for vacuole function in S. cerevisiae. Curr Biol *8*, 1219-1222.

Correa-Cerro, L. S., and Mandell, J. W. (2007). Molecular mechanisms of astrogliosis: new approaches with mouse genetics. J Neuropathol Exp Neurol *66*, 169-176.

Delague, V., Jacquier, A., Hamadouche, T., Poitelon, Y., Baudot, C., Boccaccio, I., Chouery, E., Chaouch, M., Kassouri, N., Jabbour, R.*, et al.* (2007). Mutations in FGD4 encoding the Rho GDP/GTP exchange factor FRABIN cause autosomal recessive Charcot-Marie-Tooth type 4H. Am J Hum Genet *81*, 1-16.

Di Giorgio, F. P., Carrasco, M. A., Siao, M. C., Maniatis, T., and Eggan, K. (2007). Non-cell autonomous effect of glia on motor neurons in an embryonic stem cell-based ALS model. Nat Neurosci *10*, 608-614.

Di Paolo, G., and De Camilli, P. (2006). Phosphoinositides in cell regulation and membrane dynamics. Nature *443*, 651-657.

Dove, S. K., and Johnson, Z. E. (2007). Our FABulous VACation: a decade of phosphatidylinositol 3,5-bisphosphate. Biochem Soc Symp, 129-139.

Dove, S. K., McEwen, R. K., Mayes, A., Hughes, D. C., Beggs, J. D., and Michell, R. H. (2002). Vac14 controls PtdIns(3,5)P(2) synthesis and Fab1-dependent protein trafficking to the multivesicular body. Curr Biol *12*, 885-893.

Dove, S. K., Piper, R. C., McEwen, R. K., Yu, J. W., King, M. C., Hughes, D. C., Thuring, J., Holmes, A. B., Cooke, F. T., Michell, R. H.*, et al.* (2004). Svp1p defines a family of phosphatidylinositol 3,5-bisphosphate effectors. Embo J *23*, 1922-1933.

Dubourg, O., Azzedine, H., Verny, C., Durosier, G., Birouk, N., Gouider, R., Salih, M., Bouhouche, A., Thiam, A., Grid, D.*, et al.* (2006). Autosomal-recessive forms of demyelinating Charcot-Marie-Tooth disease. Neuromolecular Med *8*, 75-86.

Duex, J. E., Nau, J. J., Kauffman, E. J., and Weisman, L. S. (2006a). Phosphoinositide 5-phosphatase Fig 4p is required for both acute rise and subsequent fall in stress-induced phosphatidylinositol 3,5-bisphosphate levels. Eukaryot Cell *5*, 723-731.

Duex, J. E., Tang, F., and Weisman, L. S. (2006b). The Vac14p-Fig4p complex acts independently of Vac7p and couples PI3,5P2 synthesis and turnover. J Cell Biol *172*, 693-704.

Escayg, A., MacDonald, B. T., Meisler, M. H., Baulac, S., Huberfeld, G., An-Gourfinkel, I., Brice, A., LeGuern, E., Moulard, B., Chaigne, D.*, et al.* (2000). Mutations of SCN1A, encoding a neuronal sodium channel, in two families with GEFS+2. Nat Genet *24*, 343-345.

Fink, J. K., Heiman-Patterson, T., Bird, T., Cambi, F., Dube, M. P., Figlewicz, D. A., Fink, J. K., Haines, J. L., Heiman-Patterson, T., Hentati, A.*, et al.* (1996). Hereditary spastic paraplegia: advances in genetic research. Hereditary Spastic Paraplegia Working group. Neurology *46*, 1507-1514.

Flanigan, K., Gardner, K., Alderson, K., Galster, B., Otterud, B., Leppert, M. F., Kaplan, C., and Ptacek, L. J. (1996). Autosomal dominant spinocerebellar ataxia with sensory axonal neuropathy (SCA4): clinical description and genetic localization to chromosome 16q22.1. Am J Hum Genet *59*, 392-399.

Frazer, K. A., Wade, C. M., Hinds, D. A., Patil, N., Cox, D. R., and Daly, M. J. (2004). Segmental phylogenetic relationships of inbred mouse strains revealed

by fine-scale analysis of sequence variation across 4.6 mb of mouse genome. Genome Res *14*, 1493-1500.

Gary, J. D., Sato, T. K., Stefan, C. J., Bonangelino, C. J., Weisman, L. S., and Emr, S. D. (2002). Regulation of Fab1 phosphatidylinositol 3-phosphate 5-kinase pathway by Vac7 protein and Fig4, a polyphosphoinositide phosphatase family member. Mol Biol Cell *13*, 1238-1251.

Gary, J. D., Wurmser, A. E., Bonangelino, C. J., Weisman, L. S., and Emr, S. D. (1998). Fab1p is essential for PtdIns(3)P 5-kinase activity and the maintenance of vacuolar size and membrane homeostasis. J Cell Biol *143*, 65-79.

Houlden, H., and Reilly, M. M. (2006). Molecular genetics of autosomal-dominant demyelinating Charcot-Marie-Tooth disease. Neuromolecular Med *8*, 43-62.

Hughes, W. E., Cooke, F. T., and Parker, P. J. (2000). Sac phosphatase domain proteins. Biochem J *350 Pt 2*, 337-352.

Ikonomov, O. C., Sbrissa, D., Mlak, K., Kanzaki, M., Pessin, J., and Shisheva, A. (2002a). Functional dissection of lipid and protein kinase signals of PIKfyve reveals the role of PtdIns 3,5-P2 production for endomembrane integrity. J Biol Chem *277*, 9206-9211.

Ikonomov, O. C., Sbrissa, D., Mlak, K., and Shisheva, A. (2002b). Requirement for PIKfyve enzymatic activity in acute and long-term insulin cellular effects. Endocrinology *143*, 4742-4754.

Ikonomov, O. C., Sbrissa, D., and Shisheva, A. (2001). Mammalian cell morphology and endocytic membrane homeostasis require enzymatically active phosphoinositide 5-kinase PIKfyve. J Biol Chem *276*, 26141-26147.

Irobi, J., Dierick, I., Jordanova, A., Claeys, K. G., De Jonghe, P., and Timmerman, V. (2006). Unraveling the genetics of distal hereditary motor neuronopathies. Neuromolecular Med *8*, 131-146.

Kearney, J. A., Wiste, A. K., Stephani, U., Trudeau, M. M., Siegel, A., RamachandranNair, R., Elterman, R. D., Muhle, H., Reinsdorf, J., Shields, W. D., *et al.* (2006). Recurrent de novo mutations of SCN1A in severe myoclonic epilepsy of infancy. Pediatr Neurol *34*, 116-120.

Kennedy, M. J., and Ehlers, M. D. (2006). Organelles and Trafficking Machinery for Postsynaptic Plasticity. Annu Rev Neurosci.

Kleopa, K. A., and Scherer, S. S. (2006). Molecular genetics of X-linked Charcot-Marie-Tooth disease. Neuromolecular Med *8*, 107-122.

Kohrman, D. C., Harris, J. B., and Meisler, M. H. (1996). Mutation detection in the med and medJ alleles of the sodium channel Scn8a. Unusual splicing due to a minor class AT-AC intron. J Biol Chem *271*, 17576-17581.

Lemaire, J. F., and McPherson, P. S. (2006). Binding of Vac14 to neuronal nitric oxide synthase: Characterisation of a new internal PDZ-recognition motif. FEBS Lett.

Lemmon, M. A. (2003). Phosphoinositide recognition domains. Traffic *4*, 201-213.

Li, J., Bai, Y., Ghandour, K., Qin, P., Grandis, M., Trostinskaia, A., Ianakova, E., Wu, X., Schenone, A., Vallat, J. M.*, et al.* (2005a). Skin biopsies in myelin-related neuropathies: bringing molecular pathology to the bedside. Brain *128*, 1168-1177.

Li, J., Bai, Y., Ianakova, E., Grandis, M., Uchwat, F., Trostinskaia, A., Krajewski, K. M., Garbern, J., Kupsky, W. J., and Shy, M. E. (2006). Major myelin protein gene (P0) mutation causes a novel form of axonal degeneration. J Comp Neurol *498*, 252-265.

Li, S., Tiab, L., Jiao, X., Munier, F. L., Zografos, L., Frueh, B. E., Sergeev, Y., Smith, J., Rubin, B., Meallet, M. A.*, et al.* (2005b). Mutations in PIP5K3 are associated with Francois-Neetens mouchetee fleck corneal dystrophy. Am J Hum Genet *77*, 54-63.

Liu, S. H., Marks, M. S., and Brodsky, F. M. (1998). A dominant-negative clathrin mutant differentially affects trafficking of molecules with distinct sorting motifs in the class II major histocompatibility complex (MHC) pathway. J Cell Biol *140*, 1023-1037.

Lupski, J. R., de Oca-Luna, R. M., Slaugenhaupt, S., Pentao, L., Guzzetta, V., Trask, B. J., Saucedo-Cardenas, O., Barker, D. F., Killian, J. M., Garcia, C. A.*, et*

al. (1991). DNA duplication associated with Charcot-Marie-Tooth disease type 1A. Cell *66*, 219-232.

Maksakova, I. A., Romanish, M. T., Gagnier, L., Dunn, C. A., van de Lagemaat, L. N., and Mager, D. L. (2006). Retroviral elements and their hosts: insertional mutagenesis in the mouse germ line. PLoS Genet *2*, e2.

Marks, M. S. (2008). FIG4, Charcot-Marie-Tooth disease, and hypopigmentation: a role for phosphoinositides in melanosome biogenesis? Pigment Cell Melanoma Res *21*, 11-14.

Marks, M. S., and Seabra, M. C. (2001). The melanosome: membrane dynamics in black and white. Nat Rev Mol Cell Biol *2*, 738-748.

Martyn, C. N., and Hughes, R. A. (1997). Epidemiology of peripheral neuropathy. J Neurol Neurosurg Psychiatry *62*, 310-318.

McKinney, B. C., Chow, C. Y., Meisler, M. H., and Murphy, G. G. (2008). Exaggerated emotional behavior in mice heterozygous null for the sodium channel Scn8a (Na1.6). Genes Brain Behav.

McNiven, M. A. (2005). Dynamin in disease. Nat Genet *37*, 215-216.

Michell, R. H., Heath, V. L., Lemmon, M. A., and Dove, S. K. (2006). Phosphatidylinositol 3,5-bisphosphate: metabolism and cellular functions. Trends Biochem Sci *31*, 52-63.

Monani, U. R. (2005). Spinal muscular atrophy: a deficiency in a ubiquitous protein; a motor neuron-specific disease. Neuron *48*, 885-896.

Naef, R., and Suter, U. (1998). Many facets of the peripheral myelin protein PMP22 in myelination and disease. Microsc Res Tech *41*, 359-371.

Nagai, M., Re, D. B., Nagata, T., Chalazonitis, A., Jessell, T. M., Wichterle, H., and Przedborski, S. (2007). Astrocytes expressing ALS-linked mutated SOD1 release factors selectively toxic to motor neurons. Nat Neurosci *10*, 615-622.

Nicot, A. S., Fares, H., Payrastre, B., Chisholm, A. D., Labouesse, M., and Laporte, J. (2006). The Phosphoinositide Kinase PIKfyve/Fab1p Regulates Terminal Lysosome Maturation in Caenorhabditis elegans. Mol Biol Cell *17*, 3062-3074.

Niemann, A., Berger, P., and Suter, U. (2006). Pathomechanisms of mutant proteins in Charcot-Marie-Tooth disease. Neuromolecular Med *8*, 217-242.

Niwa, H., Yamamura, K., and Miyazaki, J. (1991). Efficient selection for high-expression transfectants with a novel eukaryotic vector. Gene *108*, 193-199.

Oliver, P. L., Bitoun, E., and Davies, K. E. (2007). Comparative genetic analysis: the utility of mouse genetic systems for studying human monogenic disease. Mamm Genome *18*, 412-424.

Pareyson, D., Scaioli, V., and Laura, M. (2006). Clinical and electrophysiological aspects of Charcot-Marie-Tooth disease. Neuromolecular Med *8*, 3-22.

Park, M., Salgado, J. M., Ostroff, L., Helton, T. D., Robinson, C. G., Harris, K. M., and Ehlers, M. D. (2006). Plasticity-induced growth of dendritic spines by exocytic trafficking from recycling endosomes. Neuron *52*, 817-830.

Pasinelli, P., and Brown, R. H. (2006). Molecular biology of amyotrophic lateral sclerosis: insights from genetics. Nat Rev Neurosci *7*, 710-723.

Pierson, C. R., Tomczak, K., Agrawal, P., Moghadaszadeh, B., and Beggs, A. H. (2005). X-linked myotubular and centronuclear myopathies. J Neuropathol Exp Neurol *64*, 555-564.

Previtali, S. C., Quattrini, A., and Bolino, A. (2007). Charcot-Marie-Tooth type 4B demyelinating neuropathy: deciphering the role of MTMR phosphatases. Expert Rev Mol Med *9*, 1-16.

Raeymaekers, P., Timmerman, V., Nelis, E., De Jonghe, P., Hoogendijk, J. E., Baas, F., Barker, D. F., Martin, J. J., De Visser, M., Bolhuis, P. A., and et al. (1991). Duplication in chromosome 17p11.2 in Charcot-Marie-Tooth neuropathy type 1a (CMT 1a). The HMSN Collaborative Research Group. Neuromuscul Disord *1*, 93-97.

Rainier, S., Sher, C., Reish, O., Thomas, D., and Fink, J. K. (2006). De novo occurrence of novel SPG3A/atlastin mutation presenting as cerebral palsy. Arch Neurol *63*, 445-447.

Raposo, G., and Marks, M. S. (2007). Melanosomes--dark organelles enlighten endosomal membrane transport. Nat Rev Mol Cell Biol *8*, 786-797.

Robinson, F. L., and Dixon, J. E. (2006). Myotubularin phosphatases: policing 3-phosphoinositides. Trends Cell Biol *16*, 403-412.

Robinson, F. L., Niesman, I. R., Beiswenger, K. K., and Dixon, J. E. (2008). Loss of the inactive myotubularin-related phosphatase Mtmr13 leads to a Charcot-Marie-Tooth 4B2-like peripheral neuropathy in mice. Proc Natl Acad Sci U S A.

Rudge, S. A., Anderson, D. M., and Emr, S. D. (2004). Vacuole size control: regulation of PtdIns(3,5)P2 levels by the vacuole-associated Vac14-Fig4 complex, a PtdIns(3,5)P2-specific phosphatase. Mol Biol Cell *15*, 24-36.

Rusten, T. E., Rodahl, L. M., Pattni, K., Englund, C., Samakovlis, C., Dove, S., Brech, A., and Stenmark, H. (2006). Fab1 phosphatidylinositol 3-phosphate 5-kinase controls trafficking but not silencing of endocytosed receptors. Mol Biol Cell *17*, 3989-4001.

Rutherford, A. C., Traer, C., Wassmer, T., Pattni, K., Bujny, M. V., Carlton, J. G., Stenmark, H., and Cullen, P. J. (2006). The mammalian phosphatidylinositol 3-phosphate 5-kinase (PIKfyve) regulates endosome-to-TGN retrograde transport. J Cell Sci *119*, 3944-3957.

Sbrissa, D., Ikonomov, O. C., Deeb, R., and Shisheva, A. (2002). Phosphatidylinositol 5-phosphate biosynthesis is linked to PIKfyve and is involved in osmotic response pathway in mammalian cells. J Biol Chem *277*, 47276-47284.

Sbrissa, D., Ikonomov, O. C., Fu, Z., Ijuin, T., Gruenberg, J., Takenawa, T., and Shisheva, A. (2007). Core protein machinery for mammalian phosphatidylinositol 3,5-bisphosphate synthesis and turnover that regulates the progression of endosomal transport. Novel Sac phosphatase joins the ArPIKfyve-PIKfyve complex. J Biol Chem *282*, 23878-23891.

Schmitt-John, T., Drepper, C., Mussmann, A., Hahn, P., Kuhlmann, M., Thiel, C., Hafner, M., Lengeling, A., Heimann, P., Jones, J. M.*, et al.* (2005). Mutation of Vps54 causes motor neuron disease and defective spermiogenesis in the wobbler mouse. Nat Genet *37*, 1213-1215.

Schroder, J. M. (2006). Neuropathology of Charcot-Marie-Tooth and related disorders. Neuromolecular Med *8*, 23-42.

Schymick, J. C., Talbot, K., and Traynor, B. J. (2007). Genetics of sporadic amyotrophic lateral sclerosis. Hum Mol Genet *16 Spec No. 2*, R233-242.

Senderek, J., Bergmann, C., Weber, S., Ketelsen, U. P., Schorle, H., Rudnik-Schoneborn, S., Buttner, R., Buchheim, E., and Zerres, K. (2003). Mutation of the SBF2 gene, encoding a novel member of the myotubularin family, in Charcot-Marie-Tooth neuropathy type 4B2/11p15. Hum Mol Genet *12*, 349-356.

Snipes, G. J., Suter, U., Welcher, A. A., and Shooter, E. M. (1992). Characterization of a novel peripheral nervous system myelin protein (PMP-22/SR13). J Cell Biol *117*, 225-238.

Stendel, C., Roos, A., Deconinck, T., Pereira, J., Castagner, F., Niemann, A., Kirschner, J., Korinthenberg, R., Ketelsen, U., Battaloglu, E.*, et al.* (2007a). Peripheral nerve demyelination caused by a mutant Rho GTPase guanine nucleotide exchange factor, frabin/FGD4. Am J Hum Genet, preprint.

Stendel, C., Roos, A., Deconinck, T., Pereira, J., Castagner, F., Niemann, A., Kirschner, J., Korinthenberg, R., Ketelsen, U. P., Battaloglu, E.*, et al.* (2007b). Peripheral nerve demyelination caused by a mutant Rho GTPase guanine nucleotide exchange factor, frabin/FGD4. Am J Hum Genet *81*, 158-164.

Strahl, T., and Thorner, J. (2007). Synthesis and function of membrane phosphoinositides in budding yeast, Saccharomyces cerevisiae. Biochim Biophys Acta *1771*, 353-404.

Suter, U. (2007). Phosphoinositides and Charcot-Marie-tooth disease: new keys to old questions. Cell Mol Life Sci *64*, 3261-3265.

Szigeti, K., Garcia, C. A., and Lupski, J. R. (2006). Charcot-Marie-Tooth disease and related hereditary polyneuropathies: molecular diagnostics determine aspects of medical management. Genet Med *8*, 86-92.

Tersar, K., Boentert, M., Berger, P., Bonneick, S., Wessig, C., Toyka, K. V., Young, P., and Suter, U. (2007). Mtmr13/Sbf2-deficient mice: an animal model for CMT4B2. Hum Mol Genet *16*, 2991-3001.

Umikawa, M., Obaishi, H., Nakanishi, H., Satoh-Horikawa, K., Takahashi, K., Hotta, I., Matsuura, Y., and Takai, Y. (1999). Association of frabin with the actin cytoskeleton is essential for microspike formation through activation of Cdc42 small G protein. J Biol Chem *274*, 25197-25200.

Valentijn, L. J., Baas, F., Wolterman, R. A., Hoogendijk, J. E., van den Bosch, N. H., Zorn, I., Gabreels-Festen, A. W., de Visser, M., and Bolhuis, P. A. (1992). Identical point mutations of PMP-22 in Trembler-J mouse and Charcot-Marie-Tooth disease type 1A. Nat Genet *2*, 288-291.

Verhoeven, K., De Jonghe, P., Coen, K., Verpoorten, N., Auer-Grumbach, M., Kwon, J. M., FitzPatrick, D., Schmedding, E., De Vriendt, E., Jacobs, A.*, et al.* (2003). Mutations in the small GTP-ase late endosomal protein RAB7 cause Charcot-Marie-Tooth type 2B neuropathy. Am J Hum Genet *72*, 722-727.

Volpicelli-Daley, L., and De Camilli, P. (2007). Phosphoinositides' link to neurodegeneration. Nat Med *13*, 784-786.

Vowels, J. J., and Payne, G. S. (1998). A dileucine-like sorting signal directs transport into an AP-3-dependent, clathrin-independent pathway to the yeast vacuole. Embo J *17*, 2482-2493.

Walker, F. O. (2007). Huntington's Disease. Semin Neurol *27*, 143-150.

Wallengren, J. (2005). Neuroanatomy and neurophysiology of itch. Dermatol Ther *18*, 292-303.

Yamanaka, K., Chun, S. J., Boillee, S., Fujimori-Tonou, N., Yamashita, H., Gutmann, D. H., Takahashi, R., Misawa, H., and Cleveland, D. W. (2008). Astrocytes as determinants of disease progression in inherited amyotrophic lateral sclerosis. Nat Neurosci *11*, 251-253.

Zannolli, R., Buoni, S., de Santi, M., Miracco, C., Vonella, G., Tassini, M., Vivi, A., Viviano, M., Rossi, T., Orsi, A.*, et al.* (2008). New neurocutaneous syndrome with defect in cell trafficking and melanosome pathway: The future challenge. Brain Dev.

Zhang, X., Chow, C. Y., Sahenk, Z., Shy, M. E., Meisler, M. H., and Li, J. (2008). Mutation of FIG4 in patients causes a rapidly progressive, asymmetric neuronal degeneration. Brain, in press.

Zhang, Y., Zolov, S. N., Chow, C. Y., Slutsky, S. G., Richardson, S. C., Piper, R. C., Yang, B., Nau, J. J., Westrick, R. J., Morrison, S. J.*, et al.* (2007). Loss of Vac14, a regulator of the signaling lipid phosphatidylinositol 3,5-bisphosphate, results in neurodegeneration in mice. Proc Natl Acad Sci U S A *104*, 17518-17523.

Zhang, Y. W., and Xu, H. (2007). Molecular and cellular mechanisms for Alzheimer's disease: understanding APP metabolism. Curr Mol Med *7*, 687-696.

Zuchner, S., Noureddine, M., Kennerson, M., Verhoeven, K., Claeys, K., De Jonghe, P., Merory, J., Oliveira, S. A., Speer, M. C., Stenger, J. E.*, et al.* (2005). Mutations in the pleckstrin homology domain of dynamin 2 cause dominant intermediate Charcot-Marie-Tooth disease. Nat Genet *37*, 289-294.

Zuchner, S., and Vance, J. M. (2006). Molecular genetics of autosomal-dominant axonal Charcot-Marie-Tooth disease. Neuromolecular Med *8*, 63-74.